Universität Bonn

Physikalisches Institut

Investigations into the DNP characteristics of electron and proton irradiated polyethylene and polypropylene

Falmer Scott Reeve

To achieve a significant enhancement of the nuclear polarisation of solid state target materials one must use the method of dynamic nuclear polarisation. This necessitates unpaired electrons, that can be created as paramagnetic structural defects by the irradiation of materials. To this end polyethylene (PE) and polypropylene (PP) materials were irradiated by 13 MeV protons at a temperature of 120 K and over a temperature range of 87 K to 210 K with ~20 MeV electrons. The identification of the radical types that are created, as well as the quantification of the unpaired electron density, was made in a conventional ESR spectrometer. Samples were polarised in a 2.5 T magnetic field at a temperature of 1 K.
It was found that the irradiation temperature has an effect on the nuclear relaxation times of the materials. Higher irradiation temperatures result in lower radical yields and consequently longer relaxation times. Both materials exhibit an increase of polarisation values for an increase in irradiation temperature. The largest polarisation values were obtained in the PE materials of around 20% when irradiated at a temperature of 210 K, but PP only reached a maximum of 8% at the same irradiation temperature. Better results for the PP materials, in terms of polarisation values, were obtained by the heating of the samples at room temperature post irradiation. Here it was possible to obtain results of 14% polarisation.

Investigations into the DNP characteristics of electron and proton irradiated polyethylene and polypropylene

Dissertation
zur
Erlangung des Doktorgrades (Dr. rer. nat.)
der
Mathematisch-Naturwissenschaftlichen Fakultät
der
Rheinischen Friedrich-Wilhelms-Universität Bonn

von
Falmer Scott Reeve
aus
Chatham

Bonn, September 2017

Dieser Forschungsbericht wurde als Dissertation von der Mathematisch-Naturwissenschaftlichen Fakultät der Universität Bonn angenommen und ist auf dem Hochschulschriftenserver der ULB Bonn `http://hss.ulb.uni-bonn.de/diss_online` elektronisch publiziert.

1. Gutachter:	Priv.-Doz. Dr. Stefan Goertz
2. Gutachter:	Prof. Dr. Berhard Ketzer
Tag der Promotion:	19.01.2018
Erscheinungsjahr:	2018

Contents

CHAPTER 1

Introduction

The dawn of modern physics was in the late nineteenth century when the negatively charged electron was discovered by Thomson in a series of experiments analysing deflected cathode ray tracks in a magnetic field. The charge/mass ratio could be determined from these tracks, leading to the conclusion that either the charge of the electron is large or, as later discovered, the mass of the electron is particularly light. For outside observers the atom is electrically neutral and considering the negative charge of the electrons the question naturally arises as to what makes up the electrically balancing positive charge. Scattering experiments by Rutherford of alpha-particles on gold foils in the 1910s gave detailed information about the mass and the charge distribution within the atom [1]. Only a small proportion of the alpha-particles were scattered, but most of the alpha particles passed through the foils without any scattering at all, leading to the conclusion that the atom must be practically empty and that virtually all of the mass of the atom is situated in a spatially concentrated, positively charged centre. It was later shown that the positive charge of the so-called nucleus could be accounted for by an integer number of the hydrogen nucleus, later called the proton. The atomic model proposed by Bohr in 1914 gave the first "complete" theory for the atomic structure [2], [3]. Bohr's model, consisting of a positively charged nucleus containing protons surrounded by the same amount of electrons on fixed circular orbitals, had success in calculating the excitation spectra of hydrogen, but failed for heavier atoms. Chadwick's studies of atomic disintegration provided the solution in 1932 with the discovery of the neutron that makes up the additional mass observed for nuclei [4]. From this point on nuclei have been considered to be made up of positively charged protons and the non-charge carrying neutrons. This is thought by many to be the end of the classical physics era and the genesis of modern day hadron and nuclear physics.

The next major scientific development would take another 30 years, when in 1964 Gellmann and Zweig postulated the existence of charge carrying quarks as the fundamental building blocks of hadrons, of which the proton and the neutron are probably the best known, as they make up the matter we see around us [5], [6]. The interaction of quarks is described by the theory of the strong nuclear force (QCD) and contains the phenomena of confinement which isolates the quarks into hadronic groups of mesons (two quarks - quark + anti-quark) and baryons (three quarks), so that quarks cannot be directly observed as they cannot be isolated singularly. For this reason much of what we know about quarks has been deduced from observations in experiments involving hadrons and their interactions. Theoretical models have long predicted higher multiplicity of quark groups, however only these two groups of hadrons had ever been confirmed experimentally until 2015 when the LHCb collaboration at CERN for the first time reported results consistent with pentaquark states [7].

The quarks are grouped into three flavour families containing the up (u) and down (d) quarks, the charm (c) and strange (s) quarks, and the top (t) and bottom (b) quarks, as well as the same grouping again for their corresponding antiparticles. Each quark carries a charge (-1/3e or 2/3e), where the sum of the individual quark charges gives the charge of the hadron in its entirety, and a colour charge (red, green or blue, anti-red, anti-green, anti-blue) that when summed for the colour component gives a white hadron, i.e., colour/anti-colour for mesons and all three colours, or anti-colours for baryons.

In modern day scattering experiments the substituents of matter are probed with high energy gamma and particle beams, which have a relativistic momentum p and thus according to de Broglie a wavelength $\lambda = \mathrm{h}/p$ [8]. Due to the associated diffraction of waves on structures this places limitations on the resolution of these probes. The ever increasing focus on the resolution of smaller structures entails the need to increase the momentum and hence the energy of the projectiles. In scattering experiments high energy projectiles can transfer energy to scattering materials, resulting in the excitation of the materials with a subsequent creation of new particles. The energy and angle dependencies of the collisional products give insight into the dynamics of the interactions and thus also into the internal structure of the target materials.

At energies, just above the nucleon masses, detailed information in the non-perturbative region of QCD can be extracted for the binding energies of the nucleon systems by their resonance excitations. Here double polarised experiments play a stand out role, since the cross section as determined in unpolarised experiments are averages over all spin states and the dominant resonances mask the contribution of spin specific reactions. Baryonic resonances have been a focus of study for quite a long time and yet a complete and detailed spectrum of all excited baryonic states is still incomplete, as for many predicted resonances the mass, width and decay coupling constants are still missing. Other resonances predicted by the quark models are still missing completely. Baryonic resonances are observed as a broad spectrum of overlapping resonances, that can only be fully disentangled by analysing the spin dependence of the individual contributions to the cross sections, for which highly sophisticated double polarisation experiments are needed in which the polarisation of both the incoming particle and the target materials can be determined to high precision and their relative orientation manipulated. Due to the low probability of these spin dependent reactions only solid state targets with high scattering densities provide adequately high luminosities, even at low beam intensities, for these types of experiments.

The ELSA facility, including the current experiments, is run and maintained by groups affiliated with the Physics Institute (PI) and the Helmholtz-Institut für Strahlen- und Kernphysik (HISKP) and consists of two injector linacs, a booster synchrotron allowing tunable energies in the range of 0.5 GeV to 1.6 GeV and, finally, a stretcher ring providing electron end energies between 0.5 GeV to 3.2 GeV, and can provide polarised and unpolarised beams to the experiments. The combination of the polarised electron beam, provided by ELSA, together with the polarised solid state target, which is situated within the large acceptance detector Crystal Barrel/TAPS, allows the realization of a double polarisation experiment for the spectroscopy of the excitation of baryon resonances. In this experiment photoproduction reactions of energy tagged photons, produced as coherent bremsstrahlung of electrons off a diamond crystal, produce baryonic resonances that are analysed using a method called partial wave analysis (PWA). Due to the large amount of accessible observables, these types of photoproduction experiments are extremely sensitive to small coupling phenomena that are believed to be the source of the missing resonances predicted by QCD that have eluded experimental verification.

In particular the constant effort to improve the quality of the polarised beams and the target materials has shown a great improvement in the quality of the data that can be extracted from the scattering experiments. Here double polarisation experiments have thus become the indispensable tool for the determination of spin structure of protons and neutrons. The development of new target materials has been ongoing since the earlier 1960s and polymers have been discussed as serious candidates for solid

state target materials for at least the last two decades. One of the main attractions is that a polymer target could be formed to fit the geometry of practically any experimental setup and provide a highly dense, uniform material which, at least in theory, provides a filling factor close to unity. Solid state target experiments are conducted at low temperatures and the need for cooling away any additional heat input from the incident beam into the target material must be taken into consideration. This means that to ensure sufficient cooling the material must be porous or at least formed in such a manner to increase the surface area to volume ratio of the material. In practice this is realised in the form of crystals or frozen beads. However, if one was to machine the material to form discs, between which a coolant could permeate, the filling factor could be greatly improved.

To achieve high levels of polarisation in the solid state targets the method of dynamic nuclear polarisation (DNP) is used which requires the introduction of paramagnetic centres into the scattering materials. The paramagnetic centres, in the form of unpaired electrons, can be nearly fully polarised in high magnet fields at low temperatures and the process of microwave irradiation allows a transfer of this polarisation to the nuclei via a coupling of the electronic and nuclear systems. The characteristics of the electron coupling determines the eventual build-up and relaxation times of the nuclear subsystem and its effectiveness in terms of reaching high polarisation values. The stability of these paramagnetic sites, the so-called radicals, in solid target materials are usually very sensitive to elevated temperatures. Most commonly used target materials are stored in liquid nitrogen (at 77 K) as at this temperature the radicals are stable. Studies into the types of radicals that can be created by irradiation processes in polymers suggest that it could be possible to create room temperature paramagnetic centres within these materials. This would be a major benefit especially with an eye to loading and unloading of samples into cryogenic systems.

The study of the characteristics of polymers has been ongoing since their conception as macromolecules in the 1920s [9]. A lot of research was done in the past on irradiated polymers, for the most part in the 1960s and 1970s, centring on the radiation chemistry and structural changes of the polymers due to ionising radiation. This research was predominately focussed on the change in macroscopic material characteristics, with the aim of modifying polymers for their commercial use. It was shown that the irradiation environment was one of the decisive factors in the modification of the molecular structures, and that the characteristic parameters that could be relevant for DNP, such as the radical types, their yields and distributions, are all highly dependent on the irradiation temperature and the atmosphere in which the materials are irradiated and subsequently stored. Yet papers on the polarisation characteristics of polymers, especially irradiated polymers, from this time are few and far between, not surprising considering these types of experiments using the polarisation of nuclei were just at their commencement.

The polarisation characteristics of these materials first became a topic of interest, when it was realised that the high dilution factors of hydrocarbon polymers could potentially make polymers the ideal target for solid state polarised target experiments. The advancement of the polymers has albeit been hindered by the immediate success of other target materials, especially with respect to chemically doped materials. Notwithstanding the favourable results obtained with alcohols and diols, the polymers have remained an interesting prospect, with a multitude of researchers in the field of polarised targets returning at some point to the examination of their polarisation characteristics. Herein lies the problem. The polymer macromolecule is an extremely complex system. Sporadic investigations will never do the polymer systems justice and one needs to understand the radical creation mechanism and the temperature dependent evolution of the radical system to fully grasp how the polymer system can be utilised to maximise nuclear polarisation. Many studies have shown some promising results, however rarely have these studies been used to optimise the polarisation characteristics of the materials. There are many indications that polymer targets could be the way forward for double polarisation scattering experiments, however, due to the increased number of parameters, the effort involved is somewhat greater for macro-

molecular systems than is the case for short chain molecules, like many common target materials, e.g., butanol.

Some early work at the end of the 1960s was conducted by Hill et al. in Illinois, USA, studying the polarisation characteristics of polyethylene (PE) irradiated in the air-cooled reactor cores of the Argonne National Laboratory reactor facility. These radicals appeared to be very stable and when stored at room temperature for periods up to a week showed no noticeable decay in the radical concentration or on their maximum polarisation values. The reports gave maximum polarisations at 1 K and in a 2.5 T magnetic field of around 10%, when samples where irradiated to a spin concentration in the order of 10^{19} e^-/g [10]. Also in the late 1960s at CERN, Switzerland much effort was placed into the doping of different proton rich polymer materials with chemically stable free radicals, among others BPA, DPPH, PAC and porphyrexide [11]. The materials were doped by solution with the radical in solvents, e.g., toluene or benzene, where the solvent was subsequently evaporated leaving behind, in the ideal case, a polymer material with a homogeneous distribution of the radical interspersed within the molecular structure. Results showing polarisations of around just over 20% were achieved in plexiglas and polystyrene (PS) when measured under similar conditions to those used by the before mentioned researchers from Illinois. The laborious and non-trivial task in this procedure is finding a common solvent for the radical/base material combination.

As well as the blending of the radical with the polymer in a common solvent the free radicals can also be introduced into a polymer by diffusion from vapour [12]. The diffusion method does have its limitations as 1) the diffusion process is initiated by a heating of the sample material to "open" the structure, however many radicals are not stable at elevated temperatures, and 2) the radical diffusion mobility is highly restricted by the size of the radical and can cause skin effects where only the surfaces of materials can be doped, leading to an inhomogeneous distribution of the radical with respect to the material as a whole. In the mid 1990s the research group at PSI, Switzerland managed to show DNP of deuterated samples of PE foils achieving polarisations of ±10% [13] and of protons in thin PE foils and small tubes, chemically doped via diffusion at 80 °C of TEMPO to a spin density of 2×10^{19} e^-/cm^3, to values of $+64\%/-56\%$ in a 2.5 T magnetic field at temperatures below 0.3 K [14]. Kumada et al. gave results for proton polarisations of up to 32% in low density PE and 23% in high density PE, doped by the same method employed by the PSI group, but doped only to about half of the spin concentration and measured at a higher temperature and magnetic field (1.4 K and 3.35 T) [15].

Most of the recent research on polarised polymer target materials has focussed on the base polymer PE, and most emphasis has been placed on its deuterated version CD_2. Crabb reported results obtained for CD_2 irradiated to an incident dose of approximately 1×10^{15} e^-/cm^2, where a maximum polarisation of ~30% was reached in a magnetic field of 6.55 T and at a temperature of 1 K [16],[17]. Similar results were shown by Wang et al. for slightly higher doses but at a temperature of 150 mK and a magnetic field of 2.5 T [18]. However there are also some recent results from irradiated CH_2 measured at 5 T and 1 K that give polarisations of -23%/+25% when PE was irradiated with 19 MeV electrons to a dose of 1×10^{15} e^-/cm^2 [19]. The challenge of trying to put these results into a coherent picture to qualify the materials proves extremely difficult, due to the completely different experimental setups and preparation methods of the materials, however, at least PE seems to have potential to be successfully used as polarised target material.

The aim of polarised target material research is to find materials that fulfil certain base criteria and then to optimize the parameters of the material in such a way that high nuclear polarisations can be achieved. This process has been applied in this work to the base materials of PE and PP in their "normal" molecular form of CH_2 and CH_2CHCH_3, respectively, in the start of a systematic study on the influence of the irradiation temperature on the proton polarisation characteristics. For DNP to be successful unpaired electrons must be introduced into the materials. The structures of these paramagnetic sites

have a large influence on the polarisation characteristics of the materials and can be analysed using the method of electron spin resonance (ESR) spectroscopy. An introduction into the basic principles of the continous wave (CW) ESR analysis and the energy splitting in general of the spin states in magnetic fields will be given in chapter 2. A short overview of some of the historical developments of DNP, and of the descriptive theories that lay the foundation for understanding how polarisation in such materials is actually produced, will be given in chapter 3.

With regards to the choice of a base material one looks to optimize the target specific figure of merit (FOM). A detailed discussion of the FOM for a polymer type target material, in particular for PE and PP, will therefore be given in chapter 4 with comparisons to some commonly used materials detailing the various possibilities for introducing paramagnetic centres into these materials, as these centres are of paramount importance for the application of DNP methods. Another one of the defining characteristics of polymers is their crystallinity. A short discourse on the subject will be provided in chapter 5. The terminology, as well as some of the influencing factors, will be described and the results of the crystallinity determination for the sampled materials, by the chosen method of differential scanning calorimetry (DSC), will be presented. Furthermore, the possible influence of the crystallinity on irradiation yields, radical creation and polarisation characteristics will be discussed in the subsequent chapter 6, where first an introduction into the radiation chemistry of materials will be given, followed by a detailed description of the procedure for the irradiation of the chosen materials, focussing on the different irradiation facilities that were used for this study and the considerations for each of the individual irradiation programmes.

The radical identification and quantification, post irradiation, is important if one wishes to influence the polarisation characteristics of a material, as one must first understand how the polarisation is related to the ESR signal. A brief introduction into the radicals that are expected to be created in PE and PP during the irradiation processes is given in chapter 7. Concluding this chapter the decay mechanisms of the materials are presented, as changes in the structural configurations will necessarily influence the polarisation ability of the materials. In chapter 8 the measured radical yields and ESR signals will be presented and analysed with regards to the spectra. Beforehand the method of determining the spin density will be demonstrated. The change of the radicals at elevated temperatures will be shown as a conversion and/or decay process of these radicals.

After the initial analysis of the materials by ESR and DSC the polarisation measurement was conducted in a helium-refrigerator at temperatures of $\sim$1 K and at a magnetic field of 2.5 T. The basic setup of the polarised target test facility and the working principle of the refrigerator will be presented in chapter 9, as well as the method of polarisation determination. The polarisation and relaxation results obtained in the aforementioned cryostat will be presented and discussed in chapter 10 with an attempt to sum up the results into a coherent picture. The final chapter 11 is the summary of the work and will give an outlook into possible future research, trying to detail the best way to proceed in this research field with the most promising, but also realistic, procedures.

CHAPTER 2

Spin dynamics

Target materials contain an ensemble of nuclear and electronic particles, each having magnetic moments. These magnetic moments interact with each other, but also with the external magnetic field within which they are placed. This chapter starts with the basic interaction of a magnetic moment with an external magnetic field. This results in an energy splitting of the spin states, so that the resulting energy levels are indicative of the underlying spin structure. An analytical method that is based on the principle of the induced transition between electronic states is called electron spin resonance (ESR) spectroscopy and has become a vital tool in the analysis of irradiated materials. The observed spectra of irradiated materials show transitional lines that are not sharp but are broadened by mechanisms that all have a large influence on the ability of the materials to build up polarisation and therefore will be discussed.

2.1 Particles with spin in magnetic fields

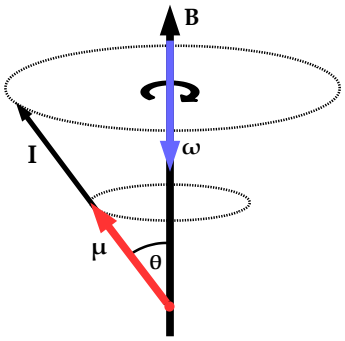

Figure 2.1: Precession of a nuclear magnetic moment in a magnetic field.

In a classical physics description the interaction of a magnetic moment $\boldsymbol{\mu}$ of a particle placed in a magnetic field $\boldsymbol{B}$ gives rise to a torque $\boldsymbol{T}$ on the particle

$$\boldsymbol{T} = \boldsymbol{\mu} \times \boldsymbol{B} = \frac{\mathrm{d}\boldsymbol{L}}{\mathrm{d}t} \tag{2.1}$$

with the time dependent change of the angular momentum being $\mathrm{d}\boldsymbol{L}/\mathrm{d}t$. This means that the magnetic moment of the particle precesses around the field axis at an opening angle of θ with an angular frequency ω, as contributions are only given in the perpendicular plane to the field axis, i.e., $\mathrm{d}L_{\parallel}/\mathrm{d}t = 0$. The situation for the proton is shown in figure 2.1. In this case the magnetic moment and the spin of the particle are parallel, whereas in the case of the electron the vector of spin and magnetic moment are opposing. For an ensemble of magnetic moments, with the resultant total magnetisation being the directional sum of all magnetic moments per unit volume, it follows that the change of the magnetisation can be written as

$$\frac{\mathrm{d}\boldsymbol{M}}{\mathrm{d}t} = \gamma \boldsymbol{M} \times \boldsymbol{B}, \tag{2.2}$$

where the gyromagnetic ratio γ gives the relationship $\mu_I = \gamma_I I$ for nuclear systems and $\mu_S = \gamma_S S$ for electronic systems, and the angular momentum of the particles are given by their spin, either I or S. In a static field B_z in equilibrium it follows that:

$$\frac{\mathrm{d}M_x}{\mathrm{d}t} = \gamma M_y B_z, \qquad \frac{\mathrm{d}M_y}{\mathrm{d}t} = \gamma M_x B_z, \qquad \frac{\mathrm{d}M_z}{\mathrm{d}t} = 0.$$

In principle the solutions are straight forward, as this is a simple harmonic oscillation (SHO) with

$$M_x(t) = M_x(0)\cos(\omega t), \quad M_y(t) = M_y(0)\sin(\omega t) \text{ and } M_z(t) = M_z(0) = \text{constant}.$$

In total this means that in equilibrium there is a constant magnetisation in field direction and each magnetic moment precesses around the field axis, though in the sum, as there is no preferential direction of the magnetic moments in the xy-plane, this means that the magnetisation in the plane disappears, as the phases of the magnetic moments are de-coherent.

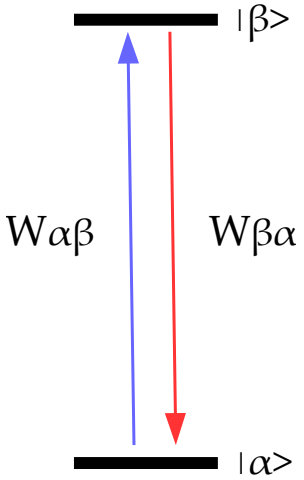

Figure 2.2: Transitions between two energy states.

The net magnetisation is in the direction of the field, typically allocated to the z-axis, and for this reason processes that are observed parallel to this axis are termed longitudinal, whereas those perpendicular are termed transverse. The net magnetisation has its origins in the unequal populations of the spin states, so for a particle with two spin states α and β the net magnetisation is longitudinal with $M_z \propto n_\alpha - n_\beta$, where n_α and n_β are the populations of the two energy states. Instead of considering the special static case in equilibrium one can also consider the generalised situation which includes relaxation processes, where the states are perturbed and attempt to relax back to equilibrium by the redistribution of the energy state populations. If one takes into account that the rate of relaxation is related to the transition from one state to the other, then the rate constants between the energy levels can be given as $W_{\alpha\beta}$ and $W_{\beta\alpha}$ (see figure 2.2). However the theory of relaxation predicts that the rate constants of transitions of a system are equal if the same underlying mechanisms are involved, so it would follow that $W_{\alpha\beta} = W_{\beta\alpha} = W$. Due to the difference in the populations of the states, the transition processes must then be related to the differences of the populations to their equilibrium values, as otherwise it would follow that in equilibrium $n_{\alpha 0} = n_{\beta 0}$ and for the magnetisation $M_{z0} = 0$, which is obviously not true. Using the rate equations one can then write the time dependence of the magnetisation in z-direction as

$$\frac{\mathrm{d}M_z}{\mathrm{d}t} = \frac{\mathrm{d}n_\alpha}{\mathrm{d}t} - \frac{\mathrm{d}n_\beta}{\mathrm{d}t} = (W(n_\beta - n_{\beta 0}) - W(n_\alpha - n_{\alpha 0})) - (W(n_\alpha - n_{\alpha 0}) - W(n_\beta - n_{\beta 0})) \tag{2.3}$$

$$= -2W(n_\alpha - n_\beta) + 2W(n_{\alpha 0} - n_{\beta 0}) \tag{2.4}$$

where the equilibrium magnetisation is given by $M_{z0} = n_{\alpha 0} - n_{\beta 0}$ and the magnetisation at any given point in time is still $M_z = n_\alpha - n_\beta$. Thus the time dependence of the magnetisation in z-direction then can be written as

$$\frac{\mathrm{d}M_z}{\mathrm{d}t} = -2W(M_z - M_0) \tag{2.5}$$

and it becomes evident that the rate constant $2W$ is in fact the inverse of the spin-lattice relaxation time T_1, as given by the Bloch equations [20]. For completeness one can further consider a system in

which the initial magnetisation in the *xy*-plane is indeed coherent and then de-phases with time. The basis solutions of motion of the magnetisation in the plane should still be an oscillation, as given for the solution of the SHO previously described, though modified by a phase factor R_2 that describes the rate of de-coherence. The assumption of the same rate constant is justified if the system is considered isotropic ($B_x = B_y$) and gives the general solutions

$$M_x(t) = M_x(0)\cos(\omega t)\exp^{-R_2 t}, \tag{2.6}$$

$$M_y(t) = M_y(0)\sin(\omega t)\exp^{-R_2 t} \tag{2.7}$$

to the differential equations

$$\frac{\mathrm{d}M_x}{\mathrm{d}t} = \gamma(\boldsymbol{M}\times\boldsymbol{B})_x - R_2 M_x, \tag{2.8}$$

$$\frac{\mathrm{d}M_y}{\mathrm{d}t} = \gamma(\boldsymbol{M}\times\boldsymbol{B})_y - R_2 M_y. \tag{2.9}$$

The last two equations are the Bloch equations for the transverse relaxation with the rate constant $R_2 = 1/T_2$ being the inverse of the spin-spin relaxation time.

2.2 Basic principles of ESR

Since its discovery by Zavoisky in 1944 [21],[22] electron spin resonance (ESR) spectroscopy has become a standard tool for the analysis of paramagnetic species and is a research field that is continuously developing with a wide variety of applications and analytical methods now in use. In its simplest form ESR spectroscopy is a non-invasive method used for the detection of unpaired electrons and can be applied to a wide variety of materials, irrespective of their aggregate state and can be used to quantify crystal defects caused by irradiation (spin density measurements). Beyond the characterisation of radicals with respect to their electronic structure it is also possible to monitor changes in local structure and molecular dynamics as the unpaired electrons interact with their surrounding environment, and with the development of new methods it has become possible to measure the distribution of the paramagnetic centres by measurement of average distances between these paramagnetic centres, typically in the range of 0.5 nm - 8 nm, as well as the direct measurement of electronic relaxation times.

ESR has a wide scope of application as unpaired electrons are found in many materials and reactions, including paramagnetic metal ions, e.g., Cu^{2+}, Mn^{2+} and Mo^{5+}, organic radicals during chemical processes (electron transfer reactions, e.g., photosynthesis) and at the sites of structural defects and colour centres in crystals. The paramagnetic centres of interest in this work are those created in polymeric materials, i.e., organic materials by irradiation and are in this sense structural defects.

The structure of the lines seen in the ESR spectra gives insight into the radical configuration, line form and various broadening mechanisms and their magnetic field dependence. Irradiated materials show absorption signals in ESR spectroscopy, meaning that there has been a structural change of the molecule resulting in “free” electron spins, which can couple to an external magentic field and to the nuclear magnetic fields, creating different energy levels and resulting in the observed resonance phenomena. The following chapter provides the fundamentals needed to understand the energy splitting of a resonance phenomena arising from the interaction of a particle with these fields. This is by no means restricted to this research field and many parts can in principle be applied to nuclear magnetic resonance (NMR), where electron specific parameters can be interchanged with those of the nuclei.

2.2.1 Energy splitting in magnetic fields

In classical physics a rotating charge q in a magnetic field $\boldsymbol{B}$ has an angular momentum $\boldsymbol{J}$ and a magnetic moment $\boldsymbol{\mu} = q\boldsymbol{J}/(2m)$, where m is the mass of the particle. This magnetic moment can couple to the external field, where the energy of the coupling is then given by $E = -\boldsymbol{\mu} \cdot \boldsymbol{B}$. In quantum mechanical terms the spin of a particle $\boldsymbol{S}$ can be considered to be an intrinsic angular momentum of the particle and is quantised by the factor $\hbar$. Furthermore, the classical approach must be modified by Dirac quantum mechanics and a parameter g is introduced to scale the angular momentum. The electronic Zeeman spin Hamiltonian for an unpaired electron in an external magnetic field $\boldsymbol{B}$ is then given by

$$\mathscr{H}_S = g_e \mu_B \boldsymbol{S} \cdot \boldsymbol{B} \tag{2.10}$$

where g_e is the g factor of the free electron and $\mu_B = e\hbar/2m_e$ is the Bohr magneton. Within this equation it is taken into consideration that the magnetic moment and the spin are related by

$$\boldsymbol{\mu}_e = -g_e \mu_B \cdot \boldsymbol{S}. \tag{2.11}$$

The experiments of Stern and Gerlach showed the quantisation of the spin [23], with the length of the spin vector given by

$$|\boldsymbol{S}| = \hbar \sqrt{S(S+1)} \tag{2.12}$$

with S the spin quantum number. In an external field the degeneracy of the electron spin states is lifted and the magnetic moment has only two possible orientations relative to the nominal field direction. So in units of $\hbar$ the spin in the field direction has a value of $S_z = m_S$ with $m_S = \pm 1/2$. The other components of the spin S_x and S_y cannot be determined simultaneously with S_z, according to the Heisenberg uncertainty principle. However, the components of the spin that are perpendicular to the magnetic field cancel each other out in an ensemble of spins, due to the precession of the magnetic moments around the field-axis. This means one needs only consider the z-component of the magnetic moment

$$\mu_{e,z} = -g_e \mu_B m_S \tag{2.13}$$

so that the corresponding energy in a magnetic field B_0 of the state corresponding to m_S is given by

$$E = -\mu_{e,z} B_0 = g_e \mu_B m_S B_0. \tag{2.14}$$

So whereas the spin has no preferential orientation when no magnetic field is applied, the application of a magnetic field leads to an alignment with the external field, resulting in a two level energy system (electronic Zeeman splitting). Each of these energies then has an energy that can be calculated to

$$\begin{aligned} E(m_S = +1/2) &= +\frac{1}{2} g_e \mu_B B_0, \\ E(m_S = -1/2) &= -\frac{1}{2} g_e \mu_B B_0. \end{aligned} \tag{2.15}$$

In ESR spectroscopy the transition between these energy states, induced by microwave irradiation, is measured. The driving mechanism is the coupling of the magnetic field component of the electromagnetic wave with the magnetic moment of the electron. The transitional energy of a photon with the Larmor frequency ν, needed to transfer the spin from the lower energy state to the higher energy state, is given by the resonance condition

$$\Delta E = h\nu = g_e \mu_B B_0. \tag{2.16}$$

The energy splitting of the Zeeman levels is directly proportional to the field, as can been seen in figure 2.3, where the higher energy level with the quantum number $m_S = +1/2$ corresponds to the spin "up" state (indicated in red) and the lower energy level with the quantum number $m_S = -1/2$ corresponds to the spin "down" state (also in red). In the simplest case this gives a simple one line transition caused by the change of orientation of the electron spin from down to up, the so-called spin-flip. The reverse process is called a spin-flop.

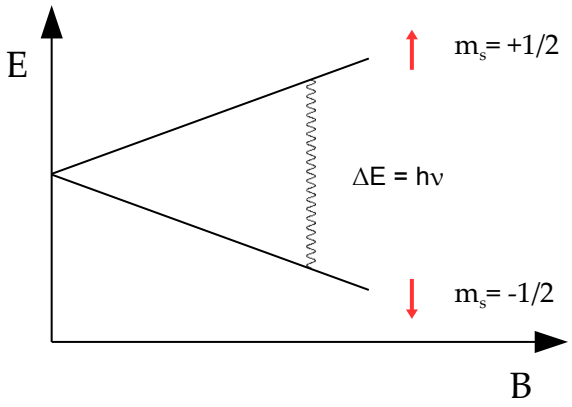

Figure 2.3: The simple ESR transition of an electron spin flip between the states $m_S = -1/2$ and $m_S = +1/2$.

A quick calculation for the typically used magnetic fields shows that the transitional energies of the irradiation in ESR spectrometers are in the microwave range, i.e., with frequencies in the region of GHz. A summary of the typical off the shelf type ESR spectrometers is given in table 2.1. The production of microwaves occurs in small ranges called bands with the allocation of the names having its origin in military communication going back to WWII. The most commonly used ESR spectrometers operate in X-band in the range 9 GHz to 10 GHz, corresponding to a central magnetic field of ~340 mT. The Bonn Polarized Target uses magnetic fields of 2.5 T, corresponding to the electronic Larmor frequency of 70 GHz, which places the electronic transitions at the higher end of the V-band (between Q- and W-band). Even so, ESR measurements in house were done with the X-band spectrometer, as a V-band spectrometer was not available. Spectrometers at higher fields are usually not sold commercially and must be custom made and these spectrometers are very expensive and are only used in laboratories that are highly specialised on ESR spectrometry.

Band	Central frequency [GHz]	Field [T]
S	3	0.107
X	9.5	0.339
K	23	0.821
Q	35	1.249
W	95	3.390

Table 2.1: Typical band, frequency and fields of commercialy available ESR-spectrometers.

In complete analogy to the electron, the spin and magnetic moment characteristics of nuclei can be summarized

$$|\boldsymbol{I}| = \hbar\sqrt{I(I+1)}, \tag{2.17}$$

$$\boldsymbol{\mu}_N = g_N\mu_N \cdot \boldsymbol{I}, \tag{2.18}$$

$$E = -\mu_{N,z}B_0 = -g_N\mu_N \mathrm{m}_N B_0. \tag{2.19}$$

Especially noteworthy is the fact that the spin and the magnetic moment for nuclei are parallel unlike in the case of the electron where they are anti-parallel. This means that the lower energy state of the nuclear Zeeman splitting has the highest quantum number, whereas the higher energy state has the lowest. Due to the inverse dependence on the particle mass the magneton of nuclei are much smaller than that of the electron, and as a result the energy splitting is also much smaller, e.g., the proton magneton is m_p/m_e=1836 times smaller than the Bohr magneton. This in turn results in an energy splitting that is approximately 660 times smaller than that of the electron, irrelevant of magnetic field strength, and in terms of the overall splitting in ESR can often be neglected, but is obviously important when considering nuclear transitions in NMR spectroscopy. The characteristic spin, g factors and frequency/magnetic field conversion constants and Larmor frequencies for X-band ESR and for a magnetic field of 2.5 T are summarised in table 2.2.

Particle	Spin	g factor	ν/B [MHz/T]	ν (0.340 T) [MHz]	ν (2.5 T) [MHz]
e	1/2	2.00232	28.025×10^3	9.5285×10^3	70.0625×10^3
^{1}H	1/2	5.58569	42.577	14.476	106.444
^{2}H	1	0.85744	6.536	2.222	16.340
^{3}He	1/2	-4.25525	32.436	11.028	81.090
^{6}Li	1	0.82205	6.266	2.130	15.665
^{7}Li	3/2	2.17096	16.548	5.626	41.371
^{13}C	1/2	1.40482	10.708	3.641	26.771
^{14}N	1	0.40376	3.078	1.046	7.694
^{15}N	1/2	-0.56638	4.317	1.468	10.793
^{17}O	5/2	-0.75752	5.774	1.963	14.436
^{19}F	1/2	5.25773	40.078	13.626	100.194

Table 2.2: Polarised target relevant NMR and ESR transition information calculated with g factors given in Appendix G7 in Lund et al. [24].

In addition to the individual Zeeman energy splitting of the spin states of the electron and of the nuclei, there exists an additional splitting that is of unique importance in ESR spectroscopy: The hyperfine splitting, in which the spin of the electron couples with the nuclear spin via the hyperfine coupling tensor $\boldsymbol{A}$. The spin Hamiltonian for the hyperfine splitting can be simply written as

$$\mathscr{H}_{\mathrm{hfs}} = \boldsymbol{S} \cdot \boldsymbol{A} \cdot \boldsymbol{I}. \tag{2.20}$$

This process will be discussed in detail in the next section 2.3.3.1 in terms of the hyperfine splitting being a source of broadening in ESR spectra. The ESR energy scheme that results from the discussed splitting mechanisms is shown in the schematic 2.4 for an electron/proton system, where the splitting is not to scale. The $m_S = \pm 1/2$ energy states of the electron are separated (indicated in red), as well as the $m_I = \pm 1/2$ states of the proton (indicated in blue), giving four energy levels. With the inclusion of the hyperfine splitting the energy of levels with the same electron and nuclear quantum numbers are shifted up, and those with opposing signs are shifted down. In the simple case of a proton coupled to an electron this gives two possible transitions of different energies. This principle can be extended to systems with a greater number of nuclei, but also to systems with different spin quantum numbers. In systems with n equivalent nuclei the number of lines in the ESR spectra is given by $2In + 1$ with an intensity distribution given by the Pascal triangle.

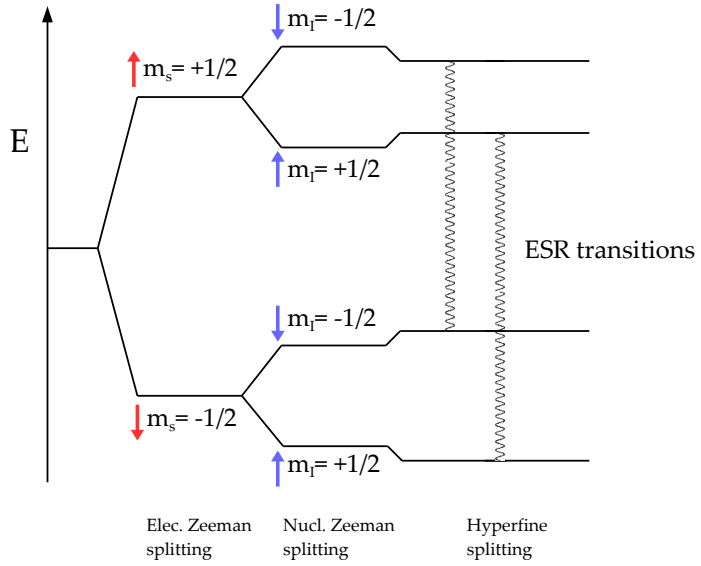

Figure 2.4: ESR energy coupling schematic for a single electron and proton, showing the electronic and nuclear Zeeman splitting and the hyperfine splitting.

2.2.2 Temperature influence on ESR detection

For a macroscopic ensemble of electron spins in thermal equilibrium the relative population of the energy states is given by the Boltzmann distribution:

$$\frac{n_+(m_S = +1/2)}{n_-(m_S = -1/2)} = \exp\left(-\frac{\Delta \mathrm{E}}{kT}\right) = \exp\left(-\frac{g_e \mu_B B_0}{kT}\right) \tag{2.21}$$

with the Boltzmann constant k and the temperature T. The lower energy state corresponding to $m_S = -1/2$ has a slightly higher population than the energy state corresponding to $m_S = +1/2$. ESR spectra are obtained by the measurement of the net absorption of the sample materials from the excitation of the lower spin state by absorption of electromagnetic irradiation, which is proportional to n_-, and the relaxation by emission of a photon from the higher spin state, which is proportional to n_+. Basically this means that the net absorption is given by the population difference $n_- - n_+$ and if one increases

this value one increases the sensitivity of the experiment. In the high temperature limit $g_e\mu_B B_0 << kT$ and it follows by Taylor expansion that $\exp(-x) \approx 1 - x$ and $n_+ \approx n_- \approx n/2$ with $n = n_+ + n_-$. Then the sensitivity of the experiment, defined as the population difference can then be summarised by the equation

$$n_- - n_+ = \frac{n g_e \mu_B B_0}{2kT}, \tag{2.22}$$

which carries the name Curie's law of magentisation. If one wishes to increase the sensitivity of the experiment, which means an improvement of the signal to noise ratio (S/N ratio), one has two factors that can be influenced for the analysis of a sample material, these factors being the magnetic field and the temperature. Increasing the magnetic field, e.g., measuring at V-, W-band or higher, means a shift to higher frequency. Due the linearity of the field/frequency relationship, the consequence would be that the waveguide diameter and sample size must be greatly reduced, cancelling the advantage gained by the improvement in the occupational states. The other preferred method is a lowering of the measuring temperature. It is common practice to measure X-band signals at 77 K by the insertion of the sample materials into an liquid nitrogen cooled dewar.

2.3 Lineshape and broadening mechanisms

2.3.1 ESR lineshapes

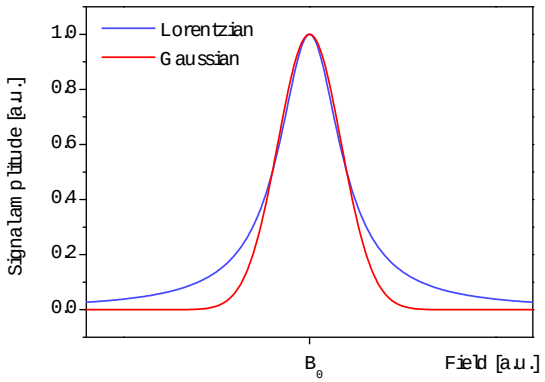

Figure 2.5: Gaussian and Lorentzian absorption spectra.

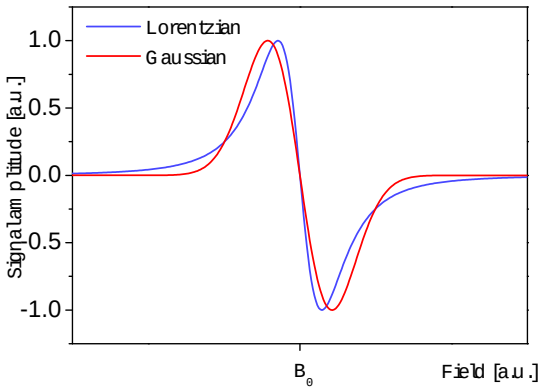

Figure 2.6: Gaussian and Lorentzian 1st derivative spectra.

Though the natural linewidth is defined by the uncertainty principle and gives the minimum possible line width in theory, in practice all lines are much broader. ESR spectra generally consist of an overlap of multiple lines which are Gaussian or Lorentzian in shape. The basic difference between the two line forms is that a Lorentzian distribution is slightly narrower through the centre and does not converge to zero as fast as the Gaussian line form in the flanks of the signal (see figures 2.5 and 2.6). Of particular importance is the lineshape of the 1st derivative of the absorption signal, as this is the signal one sees due to the measurement principle with a modulated signal, where the modulation is used to minimize noise and increase the measurement sensitivity (phase sensitive detection) [25]. Further defining characteristics of both lineshapes with regards to magnetic field, e.g., the intensity distribution and the peak widths, etc. are summarized in the ESR literature, e.g., the ESR standard on polymer research by Rånby and Rabek [26]. In most cases the actual lines seen in absorption will be a convolution of both lineshapes,

however a few generalisations can be made: Exchange narrowing in liquid solutions usually tends to produce Lorentzian shapes, whereas the broadened line observed in solid state ESR spectra is predominantly Gaussian [27]. Broadening in ESR signals can be split into two distinct groups a) homogeneous and b) inhomogeneous broadening, to be discussed in the following sections.

2.3.2 Homogeneous line broadening

Homogeneous broadening occurs when the initial and final energy states of the ESR transition are not infinitely sharp. The broadening effect is due to the fluctuation of local fields, so the actual transition energy is still well defined, however the energy states are not. Some examples of sources of homogeneous broadening are given by Portis [28]:

- The dipolar interaction of the unpaired electrons of the paramagnetic centres created, e.g., by electron-beam irradiation, give a broadening that is proportional to the inverse of the spin-spin relaxation time $1/T_2$.
- The spin-lattice interaction, giving what is sometimes termed the natural line width, broadens proportionally to the inverse of the spin-lattice relaxation time $1/T_1$. The line widths of ESR spectra tends to be much broader than the natural line width, due to the relation $T_1 >> T_2$.
- The interaction of the spins with the radiation field can cause saturation broadening. A strong continuous wave irradiation of the homogeneously broadened line, at any point within the broadened line spectra, reduces the intensity of the whole line, as all the spins interact in the same manner with the irradiation.
- The diffusion of excitation throughout sample, caused by the non-uniform microwave distribution throughout a sample material, causes fluctuations in the local fields and thus also broadening.

2.3.3 Inhomogeneous line broadening

In solids however the dominant effect of broadening is inhomogeneous. The lines consist of a distribution of resonant spin packets, whose envelope then gives the overall lineshape. Though the magnet field homogeneity and the dipolar interaction between spins with different Larmor frequencies do play a role, typically the most dominant contributions are made by the hyperfine splitting and by the anisotropy of the g tensor, both of which will discussed in the following sections.

2.3.3.1 Hyperfine splitting

The paths of the electrons on fixed orbits cross through the magnetic dipole field of the nucleus, causing a change in the local fields experienced by the electrons and a shift in their energy levels, as the nuclear magnetic dipole creates a magnetic field B_n, with which the electronic magnetic dipole interacts. This interaction is fundamentally an interaction of the electronic spin $\boldsymbol{S}$ with the nuclear spin $\boldsymbol{I}$ and is termed the hyperfine interaction. In the case of a s-wave state the wave function is spherically symmetrical and does not vanish at the position of the nucleus, i.e., $\psi(r = 0) \neq 0$, and the hyperfine splitting is isotropic and given by the Fermi contact interaction

$$A_{\text{iso.}} = \frac{\mu_0}{4\pi}\frac{8\pi}{3}(g_N\mu_N)(g_e\mu_B)|\psi(r = 0)|^2 \tag{2.23}$$

with $|\psi(r=0)|^2$ being the unpaired electron density at the location of the nucleus. The hyperfine factor is dependent on the magnetic moment of the nucleus and the probability density of the electron at the site of the nucleus. However, if this was always the case it would follow that only *s*-wave like orbitals would show any hyperfine splitting, which is plainly not true. In organic radicals one often has electrons with *p*-, *d*- or even higher states, exhibiting hyperfine splitting. The reason for this is that spin polarisation of the higher wave functions can induce a spin density in lower lying *s*-orbitals. For a wave function of the electron with an angular dependence, where the wave function vanishes at the site of the nucleus, the hyperfine coupling term has a directional dependence due to the relative orientation of the involved spins. A detailed calculation then gives the inhomogeneous hyperfine splitting term as

$$A_{\text{inh.}} = \frac{\mu_0}{4\pi}(g_N\mu_N)(g_e\mu_B)\frac{1}{r^3}(3\cos^2\theta - 1) \tag{2.24}$$

with θ being the angle between the longitudinal axis of the electron orbital and the magnetic field axis.

The hyperfine splitting influences the spectra seen in ESR spectroscopy as the energy levels of the transitions are shifted with regards to the Zeeman split lines. For the actual transition energies one can consider the field independent Hamiltonian of the hyperfine splitting

$$\mathscr{H}_{\text{hfs}} = \boldsymbol{S}\cdot\boldsymbol{A}\cdot\boldsymbol{I}. \tag{2.25}$$

The additional interaction can be seen as a perturbation of the electron/proton energy states and the full Hamiltonian for the electron/proton system can then be written as

$$\mathscr{H} = g_e\mu_B\boldsymbol{S}\cdot\boldsymbol{B} + \boldsymbol{S}\cdot\boldsymbol{A}\cdot\boldsymbol{I} - g_N\mu_N\boldsymbol{I}\cdot\boldsymbol{B} \tag{2.26}$$

where, due to the comparatively small contribution, the nuclear Zeeman interaction is usually neglected in continuous wave ESR spectroscopy, as the transition rule dictates $\Delta m_I = 0$ and the energy terms cancel in the transition energies. Using the raising and lowering operators $S_\pm = S_x \pm iS_y$ and $I_\pm = I_x \pm iI_y$ the interaction can then be rewritten as:

$$\mathscr{H} = g_e\mu_B S_z B + AI_zS_z + \frac{A}{2}(I_+S_- + I_-S_+) - g_N\mu_N I_z B. \tag{2.27}$$

The mixed ladder operator term only gives a contribution for states in which the electron and proton spins are of opposing sign, i.e., for $|m_S m_I\rangle = |+1/2\,-1/2\rangle$ and $|-1/2\,+1/2\rangle$. Neglecting the nuclear Zeeman contributions, the matrix representation of the Hamiltonian then becomes:

$$\mathscr{H} = \begin{pmatrix} 1/2g_e\mu_B B + 1/4A & 0 & 0 & 0 \\ 0 & 1/2g_e\mu_B B - 1/4A & 1/2A & 0 \\ 0 & 1/2A & -1/2g_e\mu_B B - 1/4A & 0 \\ 0 & 0 & 0 & -1/2g_e\mu_B B + 1/4A \end{pmatrix} \tag{2.28}$$

In the simple case that $A << g\mu_B B$ the matrix elements $1/2A$ can be neglected and the energy terms $E(m_S\, m_I)$ for a small hyperfine splitting can be written as a perturbation of the Zeeman energy levels:

$$E(+1/2 \pm 1/2) = +\,1/2g_e\mu_B B \pm 1/4A, \tag{2.29}$$

$$E(-1/2 \pm 1/2) = -\,1/2g_e\mu_B B \mp 1/4A. \tag{2.30}$$

To obtain the general solution for the spin 1/2, 1/2 system the matrix 2.28 must be diagonalized. The generalized eigenfunctions for the energy spin eigenstates of hydrogen like atoms, including the nuclear Zeeman splitting and for an arbitrary nucleus of spin I, are given by the Breit-Rabi equation [29]:

$$E(I \pm 1/2, m) = -\frac{A}{2(2I+1)} + g_N \mu_N m B \pm \frac{A}{2}\sqrt{1 + \frac{4mx}{(2I+1)} + x^2} \tag{2.31}$$

with the total angular momentum given by $J = 1/2$ and the quantum number $m = m_J + m_I$ and with the variable:

$$x = \frac{(g_J \mu_B - g_N \mu_N)B}{A}.$$

2.3.3.2 Anisotropic g factors

The g factor of the free electron is one of the most precisely measured fundamental constants[1]. Nonetheless, the measured value for electrons in bound systems show a deviation from this value that is a result of the spin-orbit coupling. The deviation of the isotropic contribution of the g factor in organic materials from the value for the free electron is very small, but the g factor can also be rather large, e.g. in metal centres like Fe^+ in MgO with $g_{\text{iso}} = 4.13535 - 4.2478$ [31]. This in itself would not pose a problem: The g factor in ESR is the equivalent of the chemical shift in NMR and would not change the overall lineshape of the spectra, but instead would move the spectra as a whole along the magnetic field axis with a line of centre corresponding to the g factor by

$$g = \frac{h}{\mu_B} \cdot \frac{\nu}{B} = 0.07144771 \cdot \nu[\text{GHz}]/B[\text{T}], \tag{2.32}$$

whereas the corresponding shift seen in NMR is at least a factor of 10^5 smaller

$$g_N = \frac{h}{\mu_N} \cdot \frac{\nu_N}{B} = 7.62259384 \cdot \nu[\text{MHz}]/B[\text{T}]. \tag{2.33}$$

Due to equation 2.32 a lower g value would place the ESR signal at a higher magnetic field, whereas a higher g value would shift the signal to a lower magnetic field. The main problem lies in the fact that the g factor may not be the same in all directions. This means the rotation of the sample in the magnetic field will change the spectroscopic signal form. The g factor is thus formulated as a tensor which takes the 3-dimensional components into consideration. Using the tensor formulation of the g factor the Hamiltonian for the Zeeman splitting given in equation 2.10 for the electron can be rewritten as:

$$\mathscr{H}_S = \mu_B \mathbf{B} \begin{pmatrix} g_{xx} & g_{xy} & g_{xz} \\ g_{yx} & g_{yy} & g_{yz} \\ g_{zx} & g_{zy} & g_{zz} \end{pmatrix} \mathbf{S} \tag{2.34}$$

The resulting 3x3 interaction matrix can often be diagonalized and the g factor can be simplified to a principal axes system, but does not necessarily coincide with the axes of the laboratory system. In effect this means any deviation from an isotropic g factor will necessarily lead to line broadening, an effect that is unwanted for materials that are candidates for use in experiments using DNP of nuclei at high fields. In this sense the g factor poses a larger problem for the broadening as, unlike hyperfine splitting, the g factor splitting correlates directly with the magnetic field strength. So whereas at lower fields the

[1] $g_e = 2.00231930436182(52)$ [30]

g-anisotropy may remain unresolved, the anisotropy may become highly relevant, or even dominant, when shifting to higher fields.

2.3.4 Effect of line broadening on polarisation

The dynamics nuclear polarisation theory developed by Abragam and Goldman [32], [33] was later extended to incorporate nuclear polarisation at low temperatures in the so-called Borghini model [34]. The model assumes that the ESR line is inhomogeneously broadened, predominantly by the two aforementioned mechanisms, but that the homogeneous broadening of the different spin packets is large enough to provide a sufficiently fast cross relaxation so that a common spin temperature can be achieved. This model gives a prediction of the maximum nuclear polarisation as

$$P_{I,\max} = \mathscr{B}_I\left(I\beta_L\omega_S\frac{\omega_I}{2D}\frac{1}{\eta\sqrt{1+f}}\right) \tag{2.35}$$

where $\mathscr{B}_I$ is the Brillouin function, $\beta_L = \hbar/kT_L$ is the inverse lattice temperature, ω_S and ω_I are the electronic and nuclear Larmor frequencies, D is the full ESR linewidth, and $\eta = t_Z/t_d$ is the ratio of the Zeeman and dipolar relaxation times, and finally f is the leakage factor containing all nuclear relaxation processes that are not coupled to the electronic dipolar reservoir. Especially with regards to the ESR signal the equation gives some insight in how to optimize nuclear polarisation and highlights the importance of a narrow ESR linewidth for the maximum obtainable polarisation values, especially if accompanied by a small magnetic dipole moment as is e.g the case with deuterons. This also highlights that the precise identification of the radicals created in irradiation processes are essential if one wishes to identify possibilities to improve polarisation characteristics, as a matching of the ESR width D with the nuclear Zeeman energy provides the optimized thermal contact of the electronic and nuclear reservoirs, making high polarisation values possible. In practice this means identifying radicals with narrow ESR spectra and small g factor anisotropies.

CHAPTER 3

Polarisation mechanisms

The previous chapter detailed the interaction of electronic and nuclear spins. It is these interactions that lay the foundation for the theories of polarisation. Whereas, electrons are nearly fully aligned for the standard polarised target test conditions, where temperatures are typically around 1 K and the magnetic field strength is 2.5 T, it will be shown that the simple interaction of the magnetic moments of the nuclei with the magnetic field do not lead to large polarisations. It is the use of dynamic nuclear polarisation methods that makes the high values of polarisation possible, that are needed for spin dependent scattering experiments. Here the electrons are irradiated by microwaves which subsequently interact with one or more nuclei. Thus depending on the strength of interactional mechanisms, discussed in the previous chapter, different methods exist which can lead to increased polarisation values.

3.1 Polarisation in thermal equilibrium

A polarised target is an ensemble of nuclei, situated in a magnet field and at cryogenic temperatures, where the magnetic moments are aligned with regards to the the magnetic field axis. The statistical distribution of the alignment in thermodynamic equilibrium (abbreviated to TE) can be described by the Boltzmann statistics. This details the occupational density N_i of the different spin dependent energy states E_i, which arise from the coupling of the magnetic moments to the magnetic field:

$$N_i = n_i N \frac{\exp(-E_i/kT)}{Z} \quad \text{with} \quad Z = \sum_i n_i \exp(-E_i/kT) \tag{3.1}$$

with n_i, the degeneracy of energy state, and $N = \sum N_m$, the total number of particles occupying the state at a temperature T, and the normalization factor Z termed the partition function. To quantify the spin system the vector polarisation is used, which gives the expectation value of the spin, normalized by the value of the spin itself:

$$P := \frac{< I_z >}{I} = \frac{\sum_{i=-I}^{I} i N_i}{I \sum_{i=-I}^{I} N_i}. \tag{3.2}$$

For a two state particle system in thermal equilibrium with spin 1/2, as applies to electrons and to protons systems, the polarisation can then be written as

$$P_{\frac{1}{2}} = \frac{1}{\frac{1}{2}} \cdot \frac{\left(\frac{1}{2}\right) \cdot N_{\frac{1}{2}} + \left(-\frac{1}{2}\right) \cdot N_{-\frac{1}{2}}}{N_{\frac{1}{2}} + N_{-\frac{1}{2}}} = \frac{\exp\left(\frac{g\mu B}{2kT}\right) - \exp\left(-\frac{g\mu B}{2kT}\right)}{\exp\left(\frac{g\mu B}{2kT}\right) + \exp\left(-\frac{g\mu B}{2kT}\right)} = \tanh\left(\frac{g\mu B}{2kT}\right), \tag{3.3}$$

where the energy E_i of the corresponding states for the electrons and protons is given by the equations 2.14 and 2.19, respectively. The equivalent calculation for a spin 1 particle gives

$$P_1 = \frac{4\tanh\left(\frac{g\mu B}{2kT}\right)}{3 + \tanh^2\left(\frac{g\mu B}{2kT}\right)}. \tag{3.4}$$

The polarisation of a spin ensemble can be generalized by the use of the Brillouin function, with the factor $x = I\frac{g\mu B}{kT}$:

$$\mathscr{B}_I(x) = \left(1 + \frac{1}{2I}\right)\coth\left[\left(1 + \frac{1}{2I}\right)x\right] - \frac{1}{2I}\coth\left(\frac{x}{2I}\right) = P_I. \tag{3.5}$$

From the above equations it follows that the polarisation of both electrons and protons can be enhanced by the application of high magnetic fields at low temperatures. At polarised target test conditions with temperatures of ~1 K and with a magnetic field strength of 2.5 T the electrons are highly polarised $P_\mathrm{e} = 93.3\%$, however protons on the other hand only manage a polarisation of $P_\mathrm{p} = 0.26\%$, owing to the 658 times smaller magnetic moment of the protons in comparison to the electron. Whereas the nearly complete electron polarisation at the conditions of the experiment can be achieved with relative ease, the polarisation of the protons under equivalent conditions are less than substantial. To increase the polarisation of the protons methods are employed that utilize the coupling of the electronic and nuclear spins. Using microwave irradiation it is then possible to transfer the high electron polarisations to the nuclear system, a process called dynamic nuclear polarisation (DNP).

3.2 Dynamic nuclear polarisation

The premise of DNP is to use the coupling of the electron and nuclear spins to transfer the polarisation from the electrons to the nuclei by microwave irradiation. In this manner the nuclear polarisation can reach equivalently high polarisation values. The processes describing the interactional mechanisms that lead to the enhancement of the nuclear polarisation can very generally be split into three groups: The Overhauser effect, the solid effect and thermal mixing. Overhauser first published his theory describing the DNP effect in the early 1950s [35]. Shortly after the theory was verified experimentally by Carver and Schlichter [36]. The underlying polarisation mechanism is the saturation of the electron spin transitions by microwave irradiation and was firstly used to describe the polarisation enhancement by conduction electrons in metals. The Overhauser effect is predominantly used in NMR spectroscopy to enhance NMR signals, but relies on the stochastic interactions between the electrons and the nuclei, meaning that the enhancements of polarisation are not immense. Following the experimental verification of the Overhauser effect in metals, Abragam proposed that this effect could also apply to insulating solids [37]. A short time hereafter Abragam and Proctor, and independently Jefferies, proposed the polarisation mechanism for insulators [38], [39], the mechanism later being called the solid effect. Because this model has been shown to apply to a limited amount of materials, it cannot be used to describe the polarisation mechanism that drives the polarisation enhancement in most commonly used target materials employed by the polarised target groups throughout the world. That being said the model is very intuitive and can be used to illustrate the basic concepts of DNP mechanisms. A thermodynamic theory of DNP is given by the theory of thermal mixing originating from the work of Kessenikh [40] and also

Kozhushner and Provotorov [41]. This theory is based on the allocation and coupling of the thermal reservoirs of the electronic and nuclear spin states. As the solid effect pumps classically forbidden transitions, it is generally regarded as the less efficient mechanism.

3.2.1 Solid effect

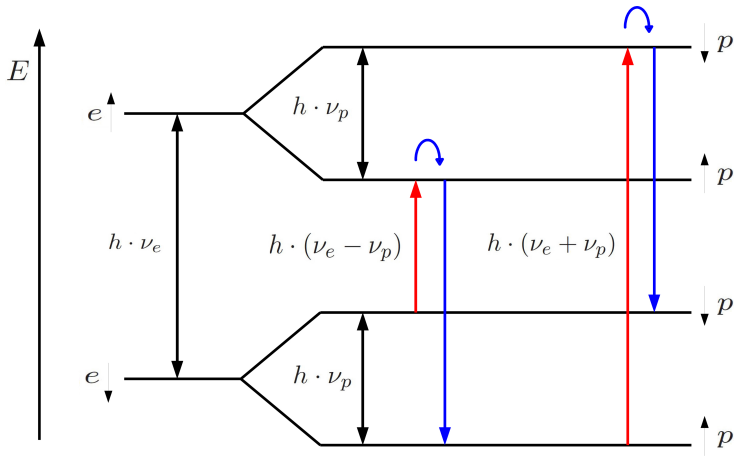

Figure 3.1: The energy-level diagram for an electron-proton pair in a magnetic field, including the induced transitions and the relaxation.

The solid effect was first verified experimentally in LiF by Abragam and Proctor [42], but one of the few examples of a target material for which the solid effect describes the polarisation characteristics is LMN-Nd^{3+}, which reached polarisation values of around 70% in the CERN setup in the late 1960s [43]. This model is based on the dipole-dipole interaction between the electron spin and the nuclear spin that leads to the hyperfine splitting of the Zeeman energy levels. It is this coupling that makes the solid effect possible. In the following it is assumed, for reasons of simplicity, that the nuclear spin belongs to a proton, however this does not necessarily need to be the case. The solid effect process is illustrated in figure 3.1 for an electron/proton pair. The ratio of the hyperfine splitting to the Zeeman splitting is very small and given by

$$q = \frac{\langle \mathscr{H}_{\text{hfs}} \rangle}{\langle \mathscr{H}_{\text{Zeeman}} \rangle} \approx 10^{-2}, \tag{3.6}$$

so that the energy eigenfunctions can be seen as a first order perturbation of the ground state, where the unperturbed energy eigenstate is $E(S_z, I_z) = g\mu_B m_S B - g_N \mu_N m_I B$. The first order perturbation can then be written as:

$$|S_z, I_z\rangle = p|S_z, I_z\rangle \pm q|S_z, I_z \pm 1\rangle, \tag{3.7}$$

with the normalisation condition of $p^2 + q^2 = 1$, where p^2 is the probability of the classically allowed state. This perturbation then allows for a simultaneous electron-nuclear spin flip, which classically would have been a "forbidden" transition. The irradiation with microwaves can then be used to cause a transition from one energy level to the other with $\Delta S_z = 1$ and $\Delta I_z = \pm 1$. As quantum mechanical transition rules apply, constraints are placed on the transitions with simultaneous spin flips of both the electron and the nucleon. The classically "forbidden" transitions can however be induced by microwave

irradiations at frequencies of $\nu_e \pm \nu_n$. Here frequencies of $\nu_e + \nu_n$ can be used to build up negative polarisation and frequencies of $\nu_e - \nu_n$ can be used to build up positive polarisation. For this to work only one of the transitions can be excited at a time, this means that the frequency width of the homogeneously broadened ESR spectrum δ must be small in comparison to the nuclear Larmor frequency ν_n.

The lower states are more densely populated and the electrons and the protons will relax back to these states. For this process to be effective the relaxation rate of the electrons must be much higher than those of the nuclei. In this manner the electron that has relaxed can be used for further transitions involving other nuclei, before the first nuclei has relaxed and consequentially this will lead to a build up of nuclei occupying the higher energy states. Due to the extremely good coupling of the electron spin to the lattice the electron relaxation rates are indeed much larger than typical nucleon relaxation rates[1].

3.2.2 Spin temperature, thermal mixing and the cross effect

The description of the solid effect relies on discrete electronic energy levels, assuming that the electronic frequency width of these states are very narrow in comparison to those of the nuclear Zeeman splitting. Realistically this only applies to systems with low electron densities, as higher electrons densities lead to a broadening and a smearing out of the energy levels due to the increased dipole-dipole interaction of the electrons. In contrast the theory of thermal mixing relies on the strong coupling between electron spins. In effect, this leads to the concept of an electron spin bath that can be described by a common temperature. The concept of a common spin temperature was first introduced by Redfield in 1955 to describe the saturation characteristics of solids in NMR spectroscopy [45], however can only be used to describe highly saturating microwave fields. This concept was then developed further in the 1960s for arbitrary fields by Provotorov et al. by the inclusion of an additional electronic spin temperature [41]. The extension of the theory to DNP was made end of the 1960s, start of the 1970s, where Borghini introduced the a spin temperature of the nuclear spin reservoir [34], [46].

The energy dependent population distributions of the spins within these three reservoirs can be described by Boltzmann statistics and are allocated reservoir specific temperatures, termed the spin-temperatures. The spin temperature given by the electronic Zeeman interaction is assigned the temperature reservoir T_{ze} and the nuclear Zeeman interaction T_{zn}. Due to the broadening mechanisms discussed in section 2.3.2 the energy levels of the electrons corresponding to the Zeeman splitting are not discrete, so that a spin temperature describing the distribution within the so-called spin-spin reservoir must be given by a separate spin temperate of T_{ss}. Without any external stimulus the system will reach a thermal equilibrium with the lattice temperature T_{l} and all reservoirs will have the same temperature $T_{\mathrm{ss}} = T_{\mathrm{ze}} = T_{\mathrm{zn}} = T_{\mathrm{l}}$.

Using microwave irradiation it is then possible to cool the spin-spin reservoir, this is illustrated in figure 3.2. If one has a split spin-spin state of width δ, then the irradiation by microwaves of the frequency $\nu_e - \delta$ will lead to a cooling of the spin-spin reservoir. This is due to the induced transition of the electrons between the electronic Zeeman levels. As effectively a small proportion of the energy is missing that is needed for the spin-flip, the energy can be extracted from the spin-spin reservoir, leading to a cooling of the electronic spin-spin system. On the other hand if the frequency of $\nu_e + \delta$ is used, the process provides a surplus of the energy needed for the spin-flip and the excess energy is then transferred to the spin-spin reservoir, leading to a cooling of the electronic spin-spin system, resulting in a population inversion corresponding to a negative temperature.

[1] $1/T_{1\mathrm{e}} \approx 10^3\,\mathrm{s}^{-1}$, whereas $1/T_{1\mathrm{n}} \approx 10^{-3}\,\mathrm{s}^{-1}$ [44]

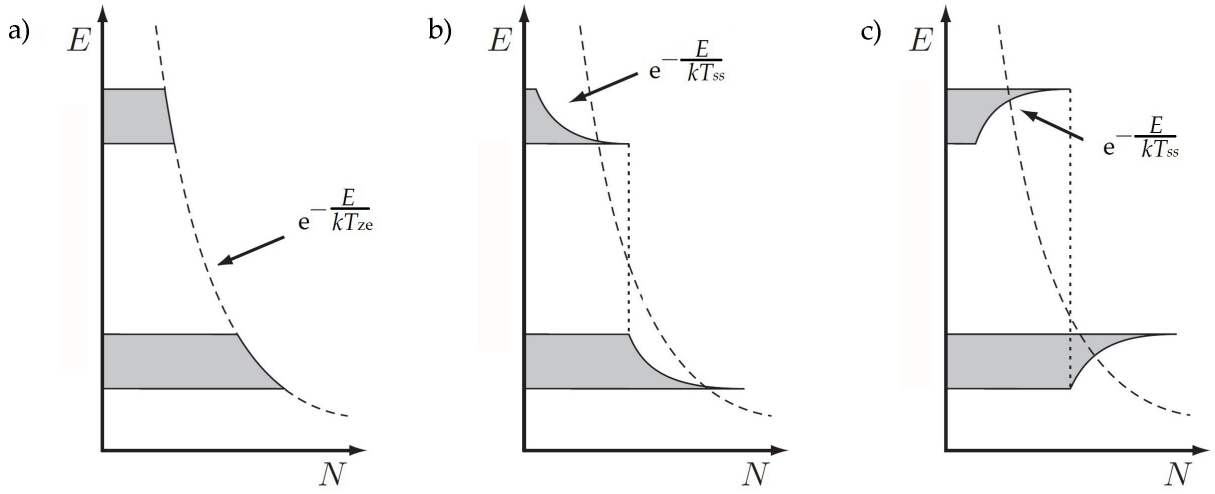

Figure 3.2: The population densities of the electron energy levels for spin-temperatures a) in thermal equilibrium $T_{ss} = T_{ze} = T_1$, b) cooling by microwave irradiation with $\nu_e - \delta$ for which $0 < T_{ss} < T_{ze}$ and c) cooling by microwave irradiation with $\nu_e + \delta$ for which $T_{ss} < 0$, $|T_{ss}| < T_{ze}$.

The coupling of the electronic spin-spin reservoir to the nuclear Zeeman reservoir leads to an equalisation of the spin-temperatures of these reservoirs, and as a result also leads to a Boltzmann distribution in the nuclear Zeeman energy levels given by equation 3.5. The process of this thermodynamic equalisation is called thermal mixing. This means a polarisation of the nuclei can be achieved by an active cooling of the electronic spin-ensemble, but for the best thermal contact between the baths, the nuclear Larmor frequency has to be close to that of the electronic width δ [33]. In a somewhat simplified picture, thermal mixing is a processes involving three spins, as opposed to two spins involved in the solid effect.

For thermal mixing to be effective a fast spectral diffusion is needed. This practically means that the ESR line width Δ is homogeneously broadened and thus $\Delta \approx \delta$. However in cases where the dominant broadening mechanism is due to the hyperfine interaction, as is the case for our irradiated polymers, the case of a fast spectral diffusion may not always apply. That being said, if the electron spin polarisation can be spread across the whole ESR spectrum sufficiently fast, i.e., there is a fast interaction between the electronic reservoirs, then thermal mixing can still apply. In systems involving multiple spectral lines one can find that the homogeneous line broadening δ is still rather small in comparison to the full ESR width Δ. In this case the spin polarisation cannot spread sufficiently fast throughout the ESR spectrum as a whole. If however two dipole coupled electrons have frequencies ν_{e1} and ν_{e2} that are close enough that they have an energy difference corresponding to the nuclear Larmor frequency ν_n, the coupling of the spin systems results in a polarisation transfer and an enhancement of the nuclear polarisation, a process termed the cross effect. In this process one electron is flipped by the microwave irradiation, but due to the coupling of the nuclear and electron spins and the energy conservation of the system this results in the simultaneous flip-flop of the electrons and a nuclear spin flip. Depending on the irradiation frequency and thus which of the electrons is flipped, this results in either positive or negative polarisation enhancement. Though this requirement is somewhat restrictive, it is believed to be a very efficient process[2] and much research in the recent years has gone into finding and designing radicals that fulfil these conditions [47].

[2] The solid effect polarisation scales with ν_n^{-2}, whereas both thermal mixing and the cross effect scale with ν_n^{-1}.

To distinguish between these mechanisms experimentally one can therefore compare the homogeneous broadened ESR linewidth δ with the total ESR linewidth Δ, as well as with the nuclear Larmor frequency ν_n. For the solid effect the condition of δ, $\Delta<\nu_n$ must hold. To distinguish between the other two effects where $\Delta>\nu_n$ one must then consider whether the ESR line is predominately homogeneously broadened, i.e., $\Delta \approx \delta$ (TM), or whether the line is mainly inhomogeneously broadened, i.e., $\Delta > \delta$ (CE) [48]. The demand of strong electronic dipolar broadening for TM means that the polarisation mechanism dominates in materials with higher radical concentrations, whereas the energy matching condition of the CE allows the mechanism to become dominant at lower concentrations, as long as the energy condition is fulfilled.

CHAPTER 4

Choice of solid state polarised target material

All target materials using DNP have in common that unpaired electrons must be brought into the overall material structure, whether this is by admixture of a paramagnetic radical, where the structure of the material is maintained, or by rearrangement of the structural configuration by irradiation. Both of these processes will be discussed, starting with the chemically doped materials, before moving on to irradiated materials where the emphasis has been placed on the ESR determined characteristics of the paramagnetic sites. Data exists on ESR measurements of some common target materials measured in V-band that are quite insightful with regards to the actual ESR lineshape at experimental conditions [49],[50][1]. For the irradiation studies the focus was placed on two types of long chained polymer molecules: Polyethylene (PE) and polypropylene (PP). To give an impression of these materials, an elementary description of PE and PP materials will be given. Why these materials are interesting for the experimental particle physicist comes down to their intrinsic characteristic properties, where the quality of the material that is to be used as a solid polarised target can be defined by the figure of merit (FOM). Detailing this definition, the relevant parameters will be discussed with regards to the use of a polymer and some comparisons will be made to butanol based targets, that are presently the standard material used in many double polarisation experiments.

4.1 Chemical doping of materials

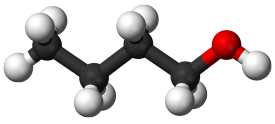

Figure 4.1: Ball and stick model of n-butanol, where the hydrogen atoms are represented by white balls, the carbon atoms are black and the oxygen atom is red.

The standard procedure for chemical doping uses materials that are liquid at room temperature and into which a free radical[2] can then be admixed and subsequently frozen. For an optimized target material one must ensure that the radical is distributed homogeneously throughout the solvent, the challenge being to find a good combination of an adequate base material, with a high dilution factor, as well as a radical with the ability to dissolve into the structure of this base material. Many combinations of free radicals and base materials have been tested, however only a few have really proven worthy of use in particle and nuclear physics experiments [51]. Some of the most implemented target materials in low intensity beam experiments have been the alcohols and diols, in particular butanol (figure 4.1) and propandiol.

[1] All values of V-band measurements mentioned in this chapter are taken from these publications.
[2] A free radical is an atom or molecule containing one or more unpaired valence electrons.

Butanol has been used as a target material in Bonn for many years and still remains one of the most successful in terms of overall performance. Butanol, in its isomeric configuration n-butanol ($CH_3(CH_2)_3OH$), has been used as a solid polarized target in many particle physics experiments and has been predominately doped for polarisation experiments by chemical means, e.g., with TEMPO [3], porphyrexide[4] and EHBA-Cr(V)[5]. Butanol has a four carbon structure with nine associated hydrogen atoms and a hydroxyl element and has two primary, one secondary and one tertiary isomers. The hydroxyl group is a polar group, with a partial positive charge on the hydrogen atom and a partial negative charge on the oxygen atom due to the two unpaired electrons in the remaining sp^3-hybrid orbitals and a partial positive charge on the bonded carbon atom, causing the overall polarity of the butanol molecule. The differences in the structural configuration of the isomers do give rise to physical and chemical differences, e.g., melting and boiling points, solubility and miscibility with water. However as far as I know, there have been no studies on how the isomeric configurations of the molecule may influence its polarisation characteristics, though as the other isomers don't offer any perceptible significant advantage over n-butanol, therein probably lies the reason. Some radicals can be directly dissolved into butanol e.g TEMPO, however for others it is necessary to dilute the butanol with water, e.g., prophyrexide. One must be cautious when doing so as the dilution factor is decreased by the admixture and has been known to reduce the radiation resistance of the material, yet the addition of water has in some cases been shown to improve the polarisation characteristics of the base material. The mutual solubility of n-butanol and water at room temperature is just under 8% by weight of water in butanol [52], placing an upper limit on the amount of water that can be used to initiate the admixture.

4.1.1 Nitroxyl radicals

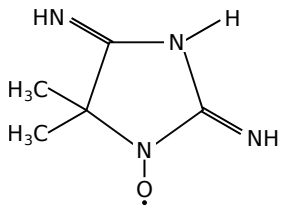

Figure 4.2: Structure of porphyrexide molecule.

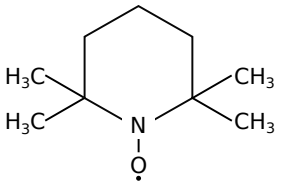

Figure 4.3: Structure of TEMPO molecule.

Both porphyrexide (figure 4.2) and TEMPO (figure 4.3) are nitroxyl-radicals. The localisation of the unpaired electron is predominantly on the N–O chemical bond and is stabilized due to the low energy of the valence electrons and the distance screening from the other atoms of the molecule [53]. This is particularly clear for a measurement in the so-called fast regime, e.g., in the liquid state at room temperature, where very high molecular rotational averaging cancels the contributions perpendicular to the magnetic field axis and only the isotropic part of the hyperfine splitting is seen. The result is an equidistant splitting into a three peak structure, which comes from the hyperfine coupling of the unpaired electron spin to the $I = 1$ nuclear spin of the ^{14}N nucleus.

[3] (2,2,6,6-tetra-methyl-piperidine-1-oxy) - $C_9H_{18}NO$
[4] (2,4-diimino-5,5-dimethyl-imidazolidine-n-oxyl) - $(C_5H_9N_4O)$
[5] (2-hydroxy-2-ethylbutyric acid) - $(Na^+(C_{12}H_{20}O_7Cr))^-$

4.1.1.1 Porphyrexide

The first stable free radical was created over a century ago, when in 1901 Piloty and Schwerin first synthesized the crystalline radical prophyrexide [54]. Porphyrexide is no longer commercially available, but the Bonn Polarised Target group has a reserve of the material stored. However, its production would not pose a great problem for most chemistry laboratories, as its production process is extensively detailed in the aforementioned publication and many papers since [55]. Porphyrexide is not room temperature stable and is usually stored at temperatures of between 0 °C and 6 °C (standard refrigeration) and is prepared as a highly crystalline powder of bright red colour. Porphyrexide can not dissolve in butanol alcohols, in fact it won't dissolve in any of the heavier alcohols either [56], and it is only with the addition of a small portion of water that it becomes possible to dissolve the dopant fully, only slightly reducing the dilution factor by an insignificant amount. It had been shown by Mango in the late 1960s that the addition of water had an effect on polarisation and relaxation characteristics, with maximum polarisations being obtained for a 5% by weight contribution of water for a fixed amount of the radical substance [57]. It was noticed that the relaxation rates of the samples increased linearly with water content up to a value of about 10%, thereafter the relaxation rate was no longer linear with water content, an observation that fits quite well with the solubility of water in butanol, as mentioned in the previous section.

With regards to the electronic structure of the radical, molecular orbital calculations show a higher electron spin density on the (N-O bonded) nitrogen atom, but also a non-negligible contribution on the second nitrogen atom (C=N-H bonded), resulting in a broad three peak structure with an additional narrower triplet splitting giving a total of nine lines [58]. However, in our target samples the splitting of the second nitrogen atom is only faintly adumbrated, as line broadening leaves the secondary components mostly unresolved. The ESR X-band width was measured as 2.6 mT in our laboratory, compared to 5.3 mT measured in V-band, which means the transition for X- to V-band causes the ESR signal to double in width. The reason is evidently the g factor anisotropy.

Nevertheless, despite a significantly broadened ESR signal, porphyrexide shows good polarisation performance at low temperatures and has been the doping radical of choice in the butanol based targets used by the Bonn Polarised Target Group for the last years, where a frozen-spin method is used to maintain high levels of polarisation [59]. Proton polarisations of ~80% are routinely reached and the samples provide relaxation times up to 600 h in a magnetic holding field of 0.5 T [60].

4.1.1.2 TEMPO

TEMPO was first synthesised in the late 1950s by Lebedev and Kazarnovskii [61] starting an intense period of research, producing literally hundreds more stable nitroxyl radicals in crystalline form. The radical is quite temperature stable and has been used to dope PE foils where temperatures of around 80 °C were applied to facilitate diffusion into the polymer structure [13]. The TEMPO/butanol combination has been used in some large scale experiments worldwide investigating baryon resonances, e.g., by Jefferson Lab Frozen Spin Target in the CEBAF Large Acceptance Spectrometer (CLAS), reaching polarisation values of up to 90% in a 5 T magnetic field at a temperature of between 100 and 200 mK whilst polarising by DNP [62]. Our standard sample for the calibration of the spin densities was made from 0.5 parts by weight of the TEMPO radical and 100 parts by weight of n-butanol, giving a spin density of $1.88 \times 10^{19}\,\mathrm{e}^{-}/\mathrm{g}$.

The ESR spectrum of the TEMPO can be explained solely by the hyperfine interaction of the free electron with the nuclear spin of the closest nitrogen atom and an anisotropic g factor. The ESR signal width in X-band (measured as 3.6 mT) is initially broader than the porphyrexide doped sample, but is

comparable to the porphyrexide signal at V-band, as the linewidth increases by only 50% to 5.45 mT. This is a consequence of the g anisotropy being 10% smaller in TEMPO than in porphyrexide.

4.1.2 EHBA-Cr(V)

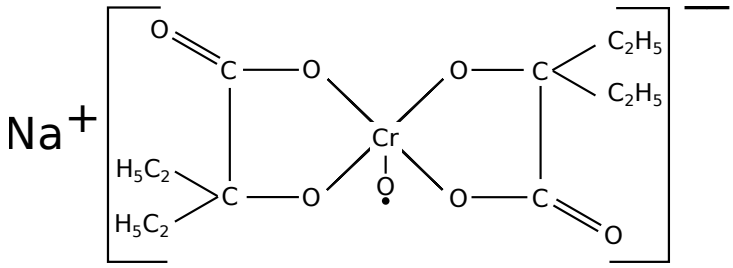

Figure 4.4: The chromium complex EHBA molecule.

The chromium complex EHBA (see figure 4.4) was first synthesised in late 1970s by Krumpolc and Roček [63] and used in the mid 1990s as the radical for target materials of the Spin Muon Collaboration (SMC) target, in which both proton and deuteron polarisations were utilized with all materials consisting of either normal or perdeuterated components [64]. The composition of the target material was 91% butanol with 5% water and 4% EHBA-Cr(V) creating a spin density of $6.35 \times 10^{19}\,e^{-}/g$ [65], which is quite high when one compares this to the porphyrexide and TEMPO doped materials and causes extensive line broadening in the ESR signals due to the spin-spin interaction of the electrons. The target material was very successful and maximum polarisations of ±94% were obtained at 2.5 T. EHBA is an interesting material because there is no hyperfine coupling contribution to the main ESR spectrum and the unpaired electron on the d-orbital of the chromium gives a three line spectrum that can be simulated by the diagonal elements of the g-tensor alone. EHBA however suffers from having an extremely large anisotropy (50% and 60% higher than porphyrexide and TEMPO, respectively). Thus, the initially very narrow signal in X-band of 1.67 mT, expands linearly with magnetic field to a width of 12.3 mT in V-band, practically excluding this material for use at much higher fields. Another disadvantage of EHBA is its light sensitivity[66].

4.2 Doping by irradiation

The inorganic compounds ammonia and lithium hydride are extremely radiation hardy materials and can be used in experiments utilizing higher intensity beams than is the case for organic materials. Ammonia has a two to three times higher resistance to radiation damage than butanol based target materials and higher beam intensities can be used without fear of causing irreparable damage. The radiation hardness in lithium hydride is in the order of a magnitude higher than that of ammonia. Both materials have high dilution factors making them extremely attractive solid state target materials.

4.2.1 Ammonia

The first successful polarisation tests of ammonia were conducted at CERN in the late 1970s by proton irradiation [67]. A short time later the method of irradiation that has proved most successful, and has now become the standard method for preparing ammonia for use in polarised target experiments, was developed in Bonn, by irradiation of ammonia by electrons in liquid argon [68], [69]. The slow

freezing of ammonia gas (NH_3) allows the compact ordering of the tetrahedron molecule into a compact structure, resulting in a solid and transparent material, which can be crushed at low temperatures to produce the small crystals used as a solid state target material. In the irradiation process the incoming electron interacts with the ammonia molecule and extracts a hydrogen atom to create the DNP active radical $\dot{N}H_2$:

$$e^- + NH_3 \rightarrow e^- + \dot{N}H_2 + \dot{H}.$$

The atomic hydrogen is caught on an interstitial lattice and though it can clearly be seen in the ESR spectra of irradiated ammonia in the far flanks of the spectrum it has no influence on the polarisation characteristics of the material. The radicals that are produced are not notably temperature stable and temperatures of ~117 K are enough to enable the recombination [70] destroying the polarisation capabilities of the material. As ammonia melts at 195.5 K and boils at 239.8 K one must handle the samples with extreme caution, especially in critical temperature periods such as sample loading. Furthermore, ammonia is caustic and can thus be quite hazardous.

The ESR spectrum of the $\dot{N}H_2$ radical is dominated in X-band by a complex hyperfine coupling resulting from the nitrogen atom and the two hydrogen atoms, however the radical also exhibits a g-anisotropy that broadens the signal[6] by 60% when measured in V-band[7]. So whereas the signal width is mainly caused by the HFS in X-band, the g-factor becomes the main broadening mechanism in V-band and higher fields.

Ammonia can be considered one of the best target materials when one considers just its maximum polarisation values, routinely achieving polarisations of >90% in dilution cryostats. However, as radiation hardy as the material is, a drop in the maximum polarisation values can be observed with age, yet annealing of the sample materials at 70-80 K can help restore the original polarisation characteristics. As established as ammonia has become the material suffers from a spin dependent contribution to the background signals from the nitrogen atoms, as these are also polarised in experiments wanting to measure the spin contributions of the protons [72]. This applies not exclusively to the abundant isotope ^{14}N, but also in lesser degree to the with 0.4% naturally occurring nitrogen isotope ^{15}N. This is unmistakably problematic when used with low intensity beams where the reaction rate is already fairly low, practically eliminating ammonia as a target material for photoproduction experiments.

4.2.2 Lithium hydride

^{7}LiH was first polarised in Saclay at the end of the 1970s, where polarisations reaching 95% were obtained for the protons of the material, but also maximum polarisations of 80% for the lithium nuclei in a magnetic field of 5.5 T [73]. Lithium hydride is stable from room temperature up to temperatures of >900 K but is highly reactive with water and must be stored in an inert atmosphere or at least completely dry. The crystalline lithium hydride samples are prepared for DNP by electron irradiation, ideally at a temperature of between 180 and 190 K [74], [75], where an irradiation to two orders of magnitude higher doses than in the organic materials is needed to create radical densities in the order of 10^{19} e^-/g. The lithium hydrides have a face-centred-cubic structure of Li and H atoms and irradiation causes an anionic vacancy in the crystal lattice by the ejection of the hydrogen atom from its lattice position, so that the vacancy can be occupied by an unpaired electron [76].

The ESR structure of the so-called lithium hydride F-center arises from the hyperfine interaction of the unpaired electron with the 6 surrounding ^{7}Li atoms ($I = \frac{3}{2}$). Where in theory this would amount

[6] The X-band width of irradiated ammonia is given by Dosert as 4.2 mT [71].
[7] The V-band width of irradiated ammonia is given by Heckmann as 6.65 mT [49].

to a signal consisting of $2nI + 1 = 19$ lines, the overlap of the broadened absorption lines leaves the components unresolved. The ESR signal then appears as a Gaussian curve with a narrow linewidth of approximately 2.4 mT [77]. The g-factor is thought to be highly isotropic with a value just under the value of the free electron and no broadening of the signal is expected at higher fields.

As with ammonia, the lithium based samples suffer from a polarisable background. Naturally occurring lithium consists to approximately 95% ^{7}Li and about 5% ^{6}Li, both of which have spin and can be polarised. The separation of the these contributions is an exceptionally difficult task.

4.3 Molecular description of PE and PP

For chemical compositions of organic and inorganic substances, proteins and DNA sequences it is common to use the CAS Registry Number (or just CAS number). Assigned by the Chemical Abstracts Service (CAS), it is a numerical identifier for the purpose that each substance can be uniquely identified. For PE and PP the identification numbers are 9002-88-4 and 9003-07-0, respectively. The CAS number is an identifier of chemical composition, but it does not say anything about how this is realised in the universal chemical structure. Being organic substances the backbone of the molecules is a long chain of carbon atoms, for PE, each with two associated hydrogen atom substitutes (CH_2 monomer - see figure 4.5) giving an overall molar mass of 14.03 g/mol. For PP the backbone of the molecule still consists of carbon atoms, however next to every methylene bridge[8] there is a carbon atom associated with a single hydrogen atom and a methyl group[9] (CH_2-CH-CH_3 monomer, i.e., C_3H_6 - see figure 4.6) giving an overall molar mass of 42.08 g/mol. In addition to the above mentioned base structures these polymers can contain small amounts of double bonds, e.g., vinylene groups[10], as well as terminal groups, e.g., methyl or vinyl.[11].

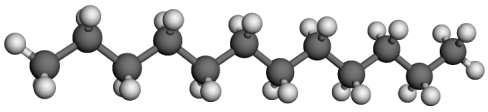

Figure 4.5: Polyethylene $(CH_2)_n$

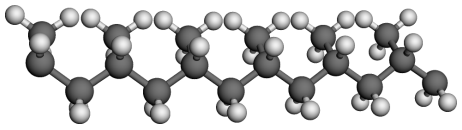

Figure 4.6: Polypropylene $(CH_2\text{-}CH\text{-}CH_3)_m$

The arrangement of the long molecular chains can be amorphous, where the chains are random and unoriented, or crystalline, where the chains are folded and packed. Most polymers are however semi-crystalline in which crystalline structures are dispersed within the amorphous regions. This will be explained in more detail in chapter 5, but generally the amorphous regions give polymers their elasticity, whereas the crystalline regions give them strength and rigidity. PE and PP are thermoplastics, meaning that no chemical bonding occurs between the chains and when heated the chains move freely and can flow, i.e., melt. A certain amount of branching is typical in polymers, i.e., a single chain can separate into Y- and X-like structures, resulting in an interconnecting crossed network rather than individual chains. The form stability of the materials can actually be increased by increasing the branching of the material by the linking of adjacent chains. This process has been applied in the industrial production for decades and is termed “cross-linking” and is achieved chemically but also by irradiation.

[8] A methylene bridge is the -CH_2- part of a molecule.
[9] A methyl group is the molecular group -CH_3.
[10] A vinylene group contains an unsaturated bond within the molecular structure -CH=CH-.
[11] The vinyl end group consists of an unsaturated double bond between the last two carbon atoms in the molecule -CH=CH_2.

In this study irradiations were conducted and subsequently the polarisation effects were measured and, based on these results, certain parameters of the irradiation process were altered for optimization. The different experimental setups influenced the choice of base material and the geometrical form of the target materials. For the initial proton beam irradiations it was necessary to use foil material: The PP foils used were bought from the distributor *Goodfellow GmbH*. [78]. Subsequent electron beam irradiations allowed the use of pelleted materials: In addition to the PP material the scope of the study was extended to include PE materials. The pelleted materials were purchased from the company *Sigma-Aldrich Chemie GmbH*. [79].

For the electron irradiations three different types of PE were used, which essentially are classified by their varying densities and branching behaviour. PE is one of the only commercially available polymers that can be produced over a wide density range (0.912 g/cm^3 to 0.975 g/cm^3), where most polymers have a constant density. The samples consisted of a highly amorphous, low density PE (LDPE, ρ = 0.925 g/cm^3) with lots of branching. This was the first type of PE manufactured and first synthesised in the 1930s by exposing ethylene gas to extremely high pressures and temperatures. The development of new catalyst techniques in the mid 1950s allowed a greater control of how PE chains grew from nucleation. This led to higher density materials with far fewer branches and a high amount of linearly arranged chains. A typical high density material (HDPE, ρ = 0.95 g/cm^3) was used as our second material. Once again it was another catalyst discovery in the 1980s that gave the next progression in the development of PE materials. The new catalysts allowed greater control over the molecular chain length and frequency of the branches. The third choice was a material out of this category, a linear low density PE (LLDPE, ρ = 0.918 g/cm^3) with a high amount of small-branching material interspersed with small crystalline regions.

All PP samples have the same density ρ = 0.9 g/cm^3 and PP is differentiated by its stereo-regularity, i.e., the relative orientation of the CH_2 and CH-CH_3 groups. The three stereo-isomeric positions are isotactic, sydiotactic and atactic, meaning that all the CH_3 groups are either on the same side of the chain, alternating or random, respectively. Isotactic PP makes up by far the bulk of the commercially produced PP, with a crystallinity typically between that of LDPE and HDPE. All samples materials of PP were of this type. Unfortunately the molecular weight of the foils for the proton irradiations was not provided by the distributor, however for the electron beam irradiations three materials of varying molecular weight were used. The average molecular weights of the samples was given as 12×10^3, 250×10^3 and 580×10^3. For simplification these substances will be referred to as PP12, PP250 and PP580.

4.4 Figure of merit

The measurement of double polarisation observables in scattering experiments relies on the determination of a counting rate asymmetry:

$$A_Z = \frac{N_\uparrow - N_\downarrow}{N_\uparrow + N_\downarrow} \tag{4.1}$$

where $N_\uparrow$ and $N_\downarrow$ are the counting rates corresponding to the orientation of the target polarisation. To deduce a physical quality from the measurement one has to take into account that one does not have a perfect target material or a perfectly polarised beam. From this it follows that the physical counting rate asymmetry can be given by:

$$A = \frac{1}{f \cdot P_T \cdot P_B} \cdot A_Z \tag{4.2}$$

where P_B and P_T are the polarisation of the beam and target, respectively, and f is the dilution factor of the target material. If we consider the statistical error for at setup in which the polarisation of target and beam, as well as the dilution factor, are determined to a high level of accuracy, then the error in the physical asymmetry is dominated by the error in the counting rate asymmetry, which for small asymmetries can be simplified [80]:

$$\Delta A \approx \frac{1}{f \cdot P_T \cdot P_B} \cdot \Delta A_Z \approx \frac{1}{f \cdot P_T \cdot P_B} \cdot \frac{1}{\sqrt{N_\uparrow + N_\downarrow}}. \tag{4.3}$$

As the total counting rate $N = N_\uparrow + N_\downarrow$ is proportional to the running time and the effective density of the target material ($N \propto \rho_{\text{eff}} t$), it follows that the time needed to acquire a precision ΔA of the physical asymmetry is then proportional to target material specific characteristics:

$$t \propto \frac{1}{\rho \cdot \kappa \cdot f^2 \cdot P_T^2} = \frac{1}{\text{FOM}} \tag{4.4}$$

with the target material density ρ, the filling factor of the target container κ, and the target material specific figure of merit FOM. The conclusion is that the quality statement of a scattering experiment is highly dependent on the quality of the target material, as defined by the FOM. In the search for new target materials the criteria is thus an improvement of this parameter.

Equation 4.4 shows the importance of the target material characteristics for polarised scattering experiments, especially of the dilution factor and the target polarisation due to their quadratic relation in the equation. For the full evaluation of the scattering asymmetry the density, filling factor and dilution factor must be determined, in addition to the maximum polarisation values. This means that for any new material the maximum possible polarisation must first be determined. Though in many cases the improvement in the individual characteristics of the FOM for PE/PP in comparison to butanol is only slight, the product of the contributions would give a noteworthy overall improvement. These characteristics will now be discussed.

Dilution factor f:

The dilution factor of a material is defined as the weighted ratio of polarisable nuclei of a substance to the total amount nuclei of the same substance. In terms of proton polarisations this is simply the amount of free protons, i.e., hydrogen atoms, in the material divided by the total amount of neutrons and protons of the material. For butanol (C_4H_9OH) this is then simply:

$$f_{\text{but}} = \frac{10}{1\times10+12\times4+16\times1} = \frac{10}{74} = 13.5\%$$

and for PE (CH_2) and PP (CH_2CHCH_3) this calculates to:

$$f_{\text{PP/PE}} = \frac{2}{1\times2+12\times1} = \frac{6}{1\times6+12\times3} = \frac{2}{14} = 14.3\%.$$

Providing all other relevant factors stay the same, and regarding the quadratic nature of the dilution factor on the FOM, this still represents an improvement of over 10% for PE/PP in comparison to butanol.

Density ρ:

Particle physics experiments with solid state polarised targets are conducted at very low temperatures, typically <1 K, for which the densities of the substances are rarely known and at best approximations can be made. In chemically doped materials the fraction by mass of the introduced radical is so low that it can be neglected in further calculations and only the density of the solvent needs to be determined. Butanol has a density of 0.81 g/cm^3 at room temperature and for the case of the typical butanol target mixture of 95% butanol and 5% water the density at a low temperature has been measured by the PSI group by gamma-ray attenuation of a target cell as $\rho = 0.94\,\mathrm{g/cm^3}$ [81]. The density measurement was at a temperature of 4 K and not at test conditions of $\sim$ 1 K or experimental conditions of $<$ 200 mK, though realistically one would not expect much change in the density at these temperatures, as the thermal expansion in the range of these temperatures is practically non existent. In addition, it is not chemically possible to consider both contributions to the density independently, as there is no phase separation between the butanol and the water, this means that for a pure butanol target or any other butanol/water combination this value would have to be measured anew.

Comparable results have also been obtained by other groups. Hassaine et al. showed that by the comparison of the refractive index determined by Brillouin scattering at room temperatures and at low temperatures it is also possible to extrapolate the density values to 0 K [82]. For butanol-glasses it has been shown that due to their differing isomeric configurations, there is a slight difference in the maximum density obtained at extremely low temperatures. For the commonly used configuration n-butanol the calculated density at 0 K is ρ=0.951 g/cm^3, which corresponds to an increase in the density of over 17% with regards to the density as determined at room temperature.

It is highly unlikely that a change in the density of the polymers will be of this magnitude, as butanol has a phase change, going from liquid to a solid, whereas the polymers are already solid at room temperature. One of the difficulties of the polymer system is the two phase model, with varying density distributions, as the thermal contraction of each material varies with the ratio of the amorphous and crystalline phases. At room temperatures the density values for the amorphous and crystalline densities for PE samples are $\rho_\mathrm{a} = 0.850\,\mathrm{g/cm^3}$ and $\rho_\mathrm{c} = 1.00\,\mathrm{g/cm^3}$ and for PP $\rho_\mathrm{a} = 0.850\,\mathrm{g/cm^3}$ and $\rho_\mathrm{c} = 0.950\,\mathrm{g/cm^3}$ [83], all of which are at least as high as the room temperature density of butanol.

There is some data on thermal expansion of polymers at low temperatures that can be used to calculate the density change. As expected the measured expansion coefficients for the linear extrapolation from room temperature show a notable difference for the values obtained for varying crystalline content. Perepechko cites results for a highly crystalline sample where the coefficient of expansion was measured as $\alpha = 8.1 \times 10^{-5}\,\mathrm{K^{-1}}$, but also for a highly amorphous sample where the expansion coefficient is given as only $\alpha = 1.34 \times 10^{-6}\,\mathrm{K^{-1}}$ [84]. In their compilation of literature data on the thermal expansion of materials at low temperatures Corruccini and Gniewek did not make any comment on the amorphous content of the listed PE material that was measured, but the relative change of length, of 2.45% at 0 K and 2.44% at 20 K with regards to the length at room temperature, corresponds quite well with the previously mentioned highly crystalline sample [85]. These results suggest that the density of our crystalline polyethylene samples, with a room temperature density of 0.95 g/cm^3, could be as high as 1.023 g/cm^3 at 1 K. If one compares this value with the maximum extrapolated density of butanol at 0 K, then this would still be an improvement of over 7% in the density factor. Though the literature is not as forthcoming with the thermal expansion coefficients of polypropylene at extremely low temperatures, there is certainly reason to believe that the relative density change will be in the same order of magnitude as the values obtained for PE [86].

Filling factor κ:

Typical alcohols targets e.g. butanol, are produced in a manner as to create beads of 2-3 mm diameter. This causes a reduction of the filling factor from unitary, due to the packing ability of the beads, but allows for a very efficient cryogenic cooling. With an increase of the size of the target container the filling factor also increases towards the value of the closest packing of equal spheres, as the loss of closest packing at the rim of the container becomes less prominent for larger volumes. However, realistically the target container is confined by the geometry of the experimental setup. The standard target containers used in the polarised target cryostat in Bonn have a diameter of 20 mm for which a filling factor of no greater than 55% can be achieved, and necessarily the filling distribution is not homogeneous throughout the target container with fluctuations of between 30% and 80%, leading to local density fluctuations throughout the target as a whole [87]. In an ideal setup it would be possible to fill the complete target area with highly polarised material. However, the impinging beam creates localised heating of the material, which locally depolarises the material due to higher relaxation rates at increased temperature. The beam energy must be effectively dissipated away from the target material, entailing adequate thermal coupling to the cryogenic bath.

The proposal is to use a polymer target material in a disc configuration that has been pre-irradiated to create paramagnetic centres for DNP. The ideal configuration, taking the need for cooling by the liquid helium between the discs into consideration, has been calculated [88]: The target geometry would then consist of discs of 2 mm thickness with a spacing of 0.5 mm between them, as illustrated in figure 4.7. A quick calculation shows that this gives us a filling factor of over 80%, which would be a substantial gain over the currently used materials in the standard container.

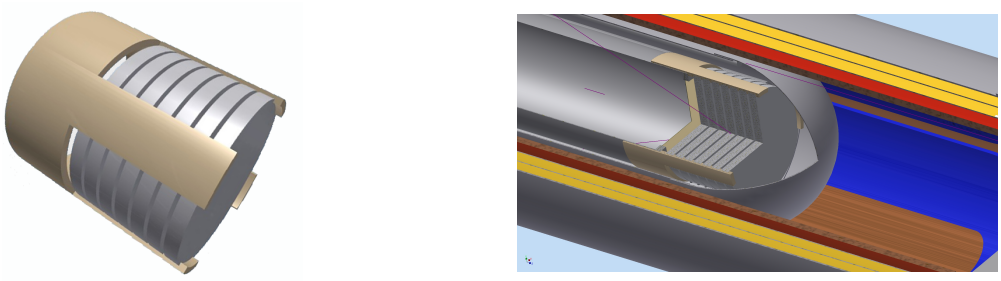

Figure 4.7: Left - polymer disc target composed of discs and spacing allowing for cooling by liquid helium, and right - the target as inserted within the cryostat nose.

Polarisation P_t

The biggest unknown in terms of target material characteristics is the maximum obtainable polarisation value. The major obstacle in making an educated guess is that there is not a prolific reference database to resort to and the polarisation mechanism of the material is not known. As the determination of maximum polarisation values of the polymers is then foremost, a direct comparison of the resulting FOM with that of the standard material would give a good impression of how much of an improvement a polymer may be:

$$P_{\text{poly}} > \sqrt{\frac{\kappa_{\text{but}}\rho_{\text{but}}}{\kappa_{\text{poly}}\rho_{\text{poly}}}} \cdot \frac{f_{\text{but}}}{f_{\text{poly}}} \cdot P_{\text{but}}. \tag{4.5}$$

By this calculation the polymer materials PE and PP must reach polarisation values of at least 80% of that of butanol, before the polymers can be considered as a suitable substitute. The open-ended question of how high the actual polarisation needs to be is dependent on the density, which would be needed to be determined for respective sample materials. For this reason absolute values can't really be set in stone, however we have some boundaries which we can apply. The estimated best and worse case scenarios are plotted in figure 4.8, where the relative improvement of the FOM is plotted against the relative polarisation with regards to the butanol polarisation. We have the lowest density of both the PE and PP samples, which certainly can be used as this sets the absolute lowest limit on the density and would entail no change in density from room temperature to very low temperatures, a proposition though completely unrealistic, could be used to estimate a worst case scenario. The best case scenario is less rigid as it is based on the values calculated and estimated in the density section above.

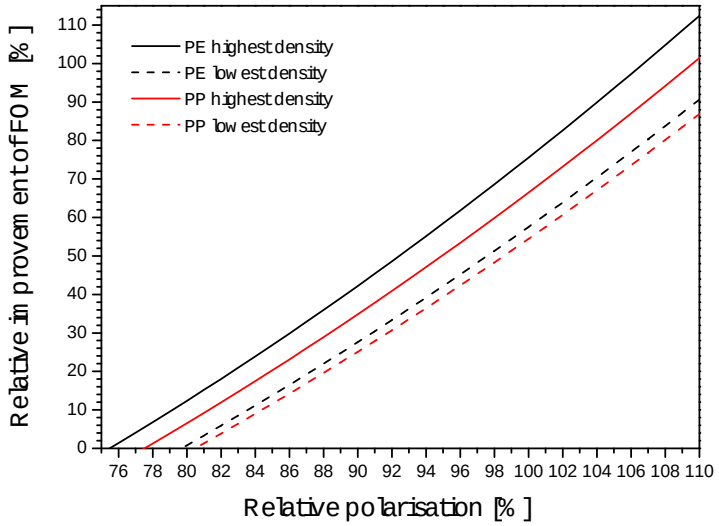

Figure 4.8: Comparison of the relative improvement of the figure of merit (FOM) versus relative polarisation values of PE/PP and butanol.

Additional considerations

Besides the above mentioned factors, that enter directly into the FOM calculation, the polymers do have some other positive characteristics that are worthy of consideration. Though not necessarily a must-have the samples are safe, stable and solid at room temperature, a characteristic that helps with their day to day handling. Another added bonus is that there are only two groups of nuclei in the material, carbon and hydrogen, unlike butanol where oxygen is also present. Whereas the hydrogen is needed for the spin dependent scattering experiments, the carbon nuclei only produce non-spin dependent background events so the polymers PE and PP lack a polarized background. The total cross section for photon scattering on polyethylene is plotted using the NIST XCOM software (see figure 4.9) and it is evident that at higher beam energies, above the creation threshold, the cross section consists predominantly of contributions from electrons/positron pairs created in the pair production process [89]. As the rate of pair production in the field of the nucleus is proportional to the square of the charge of the nucleus, we can consider a weighted ratio of the cross-sections (five carbon atoms in PE/PP for every four carbon atoms and one oxygen atom in butanol) resulting in overall 5% less background events.

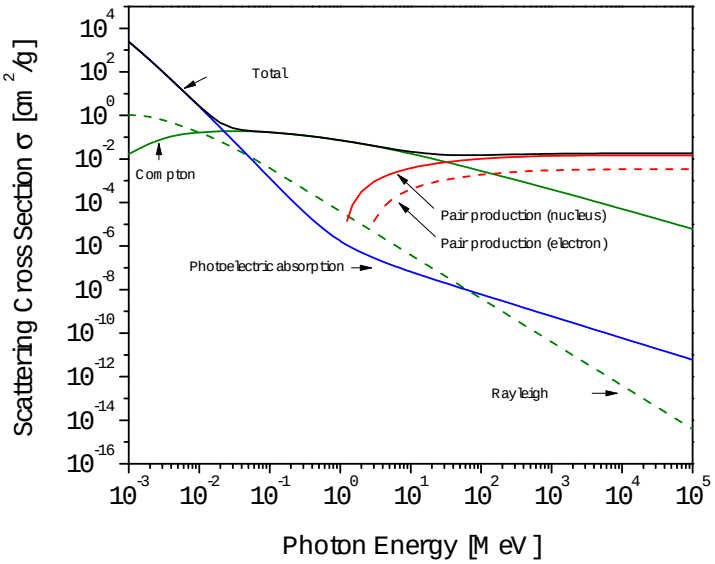

Figure 4.9: Energy dependent scattering cross section of PE with the relevant contributions highlighted.

CHAPTER 5

Crystallinity measurements of polymers

5.1 Motivation

The previous chapter showed that polymer materials are potentially interesting as target materials, due to the material characteristics defined by the FOM. Apart from these polarised target relevant defining traits, polymers exhibit a characteristic called crystallinity. Though this characteristic does not flow directly into the evaluation criteria, many studies show that the crystallinity of a polymer may influence its polarisation characteristics, as will now be discussed. Most properties of polymers are in some way influenced by their crystalline content: These can be characterised as i) mechanical properties, e.g., the hardness and brittleness of polymers increase with the crystallinity, but also make highly crystalline polymers less impact resistant, ii) optical properties, e.g., the increased ability of crystalline polymers to absorb infra-red light, iii) thermal properties, e.g., the melting point behaviour of higher crystalline content is characterised by a shift to higher temperatures as more energy is needed to melt the crystalline regions and even iv) chemical properties, e.g., the solubility of polymers decreases with increased crystallinity and it becomes harder for the solvent to diffuse into the tightly packed crystalline regions of the polymer.

The ability of a material to form a glassy-like (amorphous) state has been suggested as the main reason for an increase of the polarisation capability of many chemically doped target materials: Hill and Krumpolc demonstrated that there was a relation between the glass forming ability in inorganic polar glasses, based on amines, boron hydrides and ammonia, and the polarisation of protons [90], [91], [92]. The same can be said for organic materials. The process of freezing alcohols and diols into a solid state target material at 77 K, after the admixture of a chemical dopant, must be done rapidly to obtain a vitrified solid, as a slow cooling process facilitates the rearrangement of the molecules into crystalline structures. For some radicals it is necessary to add water to help with the solubility, but is in fact also the hindering factor in the ability of the material to form a glass-like state when the water concentration is too high, and has been shown to result in a drop in maximum polarisation values [57]. As the nuclear polarisation in many of the organic, hydrogen-rich materials in use reach higher values when these materials are chemically doped in an amorphous state, much of the research has focussed on the glass-forming ability of these materials [93]. The advantage of polymers is that many are in a glass-like state at room temperature [94], [95].

It has also been shown that for polymer materials the crystallinity of the material can influence the polarisation characteristics of the material. Kumada et al. showed that for two samples of PE, with

varying crystallinity and doped by the diffusion method with TEMPO, different polarization values were reached and indeed higher values were obtained for the lower crystallinity sample [15]. Their ESR studies showed, as one might expect, that the chemical dopant TEMPO was only localised in the amorphous regions of the polymer, as the only part of the polymer accessible for the diffusing radical coincided with the degree of amorphism of the material. But whether or not the crystallinity effects the polarisation if the radicals could indeed permeate the crystalline region, as is the case if the materials are irradiated, is still an open question. The polarising ability of a material does not necessarily coincide with the amorphism of the material in non-chemically doped materials. Irradiated inorganic materials such as ammonia and lithium-hydride reach high polarisation values and are highly crystalline: It is surely the case of having to find the right doping method to optimize the polarising capability of the material.

5.2 Determination of crystallinity

Generally the crystallinity of polymers are not given by the manufacturer/distributor and must be determined independently. Many techniques can be implemented, each based on the determination of a crystallinity dependent property. However, due to the dependence of these techniques on individual properties of the polymer, that could in fact be independent of each other, results from a direct comparison of crystallinities determined by different methods may not agree completely and thus the method of determination should always be given. Nevertheless, the concept of "degree of crystallinity", however measured, has proven very helpful in the comparative studies of polymers and is widely used for polymer classification till this day.

The underlying assumption is that polymers can be described as semi-crystalline. This means that one assumes a polymer is a two-phase structure consisting of a completely ordered region and a completely disordered region, termed the crystalline and amorphous regions, respectively. The ordered regions consist of partially aligned folded chains called lamella which branch out in 3 dimensions from a central nucleus into spoke-like fibrils that make larger spheroidal structures called spherulites [97]. A (60×60) μm cross-section of a spherulite in crystallised PP taken by an atomic force microscope is shown in figure 5.1. The lamellae imperfections and disordered, entangled material between the fibrils make up the amorphous region of the polymer. This description of a polymer may indeed be an oversimplification, e.g., geometrical voids are not considered, however it is generally accepted that the model is consistent with the overall results from crystallinity measurements.

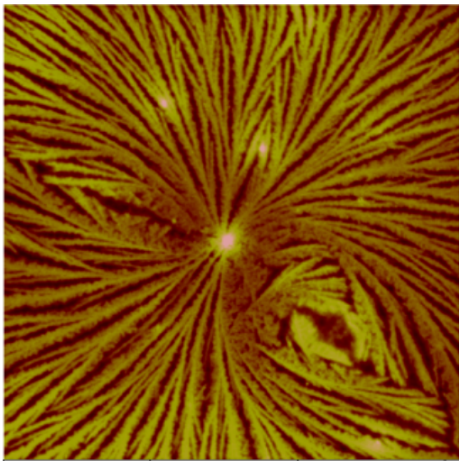

Figure 5.1: Picture of a polymer spherulite in crystalline PP [96].

Due to their production method, commercially available polymers are usually at least partially crystalline with the degree of crystallinity ranging typically from anywhere between (10–90) %. The ability of a polymer to crystallize is highly dependent on its structure: Unbranched linear molecular chains with a high degree of stereoregularity are more likely to crystallize. As an example some polymers, e.g., PP are available in atactic and isotactic form, the latter of which is much more likely to crystallize given the regularity of the methyl side chain; The irregular steric configuration of the methyl group in atactic PP makes it nearly impossible for the material to crystallize. Also, polymers with large side groups

are generally less likely to crystallize. In addition to the general molecular structure of the material intermolecular forces play a role. Strong binding due to intermolecular forces help hold the lamellae together and facilitates the crystallisation process.

Crystallisation can occur in the production process when cooling from the melt. Above the melting temperature T_m the long molecular chains of a polymer are unordered and entangled. Quick cooling (quenching) can leave a polymer in this state and the result is a highly amorphous polymer. Slow cooling of some polymers can facilitate the rearrangement of the molecular chains resulting in a highly crystalline polymer. Another way to make polymers crystallize is to evaporate them from solvents. As the solvent dissolves and the polymer concentration increases, the interaction between the chains also increases facilitating the crystallisation process. This is one of the biggest problems in chemical doping when attempting to mix radicals into polymers by simultaneous dissolution in a common solvent. The subsequent evaporation of the solvent is a slow process and if the polymer has a tendency to crystallise, this can then push the radical out of the polymer structure forming clusters, i.e., a local concentration of the radical, when ideally one would aim to achieve a homogeneous distribution of the radicals throughout the material.

For the crystallinity determination of our samples we used the DSC method, which will be detailed in the next section, however other methods are also popular. The following is a small selection of some of the more typical experimental methods [98], [99]:

5.2.1 Density measurements

The two phase description of a polymer implies that a specific weight and volume can be ascribed to the amorphous and to the crystalline parts, which in turns means that a density can be given for each of the regions. The density of the completely crystalline region ρ_c is greater than the completely amorphous density ρ_a due to the greater packing density of the chains. The weights and volumes of the regions have additivity and with the overall density ρ of the polymer the weight fraction degree of crystallinity can then be given by:

$$X_c = \frac{1/\rho_a - 1/\rho}{1/\rho_a - 1/\rho_c}. \tag{5.1}$$

The density measurement provides a simple and convenient way to determine crystallinity. Values for the amorphous and crystalline densities can be found in the literature, e.g., for PE samples $\rho_a = 0.850\,\mathrm{g/cm^3}$ and $\rho_c = 1.00\,\mathrm{g/cm^3}$ and for PP $\rho_a = 0.850\,\mathrm{g/cm^3}$ and $\rho_c = 0.95\,\mathrm{g/cm^3}$ [83].

5.2.2 X-ray diffraction

The method is based on the analysis of the angle dependent intensity distribution of Bragg peaks by x-ray scattering. The regular arrangement of atoms in the crystalline region of a polymer acts like a diffraction grating and produces sharp diffraction peaks, whereas the amorphous region gives a broad background distribution called a halo. With the spacing of the crystal planes given as d and the diffraction angle given as θ the Bragg equation is written as:

$$\lambda = 2d \cdot \sin\theta. \tag{5.2}$$

Wide angle x-ray scattering (WAXS) patterns are usually given in plots of intensity versus the opening angle 2θ and the degree of crystallinity can be calculated by the fitting and subsequent integration of the

diffraction peaks and the halo. With the total integrated area of the crystalline peaks being A_c and the integrated area of the halo A_a the degree of crystallinity can be calculated by:

$$X_c = \frac{A_c}{A_c + A_a} \tag{5.3}$$

Simple simulated WAXs spectra for a crystalline (X_c=60%) and amorphous (X_c=10%) sample are given in figure 5.2, showing (in black) the peaks from the scattering on the two planes a and b and (in red) the total intensity distribution.

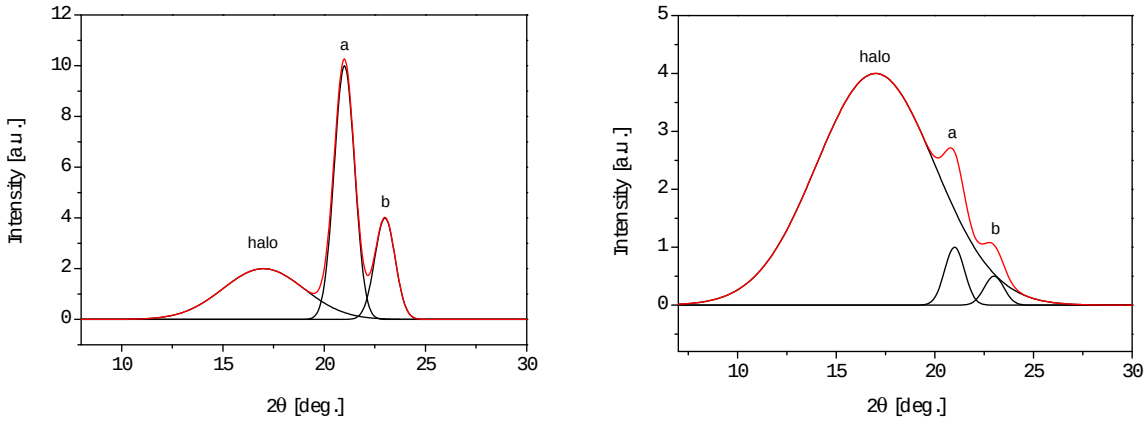

Figure 5.2: Examples of WAXS profiles for a crystalline polymer (left) and an amorphous polymer (right).

5.2.3 Infrared spectroscopy

The infrared absorption spectra obtained from crystalline materials contains all peaks seen in the amorphous material with extra peaks arising from deformational vibrations of the crystal lattice. The optical density of the material in a specific band is assumed to be proportional to the weight fraction of the absorbing material and thus the mass extinction coefficient of a material has a definitive relation to the crystallinity of that material, where the mass extinction coefficient is given by

$$\epsilon(\lambda) = \frac{1}{\rho d} \ln\left(\frac{I}{I_0}\right) \tag{5.4}$$

with ρ being the density of the material with thickness d and the ratio I/I_0 being the absorption at the specified wavelength λ. An obvious restriction in the application of this method is the need to use very thin materials. In addition the extrapolated values for the absorption of the amorphous and crystalline regions must be known. Depending on whether the absorption is measured at the wavelength corresponding to an amorphous or crystalline peak, the crystallinity can be calculated by

$$X_c = \frac{\epsilon_c(\lambda)}{\bar{\epsilon}_c(\lambda)} \qquad \text{or} \qquad 1 - X_c = \frac{\epsilon_a(\lambda)}{\bar{\epsilon}_a(\lambda)} \tag{5.5}$$

where $\epsilon_{a,c}$ are the measured mass extinction coefficients for the amorphous and crystalline regions and $\bar{\epsilon}_{a,c}$ are the mass extinction coefficients at wavelengths corresponding solely to the amorphous and crystalline states.

5.3 Differential scanning calorimetry

5.3.1 The DSC measurement principle

PE and PP are thermoplastics, meaning the application of heat leads to a softening and eventual melt of the polymers. After cooling and recrystallisation the polymers regain their original rigidity. A DSC measures the energy transferred to or from a sample in a heating process to examine changes in the thermal physical properties of the sample material. The heating chamber contains two sealed aluminium crucibles, one which contains the sample material and the other either left empty or containing a reference sample used for calibration. During the measuring process the heat input into the two crucibles is regulated separately as to maintain the sample and reference pan at the same temperature. The difference of energy that is supplied to the pans is then measured and gives the absorbed (or evolved) energy of the sample. A thermogram of the process recorded versus time (or equivalently against temperature) can then be used to evaluate the changes in the thermal properties of the material.

The measurement of the polymer crystallinity was conducted in the laboratory of Prof. Dr. S. Höger at the Institute for Organic Chemistry in Bonn with the kind assistance of Dr. J. Vollmeyer. The DSC used for the experiment was a DSC823^e with a HSS7 sensor from the company *Mettler Toledo* [100].

5.3.2 Measurement and evaluation

The sample was initially maintained at approximately 300 K for 5 min to ensure a stable initial temperature. Thereafter the temperature was increased at a rate of 10 K/min to the maximum temperature of 440 K for PE and 470 K for the PP samples. The maximum temperatures were chosen as they are at least 30 K over the estimated melting peaks of the samples, as given by the distributor, and warrant a complete melting of the crystalline structure in addition to providing enough data points after the melting peak for a decent baseline fit of the heat transfer curve. After a 5 min stability period at maximum temperature the crucibles were then cooled with a regulated liquid nitrogen flow at the same rate as the heating cycle. The heating compartment is also flooded with nitrogen as to eradicate oxygen based processes such as degradation.

Some preliminary tests were made to find the ideal sample size. In the initial cycles, after the removal of the sample pan, it was evident that the larger samples were not completely melted and thus the thermogram did not represent the homogeneous heat transfer into the sample. Following the measurement of samples of varying size and weight, it was concluded that a shaved sample of approximately 5 mg gave the best results with regards to the sample melt and the shape of the thermogram. Theoretically the melting of a monocrystalline structure would give a sharp melting peak in a thermogram, as the energy associated with melting the crystals is the same throughout the whole material. However, polymers are highly inhomogeneous with regards to the molecular chain length and one would then expect broadening of the peak structure as each molecular chain length corresponds to different melting temperature. The amorphous region on the other hand should produce a broader background structure underlying the overall thermogram over the complete range of the measurement. If one considers the crystalline and amorphous parts of the polymer independently with individual specific heat capacities $C = \mathrm{d}H/\mathrm{d}T$ one can define a percentage crystallinity:

$$X_\mathrm{c} = \frac{\Delta H_\mathrm{m}}{\Delta H_{100\%}} \times 100\% \tag{5.6}$$

where ΔH_m is the measured enthalpy of fusion and $\Delta H_{100\%}$ is the enthalpy of fusion for a sample which is 100% crystalline. ΔH_m is the heat associated with melting the crystalline structures present in

the polymer. The heat of fusion of 100% crystalline PE and PP are given by the ATHAS database as 293 J/g (or 4.11 KJ/mol) and 207 J/g (or 8.70 kJ/mol), respectively [95]. Using the thermograms of the polymer samples and integrating over the area of the total peak with a suitable baseline subtraction, as described by Gray [101], one can then obtain the crystallinity of the polymer using equation 5.6. The integrated peak represents the energy per gramme needed to melt the crystalline region, whereas the area between the extrapolated baseline and the y=0 line is the energy per gramme needed to melt the amorphous region.

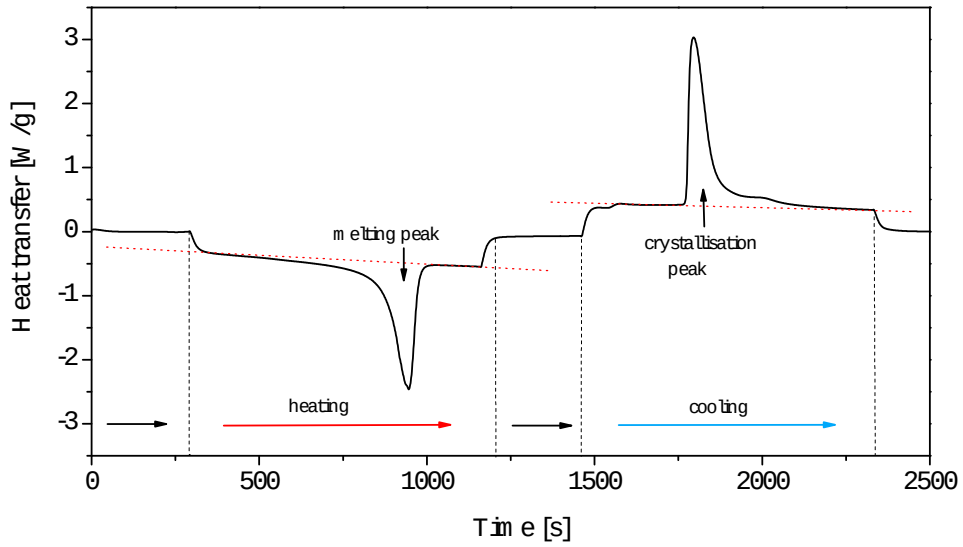

Figure 5.3: A typical DSC cycle, containing from left to right, a temperature stabilisation period, a heating period, a constant temperature period and a cooling period.

The typical form of a heat cycle thermogram showing the heat transfer versus time is shown in figure 5.3 with the red arrow indicating the heating period, the blue arrow the cooling period and the black arrows the period where the temperature is maintained at a constant value. For our purpose, the two most relevant thermal processes that can be seen on the thermogram are the endothermic melting peak in the heating part of the cycle and the exothermic re-crystallisation peak in the cooling part of the cycle, each separated from the amorphous contribution by the red dotted line representing the baseline for each peak. The clear slope of the baseline arises from the temperature dependent change in the heat capacity of the amorphous contribution.

The heating and cooling portions of the cycles, with the baseline subtracted, showing the melting peaks of the samples of PE and PP are given in figure 5.4 and the crystallisation in figure 5.5. The melting point of LLDPE was between that of LDPE and HDPE, though one might expect that the lower density of the sample would give a lower melting point. But, as one can see in the cooling cycle, the crystallisation thermogram is a mirror of the heating cycle in the tendency that the HDPE has the highest melting point, but also crystallises at a higher temperature and LDPE melts at a lower temperature, but also crystallises at a lower temperature, allowing the valid interpretation that the melting and crystallisation point of the sample is highly material specific. Another interesting point is that in the PP12 samples there are two overlapping melting peaks, but on crystallisation only one can be identified. On remelting the sample the two peaks are once again present, showing that the melt is a two phase process.

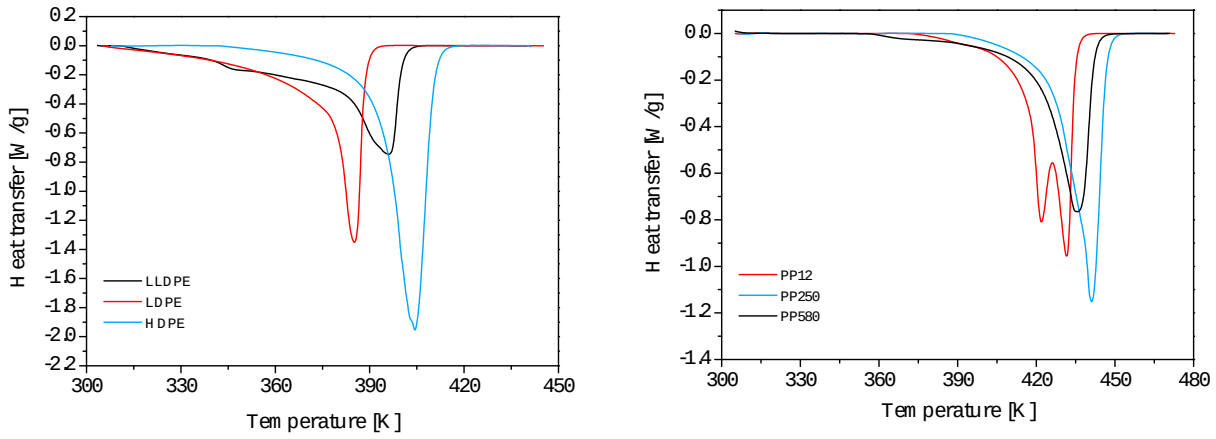

Figure 5.4: The heat transfer into the PE (left) and PP (right) samples in dependence of the temperature due to the melt.

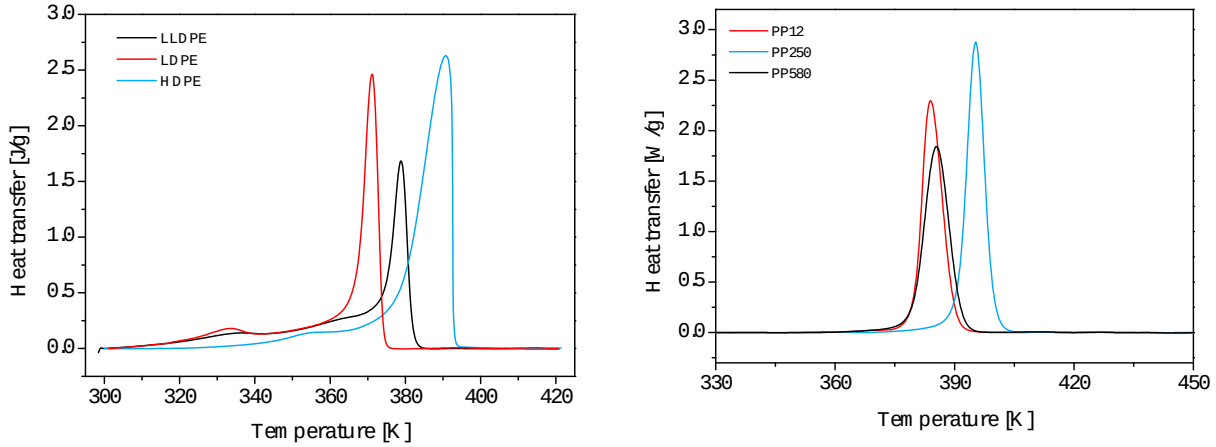

Figure 5.5: The heat transfer out of the PE (left) and PP (right) samples in dependence of the temperature due to crystallisation.

The figure 5.6 shows that the relationship of the density and the crystallinity is most certainly nearly linear for PE, as reported in the literature [102]. The explanation is as follows: In the kinetics of the crystallisation processes two parameters are important: First, the density of the nucleation centres (i.e., how many spherulites are formed) and second, the growth-rate of nucleation centres. It has been shown that the amount of centres is proportional to the molecular weight in polyethylene whilst the crystallisation-growth rate is constant [103]. No such direct correlation could be found for the molecular weight of our PP samples: Natta et al. suggested that the crystallinity of PP is dependent on the tacticity and steric regularity of the polymer [104]. They found that the crystallinity of PP increases as the molecular weight decreases, down to molecular weights of approximately 1000. Figure 5.7 clearly shows a drop in crystallinity with increasing molecular weight of PP, though the dotted red line is not a fit of any kind but just placed for visual reference. One thing that is quite noticeable is that the variation of the crystallinity in the PP samples is quite small in comparison to the PE samples. Where the scope of crystallinity for the PE samples goes from ~35% to ~70%, approximately doubling the crystallinity,

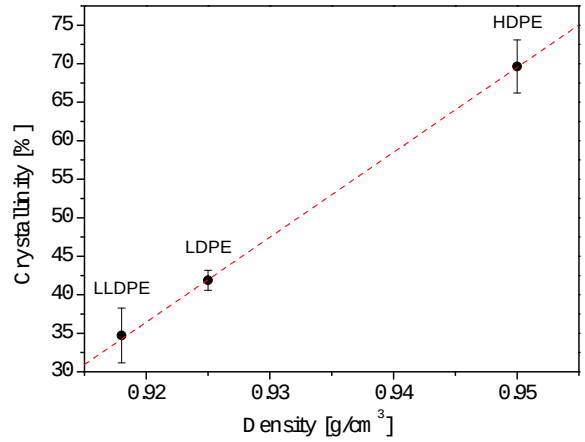

Figure 5.6: The relationship of the density and the crystallinity of the PE samples.

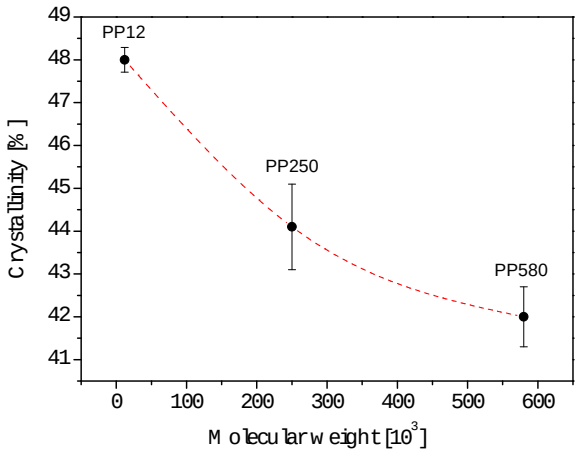

Figure 5.7: The relationship of the molecular weight and the crystallinity of the PP samples.

the PP samples have a much more limited crystallinity with a range of only ~6%. Though no values are given for the PE samples the density of PE increases with molecular weight and thus the general correlation of molecular weight to density is certainly given. If the crystallinity were to influence the polarisation characteristics of these polymers, one might expect that the effect, as measured by the differences of polarisation characteristics within the material grouping, would be more pronounced in the PE materials than in the PP materials.

CHAPTER 6

Irradiation

If one wishes to use the methods of DNP to polarise test materials, as described in chapter 3, then paramagnetic centres must be present within the materials, as it is these that can be highly polarised and are needed for the polarisation transfer to the nuclei. As polymer materials are not paramagnetic themselves, these centres must first be introduced into the materials. The method of choice in this study is the irradiation, where the interaction of the polymer medium with the projectile creates paramagnetic centres in the form of structural defects, e.g., by the breaking of chemical bonds. In this chapter the interaction of the beam with the polymer medium will be shortly described, starting from the general introduction to the interaction of particles with matter and later detailing the specific interaction of protons and electrons with polymer materials and the distribution of the interactional centres within the material. In the last part of the chapter the setups of the conducted experiments will be presented, detailing the individual irradiation facilities and the involved procedures. The irradiations are split into three separate programmes, each focussing on different irradiation aspects, starting with a heavy particle irradiation by protons at a temperature of 120 K, followed by the low temperature electron beam irradiations in liquid argon and finishing with the electron beam irradiations at temperatures between 140 K and 230 K in helium gas. The results of the spin density determinations resulting from these irradiations will be presented in chapter 8, including information on the types of structural defects that are created, with the analysis of the polarisation characteristics then following in chapter 10. The grouping of the results by the analytical methods instead of by irradiation programmes allows a direct and easier comparison of the relevant parameters.

6.1 Interaction of particles with matter

When particle beams are incident on materials an interaction between the beam and the material takes place, resulting in the loss of energy from the beam projectile. For the projectile the energy loss can be either radiative, e.g., when the charged particle beam is deflected by the field of the scattering nucleus resulting in the emission of photons, or collisional, when the electronic interaction between a charged projectile and shell electrons of the absorber materials cause ionisation, or atomic or collective excitation.

The collisional stopping power of a single element material is based on the theory developed by Bethe and Bloch in the early 1930s [105], [106], [107]. Later modifications to the theory, extending the stopping power to wider energy ranges, included shell and density corrections. Shell corrections arise

due to the interaction of the projectile with the shell electrons of the atom and are especially important at lower projectile energies, when the velocity of the projectile is low in comparison to the velocities of the bound electrons, and for heavy particles such as protons, due to their higher cross-sections [108]. The density-effect correction is relevant at the other end of the energy scale and is a relativistic effect first introduced by Fermi in the 1940s [109]. The density-effect term corrects for polarisation effects of the medium, where the stopping power is reduced as the projectiles electromagnetic field is reduced by the dielectric constant of the target medium. The effect changes the logarithmic rise of the stopping power from $\sim\ln(\beta^2\gamma^2)$ to $\sim\ln(\beta\gamma)$, leading to a flattening of the overall stopping power curve at higher energies. As the name implies the effect is dependent on the electron density of the material and thus varies for different elements, but is well documented by the literature [110],[111].

The Particle Data Group [112] gives the "Bethe-Bloch" equation in its currently accepted form as

$$-\frac{\mathrm{d}E}{\mathrm{d}x} = K \cdot z^2 \cdot \frac{Z}{A} \cdot \frac{1}{\beta^2} \cdot \left[\frac{1}{2}\ln\left(\frac{2m_\mathrm{e}c^2\beta^2\gamma^2 W_\mathrm{max}}{I^2}\right) - \beta^2 - \frac{\delta(\beta\gamma)}{2} - \frac{C}{Z}\right] \tag{6.1}$$

with

$K = 4\pi N_\mathrm{A} r_\mathrm{e}^2 m_\mathrm{e}^2$

N_A : Avogadro number 6.022×10^{23} mol^{-1}

r_e : classical electron radius 2.817×10^{-13} cm

m_e : electron mass

z : charge of projectile

Z : atomic number of absorbing material

A : atomic mass of absorbing material

$\beta = v/c$ velocity of the incident particle

I : mean excitation potential

δ : density correction

C : shell correction

where W_max is the maximum kinetic energy that can be transferred to a free electron in a single collision from an incident particle of mass M:

$$W_\mathrm{max} = \frac{2m_\mathrm{e}c^2\beta^2\gamma^2}{1 + \frac{2\gamma m_\mathrm{e}}{M} + \left(\frac{m_\mathrm{e}}{M}\right)^2}. \tag{6.2}$$

At high energies radiative effects become more important as charged particles permeate further into the field of the nucleus, resulting in energy loss by the direct emission of bremsstrahlung. For particle energies where radiative energy losses become dominant it is customary to introduce a scaling factor called the radiation length X_0 for the energy loss by length unit, similar to the intensity dependence of absorbed light when passing through a dense medium. The stopping power can then be written as

$$\left(\frac{\mathrm{d}E}{\mathrm{d}x}\right) = -\frac{E}{X_0} \qquad \rightarrow \qquad E = E_0 \exp\left(-\frac{x}{X_0}\right) \tag{6.3}$$

with the radiation length given by Jackson [113] as:

$$X_0 = \left(4N\frac{Z(Z+1)e^2}{\hbar c}\left(\frac{z^2e^2}{Mc^2}\right)^2 \ln\left(\frac{233M}{Z^{1/3}m_\mathrm{e}}\right)\right)^{-1} \tag{6.4}$$

where N is the volumetric number density of the scattering atoms. Evidently radiation losses are more important for electrons than for protons, as the radiative stopping power is suppressed by the factor m_e/m_p. However, due to the z^4 dependence, radiative losses become more important for highly

charged ions. Though it is possible to derive the radiation lengths theoretically, the radiation lengths for most elements have also been determined experimentally. A summary of these values for the radiation length (among other atomic and nuclear properties) can be found on the PDG website maintained by D. Groom [114].

So far the stopping powers have only been considered for materials containing one type of atom, however, methods exist that allow the calculation of the stopping power for composite systems. A good approximation for the stopping power for molecular compounds, like the polymers, is given by the application of Bragg's rule [115], where the contributions of each element to the total stopping power are weighted by the mass of the individual elements, so that the weighting is given by $w_i = a_i \frac{A_i}{A_m}$, with a_i, the number of atoms in the compound with atomic weight A_i, and total atomic weight of the compound of $A_m = \Sigma a_i A_i$:

$$\frac{1}{\rho}\frac{\mathrm{d}E}{\mathrm{d}x} = \frac{w_1}{\rho_1}\left(\frac{\mathrm{d}E}{\mathrm{d}x}\right)_1 + \frac{w_2}{\rho_2}\left(\frac{\mathrm{d}E}{\mathrm{d}x}\right)_2 . \tag{6.5}$$

For PE and PP the hydrogen and carbon contributions are then weighted by 0.143711 to 0.856289. The Bragg equation in its original form gives results that are quite accurate, however studies into various irradiated hydrocarbons have shown some discrepancies [116]. The reason for this is that the model does not take chemical bonding and phase effects into account, but these play a role as the energy loss of the electrons is dependent on the orbital and excitation structure of the atoms, which differ for free atoms and bound systems like molecules. The core and bond approach details how the "core" stopping power calculated by equation 6.5 can then be modified to incorporate the electronic bonding effects [117]. The differences in free, single or multi-bond systems can then be calculated by the use of correctional terms given in the literature [118].

Software exists that includes all the above mentioned factors and allows the stopping power calculation for arbitrary materials. The National Institute of Standards and Technology (NIST) provides the stopping power software ESTAR, for electrons, and PSTAR, for protons [119]. As PE and PP consist of the same weighting of elements the stopping power calculation gives the same results for both materials. To obtain the true stopping power the results must then be multiplied by the density of the material, which then give slight differences for the chosen polymeric materials of no more than 5%. The results of the stopping power calculations are presented in figure 6.1.

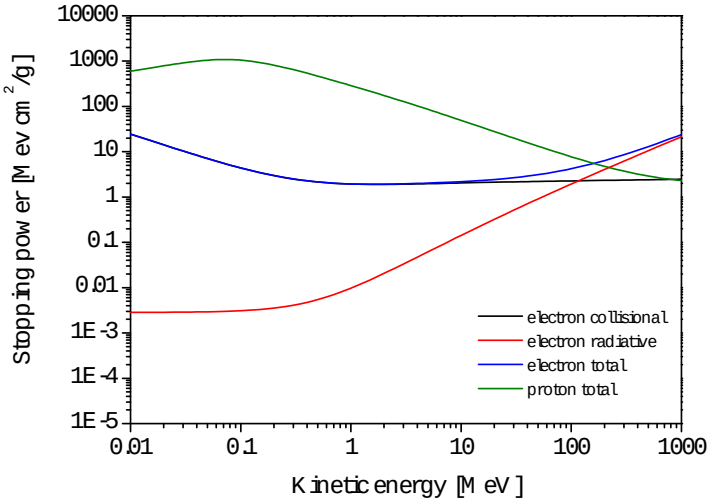

Figure 6.1: Collisional, radiative and total stopping power for incident electrons and protons on PE/PP.

In the region of energy of our irradiations of approximately 20 MeV the stopping power of the protons is 10x higher than for electrons. The proton curve is collisional over the whole range, whereas for electrons one can clearly see the dominance of radiative contributions to higher energies, though contributing just under 10% of the total energy loss at 20 MeV. At this energy, as with the proton, the electron also loses its energy mainly due to collisional losses.

6.2 Radiation chemistry of spurs in polymers

Extensive research with a wide variety of beam types has shown that the irradiation of low molecular weight hydrocarbons leads to similar results in terms of the structural defects that are created, regardless of whether the irradiation consists of γ-beams, electrons, deuterons or even higher weight particles [120], the difference being only the projectile dependent radical yields within the particular materials. The reason is that the energy of the incoming beam is initially transferred to only a minor number of individual molecules and then locally distributed through the bulk of the material, so that the general effect on the molecular structure is governed by the lower energy interactions of the secondary, tertiary, and higher order cascading electrons and radiation, caused by the initial interaction.

The deposition of energy in any medium can be separated into two distinct groups, those arising from single- and those from multi-ionization spurs, with spurs being the centres of radiation induced chemical reactions. Irradiating particles react stepwise by inelastic collisions with the medium producing secondary electrons and photons, which then create further ionizations at a greater distance from the initial ionization. The initial ionization is created by a high energy participant and thus the projectile has sufficient energy after collision to travel quite far from the site of the initial ionization. The subsequent ionizations then occur at lower energies and the ionizations are far closer together, creating bundles of reactions called multi-ionization spurs [121]. A consequence of the cascading electrons is the highly statistical nature of the reactions making it impossible to predict a well defined penetration depth from theory, and only averaging over many such reactions gives reproducible results [122]. It has been postulated that in practically all irradiated systems two separate sets of chemistry thus develop, one arising by the higher energy single ionization spurs and the other as a result of multi-ionization spurs. Hence the resulting chemistry of the irradiated system has its origin in two very different processes. The difficulty arises in distinguishing theses two processes by their final states, as they may be quite similar, or even inseparable, therefore a simple product analysis may not be very conclusive.

For γ and electron beams the proportion of multi-ionization spurs in molecules containing light elements, e.g., polymers containing H, C, N, O, F, S and Cl atoms, is very low and makes up less than 20% of the total energy deposited in the material [123]. For particles with a higher linear energy transfer (LET), such as protons and α-particles, the proportion of multi-ionisation spurs increases as the total energy of the projectile is effectively spread over a smaller material volume, due to the reduced range of the particles [124]. In this regard it may be expected that the polarisation characteristics of a proton beam irradiated target material could differ from an electron beam irradiated material, even if the same defects are created in the material, solely by the difference in the distribution of the radical centres within the target material. To highlight this point a schematic is shown in figure 6.2 of possible radical distributions in materials. It is generally assumed that irradiated polarised target materials contain a homogeneous distribution of radical sites created by singular ionisation reactions (shown on the left). A proton interaction on the other hand would create predominantly multi-ionisation spurs with a compact volume of defects (centre), whereas electron beam irradiations of polymers give a large proportion of single-ionisation spurs, creating radical pairs[1] (right).

[1] The pairwise creation of radicals in polymers is explained in section 7.1.1

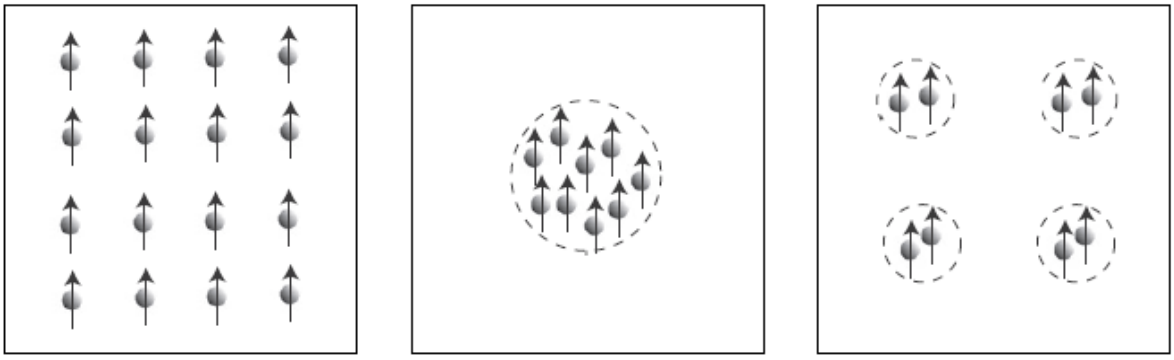

Figure 6.2: The distribution of paramagnetic centres created left) homogeneously, centre) by irradiation with heavy particles and right) in pairs by irradiation with an electron beam. Adapted from Kumada et al. [125].

6.3 Proton beam irradiations at the Cyclotron at HISKP

In the past irradiation with protons have been used to create the structural defects needed for the dynamically obtained high polarisation values in target materials: In the late 1970s at CERN a dose of 0.95×10^{15} protons/cm^2 from the 580 MeV synchro-cyclotron proton beam was used to create an unpaired electron spin density of 5×10^{18} e$^-$/cm^3 in frozen ammonia [67]. Though reaching polarisation values of over 90% ongoing difficulties with explosions and the emerging success of the electron based irradiations in the 1980s in addition to the ongoing success of chemically doped materials overshadowed any positive results obtained by this irradiation method and endeavours in this direction were halted.

As, in principle, the previously mentioned irradiations had shown promising results, it was thought that further investigations of this type were justified. An added merit was the accessibility to a specific facility and a generous grant of ample dedicated beam time. Proton irradiations took place at the Isochronous Cyclotron [126] situated in the Helmholtz-Institut für Strahlen- und Kernphysik of the University of Bonn (a schematic of the experimental area of the cyclotron is given in figure 6.3). To this purpose the protons were channelled from the cyclotron bunker to the irradiation area no. 2 in the so-called "Hochstromraum", literally translated from German as the "high current room". Here polymer materials consisting of PP in the form of foils of 0.18 mm thickness, bought from the distributor *Goodfellow GmbH.* [78] were irradiated with a proton beam of 13.5 MeV energy and at a current of 30 nA to various doses in vacuum.

The beam current can be measured as a charge deposition per unit time on the back of one of the stoppers, consisting of a galvanically isolated carbon disc connected to a charge integrator. This means that the beam can only really be measured in situ as a final current after passage through the target materials. Usually, this does not pose a problem as, especially with this irradiation area, the setup was specifically designed for the irradiation of thin foil materials, through which most of the protons can pass without being deflected. However, it was expected that the radicals created by the interaction of the traversing protons would not be room temperature stable and efforts were made to cool the sample materials: The method by which the samples were cooled did not allow for the beam current to be monitored in a constant fashion. Before the irradiation of the samples the beam current was optimized on the final stopper in the beamline terminating in the vacuum chamber containing the sample. During the irradiation of the polymer foils this stopper was shut for a few seconds and the beam current was checked for stability. Though the lack of continuous monitoring obviously brings a large systematic uncertainty

into the dose calculation at no point during the irradiation did the beam current, when checked, vary so much as to warrant a correction of the beam parameters.

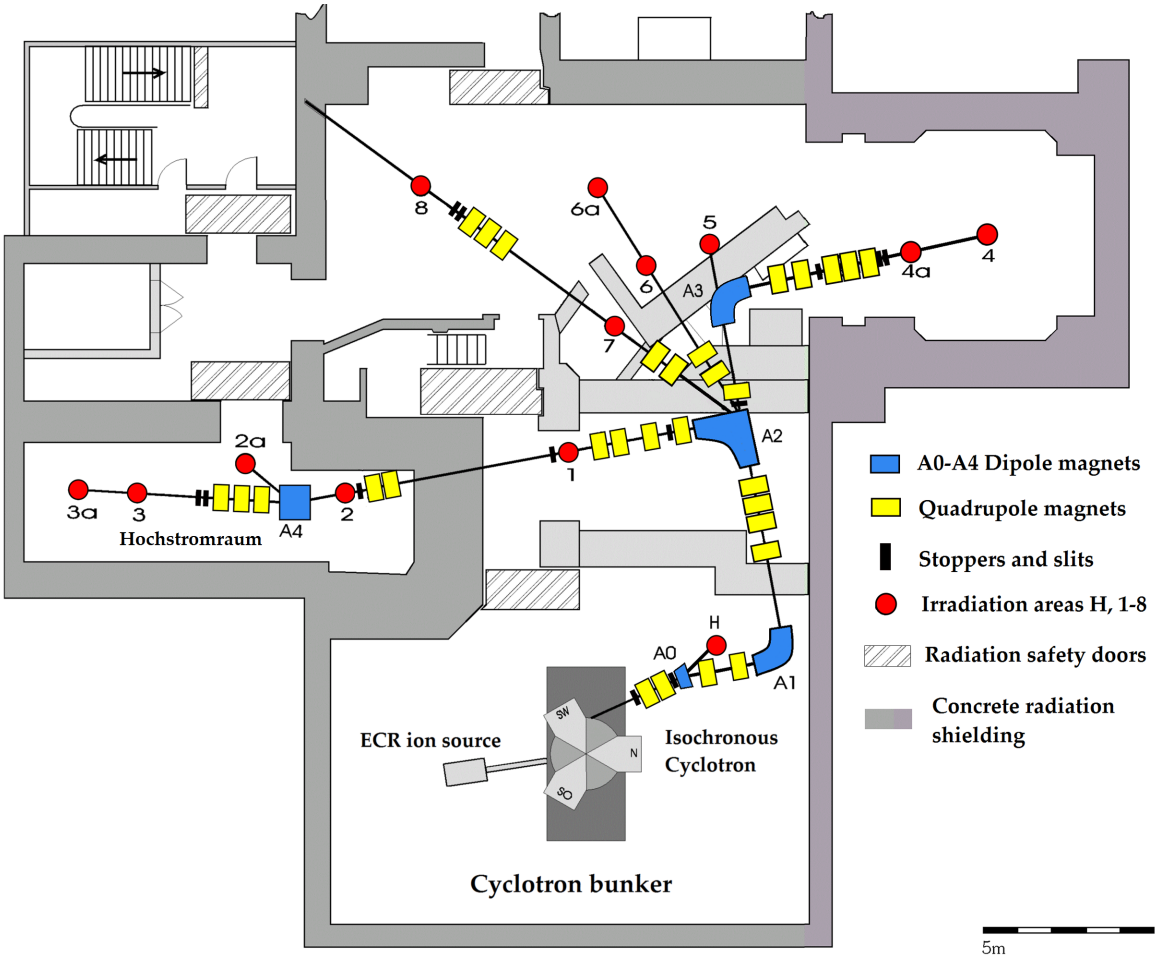

Figure 6.3: The experimental area of the Isocronous Cyclotron at the University of Bonn.

The proton beam was focused and positioned in typical fashion using quadrupole steerers and dipole magnets. The beam alignment and beam forming was judged by the florescence of a europium(III) oxide (Eu_2O_3) dummy target positioned directly in front of the sample material that could move up and down into the beamline. For the beam optimization the beam current was regulated down to a value where the florescence can only just be seen by eye on a CRT display, as the fluorescing material saturates at high currents and no beam "structure" can be resolved on the screen. A possible source of error in the alignment is due to the unknown beam trajectory on the target area, but this error can be greatly reduced by the minimisation of the spacing between the dummy target and the actual target. The problem of the beam focus lies in the positioning of the beam over the sample position. This means minimal beam losses into the aluminium aperture holding the material, when the beam is set to just fill out this aperture, but also in the uniform distribution of the beam over the target area. This error would then be mirrored in a large distribution of the spin densities, as determined by ESR.

The maximum beam current for protons at the facility is 10 µA but could not be fully utilised for the irradiations because of the large heat load on the samples and insufficient cooling power. Initial tests showed that the beam current had to be lower than 50 nA for the sample temperature to be stable

to ±3 K for a 30 min irradiation period. After some initial irradiation tests and ESR measurements of the spin concentration it was decided that irradiations of 10, 20 and 30 minutes should be conducted. For a current of I =30 nA a few brief calculations are given for the base characteristics of the 30 min irradiation: The total incident charge of Q_{tot} can be used to estimate the total amount of incident protons n_{p}, which in turn gives the dose D for the irradiated area of A =1.54 cm^2 (see equations 6.6 to 6.8):

$$Q_{\text{tot}} = I \cdot t = 30 \times 10^{-9}\,\text{A} \cdot 1800\,\text{s} = 54\,\mu\text{C} \tag{6.6}$$

$$n_{\text{p}} = \frac{Q_{\text{tot}}}{\text{e}} = \frac{54 \times 10^{-6}}{1.6 \times 10^{-19}} = 3.4 \times 10^{14} \tag{6.7}$$

$$D = \frac{n_{\text{p}}}{A} = \frac{3.4 \times 10^{14}\,\text{protons}}{1.54\,\text{cm}^2} = 2.2 \times 10^{14}\,\text{protons/cm}^2 \tag{6.8}$$

The power of the beam is given by the proton flux and proton kinetic energy:

$$P = \frac{E_{\text{tot}}}{t} = \frac{n_p \cdot E_p}{t} = 0.4\,\text{W}. \tag{6.9}$$

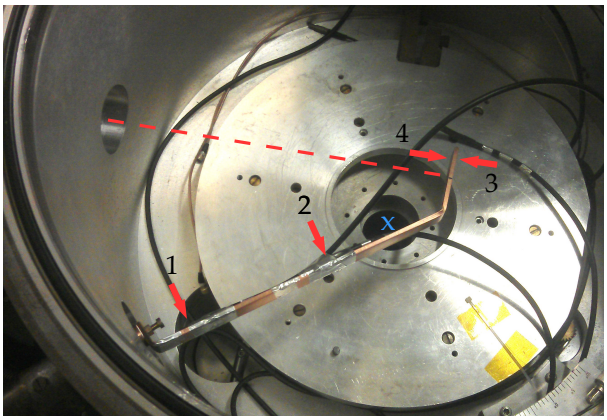

Figure 6.4: Cooling finger in the vacuum chamber for the proton irradiations.

In figure 6.4 one can see the cooling finger in the (opened) vacuum chamber, onto which the polymer samples were mounted. The proton beam enters from the hole in the chamber wall on the top left of the picture. The hole in the centre is the position where the dummy target holder can be moved up into the beamline (indicated by the blue *x*). The sample was mounted by clamping between a thin aluminium aperture of 0.3 mm thickness with a circular opening of 14 mm diameter, and copper cooling finger of 3 mm thickness, which was cooled via thermal conduction by the connection to a 25 l liquid nitrogen bath. The aim was a homogeneous irradiation of the surface area at a stable temperature and with a minimal temperature gradient throughout the whole sample material. To achieve this goal thin foil materials were chosen. The temperature along the cooling finger was measured in four places with PT100 resistors (indicated by the red arrows in the picture): 1) A few centimetres along from the vacuum feed-through, 2) halfway between sample and vacuum feed-through, 3) behind the sample position, slightly off centre as to not be in the beamline, and 4) mounted on the aluminium aperture in front of the sample. As the sample temperature could not be measured directly, the average temperature of positions 3) and 4) was used as the sample temperature and believed to be a good indication of the actual sample temperature. Once beam parameters, sample positioning and cooling was optimized the difference in temperature of both of these positions was negligible. A problem with this irradiation programme was the lack of a regulated irradiation temperature. Nevertheless, the average base temperature of all irradiations, determined as (122 ± 3) K, was very similar in all cases.

The energy specific penetration depth, given by the continuous slowing down approximate range (CSDA range), of protons in PP can be calculated by the National Institute of Standards and Technology (NIST) software PSTAR [119] to 1.936×10^{-1} g/cm^2. This gives a CSDA range of 2.2 mm for a material with the density of PP at 0.9 g/cm^3. The foil thickness was also chosen with this in mind, as one

would like the protons to pass completely through the material, as to eliminate skin effects, i.e., a high degree of radical concentration spread between the surfaces of the polymer. The detour factor (projected range/CSDA) is calculated to 0.9987, so most protons will pass through the foils in a linear fashion. The CSDA range in copper calculates to 0.41 mm, so the greater part of the protons will pass through the polymer material and transfer the rest of their kinetic energy into the copper cooling finger. The additional heat input from the protons has to be compensated by the cooling via the liquid nitrogen to maintain a constant temperature of the sample.

After the irradiation period, we continued cooling the sample materials to stop the recombination of the irradiation induced radicals. The copper finger acts as a beam dump and is activated by the energetic protons. This radioactivity was then diligently monitored, until it dropped below levels deemed safe for the removal of the sample material. On removal of the materials the vacuum chamber was flooded with helium gas and an excess pressure maintained to stop air falling in and freezing on the cooled surfaces, and to hinder contaminating the sample with reactive gases, e.g., oxygen. A small dewar containing liquid nitrogen was placed under the sample holder. After the quick release clamps were opened with a pair of long tongs, the samples and the aperture were dropped into the bath and were removed.

The irradiation of just one foil would not provide ample material for the polarisation measurement and the prior ESR analysis. This is a distinct disadvantage of the irradiation of foils, where a bulk irradiation of many foils simultaneously is not possible. This problem was discussed with my esteemed colleague G. Reicherz from the Ruhr University of Bochum in April 2014 and it was concluded that 100 mg of material should provide enough material for our target holder/NMR-coil setup to provide a large enough NMR signal for the polarisation measurement. As a single irradiation gave approximately 25 mg of irradiated material, this calculated to five irradiations total per sample parameter, four of which are needed as material for the polarisation measurement and one for the ESR measurement. For the complete irradiation programme, including preliminary testing and the dose dependent irradiations this accumulated to over 20 separate irradiations.

6.4 Electron beam irradiations

Initial electron beam irradiations took place at the LINAC1 of the ELSA facility [127] in the Physics Institute of the University of Bonn, followed by irradiations at LINAC2 of the same facility. The linacs are used as pre-accelerators for the booster synchrotron, where over the last years the emphasis has been placed on the use of the LINAC2, due to the implementation of a polarised electron source. A schematic of the linac setup is given in figure 6.5, this includes the dipole magnets (blue), quadrupole magnets (yellow), high frequency resonators (red), the electron sources and a small section of the booster synchrotron in the top right corner with the combined-function magnets (green). All previous irradiations were conducted in the irradiation area associated with the LINAC1. Irradiations using this facility have a long tradition, starting in the early 1980s with the irradiation of ammonia in liquid argon [68], [69]. Following in the polarized target tradition the new proposed direction of polymer irradiations was continued.

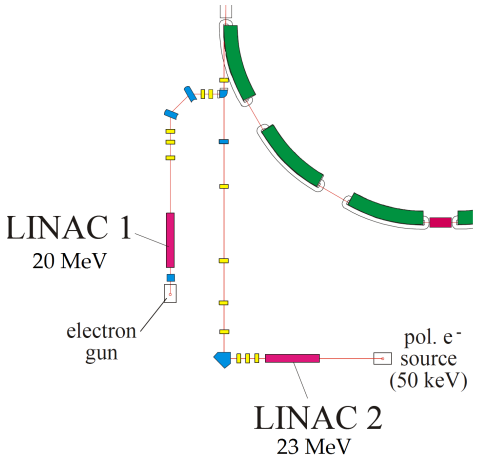

Figure 6.5: Schematic overview of the LINAC1 and LINAC2 setup.

6.4.1 Electron irradiations at LINAC1 - ELSA

A batch of three different types of PP, bought from the distributor *Sigma-Aldrich Chemie GmbH.* [79], in the form of pellets were irradiated with 20 MeV electrons to a dose equivalent to 4.2 mC of total incident charge in liquid argon at a temperature of 87 K. The sample materials consisted of 3 types of isotactic polypropylene, characterised by the difference in their molecular weights M_w. All three materials were simultaneously irradiated in a container consisting of two concentric cyclinders made of 0.25 mm thin aluminium wire mesh with diameters of 64 mm and 30 mm respectively, and a height of 4.5 cm, split into 3 compartments to ensure that all sample materials saw the same incident irradiation. In this manner over 100 cm^3 of sample material can be prepared concurrently.

In the irradiation process the most important task is getting the electrons from the source to the target material. In the beamline the focussing and positioning of the charged beam occurs by the field interaction with the quadrupole magnets and dipole steerers [128]. The irradiation cryostat is then placed in the forward direction of the LINAC1, as close as possible to the end of the beamline, as the irradiation cryostat is not directly coupled to the vacuum of the acceleration component and the beam must exit the beamline via an extraction window. To minimize scattering, and the irradiation by multiple scattered electrons, the choice of window material must be such that a very thin window can be made, but also the material must be radiation hard and durable, in addition to fulfilling the obvious criteria of being vacuum-tight. For this reason the vacuum chamber of the linac is terminated with a 125 µm Kapton foil, coated in a 5 nm sheet of titanium to further hinder the permeation of water and other gas molecules through the window. After a few centimetres in air the electrons enter the irradiation cryostat by passage through a 50 µm thick titanium window, pass through the thermally insulating vacuum, before penetrating through the 2 mm thick aluminium wall, finally entering the argon liquid vessel of 90 mm diameter containing the target holder.

To ensure a homogeneous irradiation along the horizontal axis of the material the target container is rotated at a frequency of 1 Hz. It is possible to position the beam profile in such a manner as to irradiate the whole of the incident plane of the target holder at once, but, small differences in the beam intensity along the vertical axis can cause problems in terms of accumulated dose differences. To achieve the desired result one can use the beam trajectory to advantage: The electron beam can be focussed to a circular spot of approximately 2 cm diameter and then a so-called wobble-mode used to move the beam up and down along the vertical axis in a linear fashion, pausing at the turning points. The beam trajectory is illustrated in figure 6.6, where the arrows indicate the rotation of the sample holder and the "wobble" character of the beam, ensuring a uniform irradiation of the sample materials throughout the whole of the sample container. To check the beam profile we inserted trovidur® (polyvinyl chloride - $(C_2H_3Cl)_n$) foils on the titanium windows and within the target container. The foils, initially bright orange in colour, turn black with increasing irradiation doses, making the beam dispersion visible and allowing for optimisation of the beam characteristics, quite literally on target.

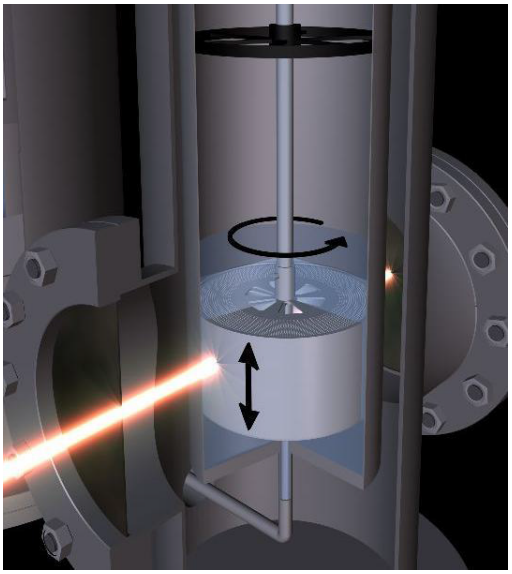

Figure 6.6: 3D drawing of the electron beam incident on the target holder in the argon cooled cryostat.

The ELSA LINAC1 uses a pulsed beam system with a pulse width of τ=1.2 µs and a repetition rate of ν_{rep}=50 Hz to produce bunches of electrons with an energy of E_{e}=20 MeV. In stable operation the linac delivers a bunch charge Q_{bunch} between (200–300) nC, giving an average current of (10–15) µC and an output beam power that can be calculated by

$$P_{\mathrm{beam}} = \left(\frac{Q_{\mathrm{bunch}} \cdot \nu_{\mathrm{rep}}}{\mathrm{e}} \right) \cdot E_{\mathrm{e}}, \tag{6.10}$$

of between 200 W and 300 W, dependent on the stable running conditions. The bunch charge can be continuously measured in a non-destructive manner with a *Bergoz* monitor [129] and the sum of the incident charge is the monitored parameter for the accumulated dose of the target material.

In irradiation dose terminology one often uses a dose calculation of incident electrons per unit area, the variable parameter during the irradiation being the number of electrons actually reaching the surface area of the target holder. The effective area of the target holder is taken to be $A = \pi/2 \cdot \bar{d} \cdot h = 24\,\mathrm{cm}^2$ with $\bar{d}$ being the average width of the container and h being the height. Based on work conducted on behalf of the Japanese Atomic Energy Agency (JAEA), it was decided that a dose of $D = 10^{15}\,\mathrm{e}^-/\mathrm{cm}^2$ would be a good starting point for the irradiation of an organic material [125], in contrast to the higher dose of $10^{17}\,\mathrm{e}^-/\mathrm{cm}^2$ used for the inorganic materials. Organic materials are more susceptible to radiation damage, or phrased in a more positive fashion, the radical creation mechanism in organic materials is generally more effective than in inorganic materials. In theory this means that $n_{\mathrm{e}} = D \cdot A = 2.4 \times 10^{16}$ electrons must be irradiated onto the target material, which calculates to an incident charge of 3.85 mC. This value was slightly overshot on the first and only irradiation, as the automatic stopping mechanism for an accumulated charge malfunctioned and the beam was stopped manually, ending with an accumulated charge of 4.2 mC.

Before the first irradiation we were naturally curious as to how much time would be needed. To get an estimation for the time needed to acquire a specified dose one can calculate the electron flux for the linac beam:

$$\text{electron flux} = \frac{Q_{\mathrm{bunch}} \cdot \nu_{\mathrm{rep}}}{\mathrm{e}} = (6.3 - 9.4) \times 10^{13}\,\mathrm{e}^-/\mathrm{s}. \tag{6.11}$$

For the desired dose, and thus the calculated incident charge, an irradiation time of only (4.5 to 7) min is required, which is exceptionally short in comparison to the inorganic materials with irradiation times exceeding 10 h. A lot of the systematic errors of the before-mentioned single-foil proton irradiations are no longer a problem in the electron beam irradiation and have the advantage of producing a significantly larger and homogeneous batch of material in just one irradiation cycle.

The sample material is immersed in liquid argon throughout the whole of the irradiation, so the sample temperature is constantly stable at 87 K. As this is a characteristic of liquid argon, the temperature is reproducible for every irradiation in this cryostat. A detailed explanation of how the cryostat cooling cycle works is given in the diploma thesis of Runkel [130]. The cryostat in its various resurrections has chiefly been used for the irradiation of ammonia, which must be inserted into the cryostat pre-cooled to liquid argon temperature. The polymer samples are much easier to handle, because they are stable at room temperature and can be inserted in the cryostat with ease at room temperature, making the loading procedure a slightly less demanding task. Once irradiated the samples are removed and stored in liquid nitrogen, ensuring a continued cooling of the materials. The plan to systematically irradiate materials to find the right dose was unfortunately halted shortly after our introductory efforts, as the LINAC1 encountered a number of ongoing issues and therefore entered a prolonged period of maintenance. It was not possible to conduct any further irradiations of materials at this site: An alternative was needed.

6.4.2 Electron irradiations at LINAC2 - ELSA

In the past all irradiations of target materials at the Physics Institute of Bonn have taken place at the LINAC1 of the ELSA facility, as previously detailed. However at present it is not possible to use this part of the accelerator. Luckily, the second linear accelerator LINAC2 is well maintained, primarily due to its association with the larger experiments at the ELSA facility, e.g., Crystal Barrel. Some modifications, e.g., to the current beamline were needed, and it is now possible to extract the electron beam into the irradiation area. The initial plan, started with the irradiations at LINAC1, was the systematic irradiation of PE and PP materials. The modifications allow the irradiation using the LINAC2, with the restriction that the linac could no longer be used parasitically, as it provides the pre-acceleration for the high energy electrons needed in the larger experiments. To this end, with limited access in times of maintenance and downtime of the larger experiments, an attempt was made to continue the irradiation programme of the materials. In addition to the PP samples, used in the previous irradiations, samples of PE, differing in density and linearity, were irradiated simultaneously, to ensure comparability, in a helium gas cryostat [131], [132]. The cryostat uses a dual regulating system, implementing a slow cycled liquid nitrogen cooled heat exchanger coupled to a closed helium gas system with a fast regulating 1000 W heater. The major advantage of this cryostat is that the irradiation temperature can be regulated to the desired temperature in the range of 90 K<T<300 K. Irradiations were conducted at temperatures of 140 K, 180 K, 210 K and 230 K. The temperature is determined by PT100-resistors in a four-wire configuration and the sample temperature is determined as the average of the temperatures before and after the irradiation chamber in the helium gas flow.

Looking at the setup of the linacs at ELSA (figue 6.5) we can see that if LINAC1 was to be used as a feeder for the booster synchrotron that due to the geometry of the setup the beam must be bent away, first clockwise, then anti-clockwise, from its initial trajectory, into an injection beamline parallel to LINAC1. If we use the LINAC2 for pre-acceleration we can bend the beam back into the part of the beamline perpendicular to the LINAC1 by retaining the same field direction for the last, shared dipole magnet. Is this way the same irradiation area can be used as before, the cryostat now being placed in the linear extension of the connection between the linacs with a new extraction window, similar to the one described for the LINAC1 irradiations.

The beam focussing, positioning and profile manipulation has been described in the previous section. The internal path of the beam within the cryostat progresses through the external window, made of 100 µm thick titanium, and through the insulating vacuum before entering the helium gas filled irradiation chamber via another titanium window of 50 µm thickness. The irradiation chamber consists of an open section in a 80 mm diameter pipe with windows in forward and backward direction. Within the irradiation chamber the sample holder, made of a meshed aluminium cylinder, contains the target material, which is cooled by the flow of helium gas channelled through the cylinder.

The end energy of LINAC2 is slightly higher than that of LINAC1 with 23 MeV instead of 20 MeV, yet the bunch charge was measured as approximately 20 nC before the before-mentioned dipole magnet, which was 10 to 15 times lower than the bunch charge produced at the LINAC1, at the same repetition rate and pulse width. A new *Bergoz* monitor [129] was installed just before the extraction window to determine the actual electron current entering the cryostat. The dipole magnet effectively acts as a highly selective energy filter and reduced the beam bunch charge to approximately only 7 nC, some 30 to 40 times lower than that previously expected from the LINAC1, scaling the electron flux, beam power by the same factors:

$$\text{electron flux} = \frac{Q_{\text{bunch}} \cdot \nu_{\text{rep}}}{\text{e}} = 2.18 \times 10^{12}\,\text{e}^{-}/\text{s}, \tag{6.12}$$

$$P_{\text{beam}} = \left(\frac{Q_{\text{bunch}} \cdot \nu_{\text{rep}}}{\text{e}} \right) \cdot E_{\text{e}} = 8.05\,\text{W}. \tag{6.13}$$

After the ESR and polarisation measurements of the previously irradiated samples it was decided to first reduce the dose from the equivalent of 4.2 mC injected charge by a third to 2.8 mC. The reasons for this will be discussed in detail in the sections 8.3 and 10.2. The injected charge of 2.8 mC still produced radical densities in the order of magnitude necessary for DNP. The reduction of the incident charge from 4.2 mC to 2.8 mC scales the dose in the same way: The calculated dose then becomes $0.73 \times 10^{15}\,\text{e}^-/\text{cm}^2$, and was used to irradiate all samples at the above given temperatures. The lower irradiation charge means the irradiation times are significantly longer than in the previous irradiation of the polymeric materials. The irradiation time needed to accumulate the calculated dose is then in the region of $2^{1/2}$ h. After the samples were irradiated at all of these temperatures, irradiations to higher doses in multiples of the initial dose were conducted for some samples at the temperatures of 180 K and 210 K. The reasons for this will become clear in the evaluation of the polarisation characteristics in section 10.3.

The lower beam current of the LINAC2, in comparison to the LINAC1, works in favour of the temperature stability as less power is deposited in the sample materials and needs to be cooled away. The disadvantage of the helium cryostat is that because it is gas cooled the samples should ideally be inserted at room temperature and removed cold. The procedure for the sample insertion in this irradiation programme was to insert the samples into the cryostat and then pump the closed system. Once the pressure reached 10^{-2} mBar the system was then flooded with helium gas and pressured to 1.5 Bar before beginning the cooling cycle. For the polymer samples this does not pose a problem, however it does restrict the use of the cryostat to materials that are solid at room temperature. An alternative procedure may be to pump the system to vacuum, then flood with helium, cool the system and then insert the sample whilst additionally flooding the system with helium gas to stop air falling in. This may provide a method to broaden the scope of operation. Though this procedure was not tested in this irradiation programme.

CHAPTER 7

Radical identification and decay

As described in the previous chapter, the interaction of irradiation with the polymer medium creates the unpaired electrons that are needed for DNP. These unpaired electrons are not created at random positions within the molecular structure, so that the unpaired electrons are found at very specific positions within the molecular chains. The resulting molecules containing at least one unpaired electron are called radicals. The analysis of ESR spectra gives insight into the type of the radical present in materials, i.e., where the bond cleavage has taken place. However, the analysis of complex spectra can be an arduous task, especially if the total spectrum consists of a superposition of many spectra arising from various different couplings within the molecular structure, which is especially true for polymers systems containing different configurations and conformations at the radical sites. A bulk of ESR studies on the creation and decay of radicals in irradiated polymers was published in the 1960s and 1970s. These studies focussed on the identification of the radicals and also on conversion mechanisms from one radical to the other. An overview of relevant studies will be presented in this chapter, with the comparison of the predicted ESR spectra with those obtained for our samples being discussed in chapter 8. Though the radicals that were produced in this study are from irradiation processes, this is not an exhaustive description of all radicals that can be created within the materials, as it is known that additional radicals can be created at extremely high doses, but also by various fracture mechanisms. For further reading a brief overview of these processes is given in the appendixes A.1 and A.2. It has also been shown that the creation of radicals in polymers comes from a spur-like formation along particle tracks. This production method will also be discussed, as the type of irradiating projectile has a fundamental influence on the radical distribution within the bulk material and may also help explain the polarisation characteristics of the polymer materials.

7.1 Identification of the irradiation induced radicals in PE and PP

7.1.1 Polyethylene

In PE materials three distinct radicals, shown in figure 7.1, can be identified that are formed at specific temperatures, either during irradiation or after subsequent heating, where the temperature stability of the radical is improved by an increase in the degree of unsaturation, i.e., the number of double bonds. This is a unique characteristic of hydrocarbons in which a number of radical subsystems can be created, in contrast to those irradiated materials that have previously been the focus of polarised target irradiation studies, where only one polarising radical type is observed. A compact way of expressing the chain-

radicals in PE is:

$$–CH_2–\dot{C}H–(–CH=CH)_n–CH_2–$$

with n= 0 being the alkyl-, n= 1 being the allyl- and n> 1 being a polyenyl-type radical, of which the first two will be discussed, as the polyenyl-type radical is created at higher doses than the scope of this work.

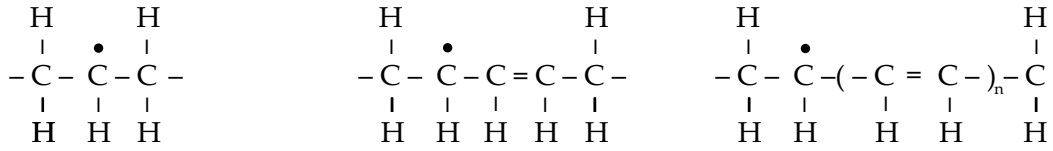

Alkyl. Allyl. Polyenyl.

Figure 7.1: Chain radicals created in PE.

7.1.1.1 Alkyl-type radical

In the low temperature irradiation process of PE an alkyl-type radical is created: The electron is localized on a p-orbital of the single carbon atom and has a hyperfine interaction with a single α- and four surrounding β-protons and no contribution from γ-protons or higher[1] [133]. A single alkyl radical is created by the initial interaction of the radiation and the molecule. The extracted hydrogen atom leaves the vicinity of the newly created radical site and combines with another hydrogen atom by extraction of a hydrogen atom from a nearby molecular chain to form molecular hydrogen. The hydrogen atom could bond with free electrons in the molecular structure, or with other atomic hydrogen atoms, however these interactions are extremely unlikely and the extraction of a nearby hydrogen atom does seem more plausible. The extraction of the second hydrogen atom results in an additional radical, leaving two identical radicals that are locally concentrated, formed by one irradiation process. The process termed the "pairwise" creation of radicals was first proposed by Miller et al. in the mid 1950s for hydrocarbons [134] and is detailed for PE by the following two step reaction:

$$1)\ –CH_2–CH_2–CH_2– \quad +e^- \quad \longrightarrow \quad –CH_2–\dot{C}H–CH_2– \quad +\dot{H} \quad +e^-$$

$$2)\ –CH_2–CH_2–CH_2– \quad +\dot{H} \quad \longrightarrow \quad –CH_2–\dot{C}H–CH_2– \quad +H_2$$

Direct evidence for this process was then given by Iwasaki and Ichikawa by the observation of $\Delta M = 2$ transitions in ESR absorption spectra of polymers, from the dipole-dipole coupling of two unpaired electrons [135], [136]. The probability of detection of the $\Delta M = 2$ spectra is given by the ratio of the $(\Delta M = 2)/(\Delta M = 1)$ transitions and is proportional to the distance separation of the unpaired electrons, due to the distance dependence of the dipole-dipole interaction. It was shown that this ratio drops for heated samples, even when the radical concentration is maintained, implying that the radicals that are

[1] The Greek letters symbolise the positions of the carbon atoms in the molecular chain with regards to the radical site: $-(CH_2)_\gamma-(CH_2)_\beta-(\dot{C}H)_\alpha-(CH_2)_\beta-(CH_2)_\gamma-$

initially close together then drift further apart. The creation of radical pairs has been shown for a wide range of γ and electron beam irradiated polymers, including PE and PP.

Earlier studies had presumed a rather simple structure of the alkyl radical arising from the equal coupling of the single α- and four β-protons giving the sextet structure seen in the ESR spectrum. If the substructure is ignored the spectrum can be estimated by equal interaction of five protons with the unpaired electron, giving a peak separation somewhere in the region of 3.1 mT[2]. With the development of higher sensitivity ESR and the use of oriented samples the actual underlying ESR structure has been shown to be much more complex: For more information, the highlights of these developments is given in the following references [137], [138], [139], [140]. Due to the line broadening in the solid the narrower substructure is smeared out in unoriented samples and as such the convolution of these lines can be estimated as broader singular lines, so that the assumption of a six line spectrum is justified. The ESR signal is highly symmetrical and an anisotropic g factor, if even present, is thought to be very minimal. This will be discussed further in section 10.3.1.

7.1.1.2 Allyl-type radical

The room temperature irradiation of PE creates the previously discussed alkyl, but in addition also a second type of radical called the allyl that is characterised by the stabilisation on an unsaturated double bond in the molecular chain. The allyl radical is known to be very stable at room temperature. Alkyl radicals are not, so that in practice room temperature irradiations produce predominately allyl radicals, as the alkyl radicals decay at a much faster rate. Alternatively, it is also possible to irradiate materials at low temperatures, e.g in liquid nitrogen, and then subsequently produce allyl radicals by a heat treatment of the materials at room temperature [141]. The alkyl radical can be created at room temperature, however the formation of a vinylene bond from the alkyl radical is thermodynamically more favourable, where the activation energy of the back reaction is at least 15-20 kcal/mole larger than the forward reaction [142]. A consequence of this is that the yield of the allylic radicals increases with the irradiation dose. It has been noted that the vinylene concentration, as measured by the intensity of UV and IR absorption bands, increases linearly with dose, but that the rate constant of the subsequent conversion does not follow in the same manner [143]. The conversion mechanism becomes more effective for higher doses. This general trend is understood to be a result of the reduction of the average distance of migration of the alkyl-radical. Waterman and Dole showed that room temperature persistent alkyl radicals are quantitatively converted to allyl radicals[144], so this suggests that there is no direct method of producing the allyl radical as its creation is a result of the migration of the alkyl radical to sites of unsaturation [145]. This means that the number of alkyl radicals that can convert to allyl type radicals is then dependent on 1) the degree of the initial unsaturation and 2) the number of addition double bonds formed by the irradiation at higher doses.

The alkyl radicals can migrate to the site of a double bond, where the radical is stabilised by bond resonance, however, the electron de-localises and has a spin distribution over three carbon atoms[3]. Lefkovits et al. calculated the electron density on the carbon atoms of the allyl radical as 0.622,
-0.231 and 0.622, respectively, giving two resonance forms and these results can be used to obtain the theoretical splitting to a septet of 1.87 mT spacing with an addition doublet splitting of 0.69 mT [146]. Whereas the splitting of the two resonant forms of the α-protons are largely temperature independent, the hindered oscillation of the methylene group of the β-protons has also been shown to be highly influenced by the temperature [141].

[2] This value is an estimate based on the peak fitting of our irradiated samples.
[3] This means that the allyl radical has three α-carbon atoms: -$(CH_2)_\beta$-$(\dot{C}H)_\alpha$-$(CH)_\alpha$=$(CH)_\alpha$-$(CH_2)_\beta$-

7.1.2 Polypropylene

Many structures have been proposed for the radicals resulting from the irradiation of PP, however a general consensus does not seem evident from the literature. The main obstacle in determining the constituents of the spectra is the fact that irradiation of the material is thought to lead to a superposition of radical structures that are primarily obtained by the removal of hydrogen atoms. In PP there are three sites from which a hydrogen atom can be removed, each of which would be expected to give an individual and distinct ESR spectrum. A hydrogen atom can be removed from the carbon backbone opposite of the methyl group or from the methylene bridge, as well as from the side-chain methyl, all shown in figure 7.2. In addition to hydrogen evolution there is also the possibility of the creation or stabilization of radicals in a double bond system, or even less likely, chain scissions. An example of the former is the allyl-type radical and of the later a chain scission could be the removal of the side chain methyl molecule (radicals IV and V in figure 7.3). The enlarged number of possible radicals in PP makes the interpretation of ESR spectra a much more difficult task, than is the case for PE, however there seems to be a tentative agreement towards the dominance of the alkyl-type I.

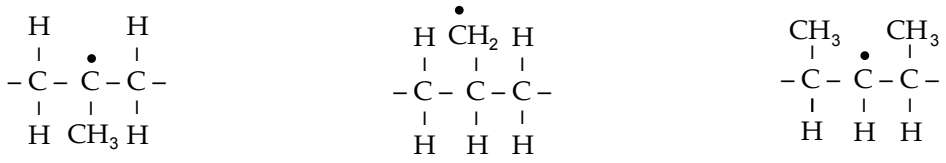

I II III

Figure 7.2: Alkyl-type radicals created in PP by the extraction of a single hydrogen atom.

IV. V.

Figure 7.3: Further examples of possible radicals created in the PP chain structure.

An irradiation of PP at 77 K produces a radical that exhibits an eight line structure in the ESR spectrum, when measured at the same temperature. The eight lines have a nearly equidistant separation of ~ 2.2 mT[4] and are produced by the interaction with the surrounding β-protons [5]. As there is a lack of an α-proton in the radical structure, it follows that there should be no angle dependence of the ESR spectra,

[4] This value is an estimate based on the peak fitting of our irradiated samples.

[5] In this case all the protons in the alkyl-type I radical depicted in figure 7.2 are β-protons as there is no hydrogen connected to the α-carbon.

which has been verified experimentally by comparision of stretched[6] and non-stretched samples [147]. This practically excludes radicals of the type III and V, as the hyperfine coupling of the α-proton in similar configurations in other hydrocarbons, e.g., in PE, has been shown to be anisotropic [137], [138], [139], [140]. Another argument against radical V is that the methyl-side groups affect the de-localisation of the unpaired electrons, even when these protons are not directly observed in the ESR spectrum [148]. This has the effect that even if the same radical is created in the confinement of the α-, β-region of the radical, the side chain methyl-groups increase the local electron density on the α-carbon, resulting in a lower hyperfine coupling with the surrounding protons. As this observation is not made for a comparison of PE and PP spectra radical V can most definitely be excluded.

It has also been suggested that the spectrum actual consists of two equally weighted, separate overlapping spectra, consisting of eight and of four lines [149]. The additional quartet may come from the equal interaction of 3 protons: There are two chain radicals that could produce this: CH_2-$CH(\dot{C}H_2)$-CH_2 (radical II) and $CH(CH_3)$-$\dot{C}H$-$CH(CH_3)$ (radical III). Loy used a deuterium-substituted PP to identify the radicals seen in the spectrum of the ^{60}Co γ-irradiated polymer [150]. Using various substitutions, certain radicals could be excluded and the multiplet was assigned to the radical I, with the quartet from the equal interaction of 3 protons attributed to the radical II. If this is true then this could potentially pose a problem for the use of PP as a solid state polarised target, because the radicals may have different g factors and this would lead to a broadened ESR signal at high fields.

Similar to the irradiations of PE, it has been shown that the number of double bonds in PP increases with dose. For this reason, in a direct comparison to the irradiated PE samples, the ESR signal of room temperature irradiated or heat treated PP samples has been interpreted as being from the allylic radical (radical IV) [147]. As enticing as this allocation seems, the hyperfine splitting of the radical is incompatible with results obtained for various other allylic radicals in hydrocarbons that display similar splitting in accordance to the spin density calculations of Lefkovits [146]. Instead Ayscough interpreted the spectrum as coming from the alkyl radical I, as with the 77 K irradiation, but with the difference that there is no overall equivalence of protons [151]. The β-protons of the methylene bridges are considered to be equivalent in pairs with an anisotropic contribution of the protons of the methyl group.

A lack of consensus on the radical conformity may come from the different samples that were used. It has been shown that the stereo-regularity has an influence on the observed spectra, shown by the substitution of the isotactic material for an atactic material [152],[153]. Different angular dependences of the β-protons in isotactic and atactic materials lead to different values of hyperfine splitting, complicating the matter further.

7.2 Decay and radical conversion processes in PE and PP

The decay of the radical concentration in polymers arises from a variety of different factors. The radicals created at low temperatures are typically stable at these temperatures. In most cases liquid nitrogen temperature is low enough to stop the recombination of these radicals, decay and/or morphing to other radical types. However, heat treatments at elevated temperatures help to shed some light onto exactly theses processes. The first thing to be expected is the reduction of the initial concentration by a decay of the initial radical, though secondary processes involving the conversion of one radical to the other may also occur. Which process is dominant is highly specific of the polymer composition and structure and

[6] Generally the anisotropic part of the hyperfine coupling is averaged out by the non-preferential orientation of the molecular axis. However, upon stretching the molecule is aligned in the direction of the stretch and the $(C\text{-}H)_\alpha$ bond is then at right angles to the molecular chain, with a random orientation in the plane perpendicular to the direction of stretching, which then gives access to the anisotropic part of the hyperfine splitting by measurement of the ESR spectrum of the sample at 0° and 90° relative to the magnetic field axis.

can be highly temperature dependent.

A paper authored by Loy in 1960 focussed on the temperature dependent decay of the alkyl radicals in PE [154]. It was shown that for samples heated "in the absence of air" there is an initially steep decay that tends towards a temperature dependent fixed value, for which the ratio of residual/initial radical concentration was inversely proportional to temperature and was independent of dose. Irradiations of PE in vacuum at low temperatures by Cracco et al. showed that the created alkyl radical was stable up to a temperature of 155 K, above which a very noticeable decay took place [155]. It was suggested that the temperature increase of the polymer allows an increase to the dispersion length of the radicals and thus makes the recombination more likely, i.e., at lower temperatures the radical can only react with its closest neighbours. The limiting value of the radical concentration upon decay in vacuum is undeniably the temperature, but it was also shown for the first time that the persistent radical at elevated temperatures was of the allyl-type, so that a conversion process must have taken place.

Similarly, Nara et al. and Forrestal and Hodgson also identified two distinct temperature regions in which the alkyl radicals, created by irradiation, decay in PP [156], [149]. This is linked with the motion of the molecular matrix that traps the free radicals. The first distinct region of decay was around the temperature of 170 K, in the region of the γ-dispersion (local mode relaxation[7]) in propylene and the second being close to 260 K, which corresponds to the β-region (connected to the glass transition temperature[8]). No change in radical concentration was observed when samples were heated to temperatures below 170 K, so the radical is obviously stable up to this temperature. Heating to temperatures above 170 K led to a drop in radical concentration with a distinct decay region above 260 K.

As polymers are heterogeneous materials, one can naturally assume that the decay mechanisms within them are governed by the differences in the surrounding molecular structures. Already in early research papers it was considered that the multi-phase system of polymers could play a role in the kinetics of creation and conversion of radicals in these materials and that decay rates in the amorphous materials were much larger than in crystalline materials. Loy proposed that cross-linking radicals are formed in the amorphous region of the polymer, whereas the frequently observed long-lived radicals were situated in the crystalline phase [154]. The stability of the radical created at 77 K and decaying at room temperature was found to vary in PE samples of "differing physical and chemical properties" [157], those being mainly the factor of crystallinity. The "morphological structure" of PE was shown by Johnson et al. to explicitly have an influence on the decay of the alkyl radical in PE [158]: Different samples of PE were prepared by melting the samples and then submerging them in baths of varying temperatures. As the rate of crystallisation is temperature dependent, this resulted in materials with a wide range of densities and thus of crystalline/amorphous fractions. It was shown that their data fitted well with a composite decay consisting of two first order decays, occurring simultaneously but independently, so that the overall concentration of the alkyl radical is given by:

$$c = c_s + c_f = c_{s,0}\exp^{-k_s t} + c_{f,0}\exp^{-k_f t} \tag{7.1}$$

or in rearranged form

$$\ln\left(\frac{c - c_s}{c_s}\right) = \ln\left(\frac{c_{f,0}}{c_{s,0}}\right) - (k_f - k_s)t \tag{7.2}$$

where c_s and c_f are the concentrations of the fast and slow decaying components, to their respective starting values $c_{s,0}$ and $c_{f,0}$ with decay constants k_s and k_f. It was shown that this decay was most certainly linked to the amorphous content of their samples, with both k_s and k_f increasing for a larger

[7] The local modes are the vibrational states of molecules in the glassy state. When thermally excited the modes are strongly damped into relaxational molecular motions.

[8] The glass transition is the transition from the glassy state into a viscous state at elevated temperatures.

amorphous volume content. The conclusion was that the fast decay could be attributed to those alkyl radicals situated in the amorphous phase, with greater mobility, and that the slow decay can then be attributed to the alkyl radicals in the crystalline phase after diffusion to the surfaces of the crystalline regions. A high crystalline sample would thus exhibit very long decay times: Zhao et al. found that the decay times of the alkyl radicals in air (and in vacuum) at room temperature in highly crystalline UHMW-PE was up to 100x (and 30x) longer than values given by the literature for HDPE [159]. This has also been illustrated for UHMW-PE (ultra high molecular weight PE, i.e., extremely high crystalline fraction) by Jahan et al., who showed that the long term stability of the radicals created at room temperature by gamma irradiation, where samples left for 2 years under these conditions still exhibited up to 20% of the initial radical concentration [160].

The same conclusions can be drawn for samples of PP where decay in the amorphous region of PP has also been noted to be faster than in crystalline region, when measured at a temperature around the glass transition temperature [161]. Gvozdic et al. demonstrated that the decay of the primary radicals in isotactic PP does not follow simple composite first order kinetics, but instead a composite of a first and a second order reaction [162]. The decay progress can be written in terms of the decay constant of the second order reaction and the initial concentration of those radicals participating in this reaction $c_{0,2}$, based on the assumption that a proportion of some of the initial radical is converted into stable radicals:

$$c_0 - c = c_{0,2} \frac{c_{0,2} k_2 t}{1 + c_{0,2} k_2 t} \tag{7.3}$$

or in rearranged form

$$\frac{t}{c_0 - c} = \frac{1}{c_{0,2}^2 k_2} + \frac{t}{c_{0,2}}. \tag{7.4}$$

Gvozdic explains the second order reaction as coming from the simple decay by recombination of two of the radicals that produce the octet structure in ESR spectroscopy: Radical A· combines with radical A· with a decay rate k_2 to form a stable product. The first order process, governed by the rate constant k_1, would then involve the displacement of the radical A· from its original location, to a position where it can "become" a stable radical. However, no explanation was given that could explain why the decay mechanisms in PE and PP should be so different.

As previously stated, the irradiation processes at low temperatures creates the alkyl-type radicals. It is only after heat treatment or irradiation at elevated temperatures that the allyl radical can be created in PE, whereas in PP there is no conversion process, but simply a reduction of the number of alkyl radicals in the material. It has been claimed that, in contrast to the alkyl radical, the allyl radical is created in a well defined region of the polymer. The conversion rate of the reaction alkyl → allyl radical was shown to be larger for greater amorphous fraction, implying that the allyl radical is mainly created in the amorphous regions of the polymers [163]. However this picture seems to be to simplistic. Waterman and Dole claimed that a large proportion of the allyl radicals observed in their experiments came from the migration of the alkyl-radicals, created at 77 K, to the sites of existing double bonds, as immediately after irradiation at 77 K no allyl radicals are detected and that it is the heat treatment that initiates the conversion of the alkyl radical to the allyl by the direct reaction of one alkyl radical with one double bond [144]. However, the amount of residual allyl radical left in the polymer after a heat treatment at 260 K was shown to be nearly linear with the initial dose. It was postulated that the room temperature conversion occurs in the amorphous regions of the polymer, but that the trapped alkyl radicals convert at a much reduced rate in the crystalline regions. Following this reasoning, as the allyl radicals also decay, albeit at a much reduced rate than the alkyl radicals, it would thus seem plausible that the long term stable radicals trapped in the crystalline regions of the polymer are converted to long term stable

allyl radicals. It would thus also seem realistic to assume that the crystalline content would influence the amount of residual radical within the polymer. This can be seen for our sample materials of PE, as demonstrated in section 8.5.

The decay mechanism of the allyl radical in PE has been studied extensively and the conclusion is that the decay follows a diffusion controlled second order process [164],[145]. The description of the kinetics was first given by Lebedev, based on diffusion based kinetics described by Waite and later adapted by Smoluchowski. The Lebedev theory postulates that the decay of a radical is a two phase kinetic process: 1) a slow movement of the radicals to a favourable position, followed by 2) a fast recombination of radicals in active volume [165]. The Smoluchowski-Waite equation describes second order diffusion-controlled bimolecular reactions, under the assumption that the initial radicals of concentration c_0 are distributed randomly within the material and that they subsequently "diffuse", meaning a migration of the radical site, by the characteristic diffusion constant D, to within a reaction cage of radius r_0 [166], in which they react to leave a concentration of c :

$$\frac{c_0}{c} = 1 + 8\pi r_0 D c_0 \cdot \left(1 + \frac{\sqrt{2} r_0}{(\pi D t)^{1/2}}\right) \cdot t = 1 + A t^{1/2} + B t, \tag{7.5}$$

with the constants $A = 8\sqrt{2} r_0^2 c_0 \sqrt{\pi D}$ and $B = 8\pi r_0 D c_0$. The description of a diffusion based decay is not just restricted to the decay of the allyl radical, but has also been used to help explain the mechanisms involved in the degradation process of polymers, especially with regards to the exposure of radical species in air [167], [168].

CHAPTER 8

ESR measurements

As discussed in section 3.2, the ability of sample materials to be dynamically polarised is highly dependent on the coupling of the electronic and nuclear spins. The coupling of these spin states leads to energy transitions that can be visualised by ESR spectroscopy. It is then possible to identify the specific radical that is created by comparison of the ESR spectra with those structures predicted by the literature, as was presented in chapter 7.

A factor that influences the polarisation characteristics of materials is the local environment of the unpaired electrons that were created in the irradiation process. Here the influencing factor is the number density of the unpaired electrons that are produced. ESR spectroscopy can be used to quantify these unpaired electrons and allows a direct comparison of the so-called spin densities of the individual materials. In this way it is possible to see how, e.g., radical yields differ between materials or if they are influenced by the irradiation temperature.

Thus, after the irradiation of the materials, the first step of the analysis of the samples was the spin density determination by ESR spectroscopy to quantify the absolute structural defects, but also to determine the form of the ESR spectra, giving an indication of the structural configuration of the created paramagnetic centres. Before going into detail of the analysis, a brief overview of the measuring systematics is given and it is explained how the ESR spectrometer is used to evaluate the concentration of the paramagnetic centres created by irradiation. All measurements with the ESR spectrometer were centred at a magnetic field of 332 mT with a sweep width of 40 mT. The sweeping rate was set so that a full field sweep takes 5 min, acquiring 512 data points in the process. Unless otherwise stated all signals were taken at a temperature of 77 K for an increased sensitivity, as detailed in section 2.2.2. The spectrum for a calibration sample was retaken on each individual day of measurement to minimize systematic errors arising from, e.g., slight differences in tuning.

8.1 Determination of the spin density

The determination of the spin density of irradiated materials using ESR is of utmost importance, as all materials that have been successfully used as dynamically polarised solid state target materials have spin densities in a very confined range: Experience has shown that spin densities in the order of $10^{19}\,e^{-}/g$ are needed for efficient DNP. For the spin density determination using ESR to quantify the irradiated materials a calibration sample is needed, which can be easily made using one of the many commercially available chemical radicals. The starting point of the analysis when using chemically doped materials is

the molecular weight m_w of the radical carrier, e.g.,

$$\text{TEMPO} : m_\text{w} = 156.2453\,\text{g/mol},$$
$$\text{porphyrexide} : m_\text{w} = 141.1512\,\text{g/mol}.$$

Determining the number of molecules of a radical carrying substance gives us access to the number of free radicals in a sample, assuming that each molecule carries a known number of unpaired electrons, e.g., in the case of TEMPO and porphyrexide each molecule carries exactly one unpaired electron. Thus, the number of paramagnetic centres of a radical carrying substance of sample mass m_r and purity p is then given by:

$$n = \frac{p \cdot m_\text{r}}{m_\text{w}}.$$

To calculate the spin density n_s of a sample mixture, i.e., a radical carrier of mass m_r admixed with a non radical carrying substance of mass m_s, the total number of carrier molecules is divided by the total mass of the mixture:

$$n_\text{s} = \frac{n}{m_\text{s} + m_\text{r}} = \frac{p \cdot m_\text{r}}{m_\text{w} \cdot (m_\text{s} + m_\text{r})}. \tag{8.1}$$

So that the samples can be used for calibration one needs a uniform distribution of the radical carrier throughout the solvent. To achieve this solutions are shaken for a short period until the free radical carrier is completely dissolved and no residue remains. Also, the mixture is dripped from an automated dripping apparatus into liquid nitrogen and frozen into clear spherical beads of approximately 1 mm to 2 mm diameter. This process of mixing the radical carrier at room temperature into a liquid, hydrogen rich substance, e.g., alcohols and diols and then freezing the mixture is the basic process for creating chemically doped solid state target materials [169]. By mixing the materials in such a manner one also creates an ideal calibration substance with which spin densities of other materials can then be determined. Using the above described method a solution of 0.5 parts by weight of TEMPO of 98% purity and 100 parts by weight of n-butanol was mixed and used as a calibration sample: The spin density of the sample can be easily calculated using equation 8.1 to be $1.88 \times 10^{19}\,\text{e}^-/\text{g}$.

The 1st derivative signal measured in the ESR must be integrated twice, as due to the measuring procedure we don't measure the actual electron spin absorption spectrum[1]. The integration of the 1st derivative gives the absorption signal of the sample and the integrated area of this spectrum is then a measure of the number of paramagnetic centres in the material. The calculated area together with the measured sample mass can then used as a reference to determine the spin density of other materials as the spin density of the calibration sample is known.

The total spin density ρ_s of the sample can be calculated from the calibration data using the formula given by Schneider and Plato, assuming that the calibration sample and the sample of interest are measured at the same power and the same sweep parameters [2] [171]:

$$\rho_\text{s} = \rho_\text{c} \cdot \frac{A_\text{s}}{A_\text{c}} \cdot \frac{m_\text{c}}{m_\text{s}} \cdot \frac{S_\text{s}(S_\text{s}+1)}{S_\text{c}(S_\text{c}+1)} \cdot \frac{g_\text{s}}{g_\text{c}} \cdot \frac{T_\text{c}}{T_\text{s}} \tag{8.2}$$

where A is the calculated area of the signal for a sample of mass m and with the g factors and the spin S, with the index s being for the measured sample and index c for the calibration sample. Assuming all samples are of the same electronic spin species and are measured at the same temperature T, and

[1] The detailed description of the phase sensitive detection by signal modulation which leads to this phenomena is given by Eaton [25]

[2] This equation is a slight modification of the original equation with the suggested corrections for the g factor dependence, suggested by Aasa and Vänngard [170]

that the g factors of PE/PP and TEMPO doped butanol are similar enough that their deviation can be neglected, then the measurement simplifies in our case to the determination of the area of the absorption signal and the sample mass :

$$\rho_s = \rho_c \cdot \frac{A_s}{A_c} \cdot \frac{m_c}{m_s}. \tag{8.3}$$

8.2 ESR of proton irradiated PP foils

In the proton irradiations only PP foil materials were irradiated. As only part of the foil could be irradiated uniformly, those areas that were not open to the direct incident proton beam were later removed. To this end, previous to the irradiation, the foil was marked by the size of the irradiation aperture, which was filled by the proton beam. This way one could ensure that only irradiated material was included in the conglomerated material. After the material was batched into groups according to their irradiation times, the foils were then subsequently further reduced in size. All foils were cut into strips, later used for the polarisation tests. Some of the strips were then reduced further still in size for the ESR measurements. Great care was taken to ensure that no specific area of the foils was preferred and that border areas as well as centre pieces all ended up in the ESR analysis. For each irradiation time 10 sample pieces were selected for the spin density analysis.

Due to the saturation characteristics of the samples the ESR measurement of the spin density had to be taken at adequately low power. At -40 dBm all samples were still in the region where the observed signal increased linearly with the square root of the power and all measurements were thus conducted at this power. One disadvantage of the foil samples was the relatively small sample size of approximately 0.0025 mg of mass, resulting is rather noisy ESR signals. For comparison, a typical sample used for the ESR analysis of the pelleted materials was in the order of ten times larger.

The results of the spin density determination for the irradiation times of 10, 20 and 30 min are summarized in figure 8.1. The analysis of the spin density shows clearly that for these irradiation times the spin density increases with irradiation time and, as was the aim of the irradiation process, spin densities in the order of 10^{19} e^-/g were created in the material. The size of the error bars result from the fitting of the noisy signals, as well a wider spread in the spin densities within a batch due to the problem of systematic errors.

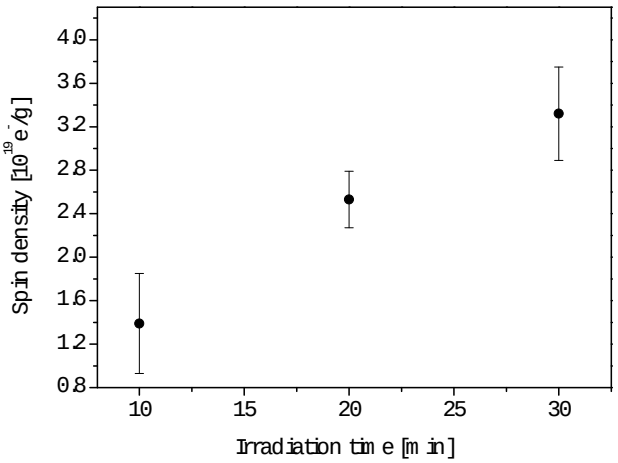

Figure 8.1: Spin density of proton irradiated PP for irradiation times of 10, 20 and 30 min.

The ESR spectrum of PP can be easily identified by the 8 peak structure arising from the hyperfine interaction, with an average peak separation of (2.3 ± 0.1) mT. In figures 8.2 and 8.3 an example of the ESR signal form and the integrated ESR signal is given. This example is of a PP foil that has been irradiated for 10 min with the parameters described in section 6.3. The peaks are indicated by the numbers in the figures. It should be noted that the structure seen in the 1st derivative spectrum, between the peaks 4 and 5, is not an additional absorption structure, but a result of the overlapping of the components, due to the broadened individual lines. The overlay of random signals from different irradiation times showed only minimal differences that are hardly discernable by eye, however extensive fitting and comparison of all the ESR curves showed there was a difference, if only very small, in the FWHM line width Γ_{tot} and of the individual line widths Γ_{line}. These results are summarized in table 8.1, together with the spin densities.

The main contribution to the width of the ESR signal comes from the hyperfine splitting, though a small contribution is certainly made by the line broadening of the individual lines. If the linewidth of the electronic signal is dominated by homogeneous broadening from the electronic dipolar interaction, then the spin-spin relaxation time can be given by $\Gamma_{line} \propto \frac{1}{T_2}$. At higher doses the individual linewidths would then increase due to the increased dipole-dipole fields seen by the unpaired electrons. As the average distance of the electrons reduces for higher concentrations, one would expect the spin-spin relaxation time to decrease, so that higher doses give broader lines. However, in solids the broadening mechanisms are from a variety of sources, so that this direct correlation is often masked by other effects (see section 2.3.2). In addition this analysis only applies if the individual line widths can be identified. In solids the ESR spectrum can consist of broad overlapping individual lines, which leads to unresolved components. Thus, if one was to determine the spin-spin relaxation time from the determination of the average linewidths of the octet, one would most certainly underestimate the relaxation time. For this reason the determination of the linewidth can be used for a comparison between the samples, but it does not give us access to the actual spin-spin relaxation time of the systems. This will be discussed further in the upcoming sections.

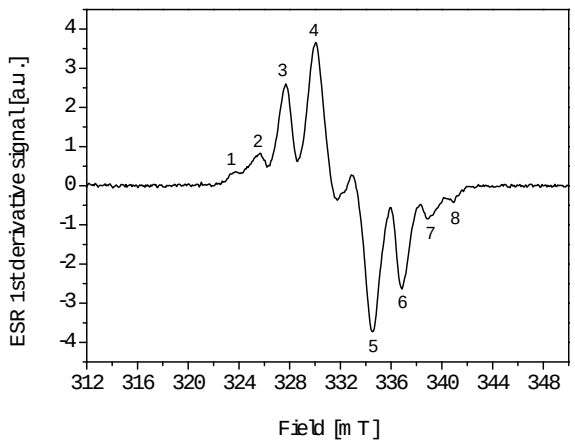

Figure 8.2: 1st deriv. ESR spectrum of proton irradiated PP foil.

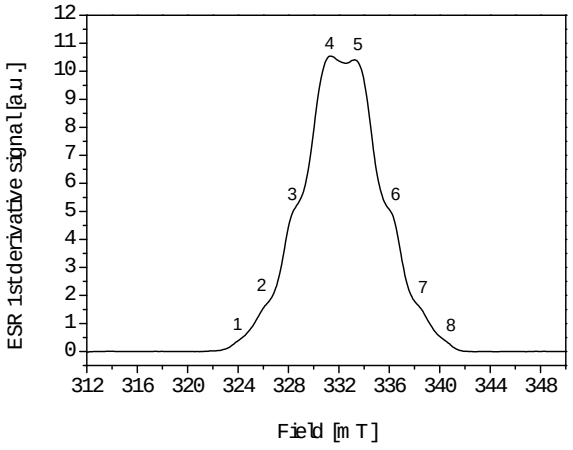

Figure 8.3: Abs. ESR spectrum of proton irradiated PP foil.

Irrad. time [min]	ρ [10^{19} e$^-$/g]	$\Delta\rho$ [10^{19} e$^-$/g]	Γ_{tot} [mT]	$\Delta\Gamma_{tot}$[mT]	Γ_{line}[mT]	$\Delta\Gamma_{line}$ [mT]
10	1.4	0.5	6.88	0.01	2.39	0.02
20	2.5	0.3	6.92	0.01	2.43	0.04
30	3.3	0.4	7.06	0.04	2.53	0.04

Table 8.1: ESR results of the irradiation of PP foils in vacuum.

8.3 ESR of PP irradiated in argon by electrons at the LINAC1

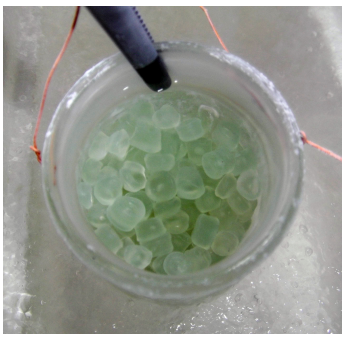

Figure 8.4: PP pellets that were irradiated in liquid argon.

For the electron beam irradiations in liquid argon three types of PP pellets were used of varying molecular weight, the individual pellets being of a size that they could be directly used in the ESR spectrometer. After the irradiation the PP samples show an intense green colouring (see figure 8.4), whereas the earlier irradiated foils only exhibited a hint of colouring. The general spectral form of all 3 measured PP sample types was the same, which implies that the type of radical created in each of the samples is also predominately the same alkyl-radical as in the previous proton irradiations. The signals, however, were of a lot higher quality than those obtained in the proton irradiations, as the sample mass was approximately ten times larger, giving a much better signal-to-noise ratio, allowing for the measurement at a lower power of -50dBm. A representative example of the ESR signal for these irradiated materials is given in figure 8.5 for the PP12 type sample with a direct comparison to the broadest ESR signal for the proton irradiated material. Evidently, the linewidths of the electron beam irradiated samples are broader than those obtained for the proton irradiations. Indications of this are that the broadening of the lines makes the individual lines less prominent as the overlap increases, whilst maintaining the central position of the lines. This is particularly apparent for the overlap in the centre of the ESR signal as the "wiggle" becomes larger for a greater overlap. The broadening is a direct consequence of the higher concentrations of unpaired electrons, as verified by the spin density determinations.

The results of the ESR analysis are given in table 8.2. Within error there is no difference in the widths of the absorption lines or the resulting total width of the ESR signal. Nor does there seem to be any significant influence of the molecular weight on the radical yield. As the initial comparison of the ESR of proton irradiated samples and the electron irradiated samples indicated, the total signal width is broader for the electron irradiated batch, as a result of the broadening of the individual lines, and the spin densities of the samples were also higher. The peak separation of (2.2 ± 0.1) mT however remains very comparable to those previously obtained. In summary, the overall spin density of all of the materials had an average of

$$\rho = (5.1 \pm 0.3) \times 10^{19}\,\mathrm{e}^-/\mathrm{g},$$

determined by the measurement of the spin densities of 10 samples each of PP12, PP250 and PP580. The average of all measured FWHM of the ESR absorption signals was

$$\Gamma_{tot} = (7.34 \pm 0.03)\,\mathrm{mT}.$$

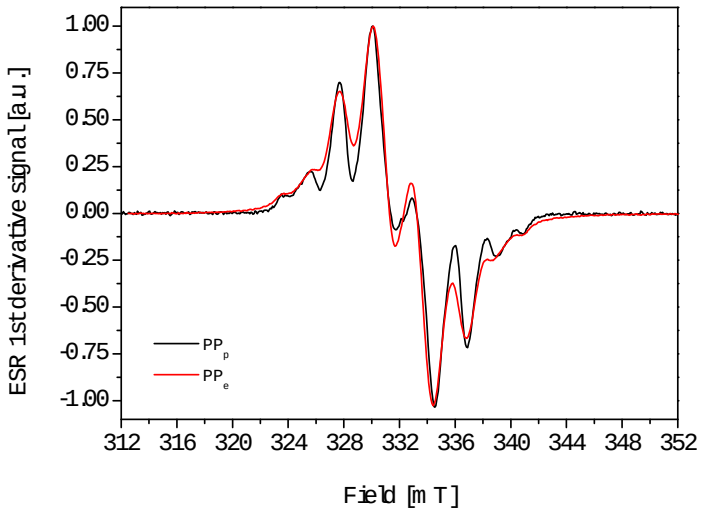

Figure 8.5: Comparison of the ESR spectra of the electron irradiated PP_e and proton irradiated PP_p.

Material	ρ [10^{19} e$^-$/g]	$\Delta\rho$ [10^{19} e$^-$/g]	Γ_{line}[mT]	$\Delta\Gamma_{line}$ [mT]
PP12	4.9	0.3	2.67	0.01
PP250	5.2	0.2	2.68	0.02
PP580	4.9	0.4	2.67	0.02

Table 8.2: ESR results of the irradiation of PE pellets in argon.

8.3.1 Decay channels of PP measured in CW-ESR

8.3.1.1 Room temperature measurement of decay channels

The polarisation characteristics of some irradiated materials can be positively influenced when the samples have been exposed to elevated temperatures for short periods of time [172], [173]. ESR spectroscopy can be used to monitor the change in spin density of heat treated samples, as well the any changes in the radical structures within the material. In this way it is possible to decide whether a change in the polarisation characteristics are more likely the result of a change in the radical structure, or whether other effects such as spin densities or the radical distribution play a greater role.

The first attempt at measuring the decay of the irradiation created radicals was to measure the sample dynamically. This meant that the sample was inserted into the spectrometer and allowed to decay at an elevated temperature. The radical decay is immediate once a certain temperature is exceeded and the sample must be inserted into the resonator as soon at it is removed from the liquid nitrogen storage and the fine tuning of the ESR spectrometer must be exceptionally fast. It is to be expected that the initial fast decay of the sample will then be slightly undervalued. A separate calibration measurement can give the real initial starting value of the radical concentration. The signal at room temperature is much weaker than in liquid nitrogen (see Curie's Law in section 2.2.2) and the signal intensity drops during the decay run, so that the measuring power was adjusted accordingly during the measurement. Every 60 s the field was automatically ramped once, covering the 40 mT range in 30 s. The octet structure is still the most dominant contributor to the overall spectrum, though a small substructure is apparent. As

the measurement concerns only the total area and not the actually rotational configuration of the radical, no attempt was made to fit the spectra of the first 10 min of decay shown in figure 8.6. As far as the identification of the predominant radical is concerned one does not see a marked change in the overall structure, disregarding the small substructure previously mentioned.

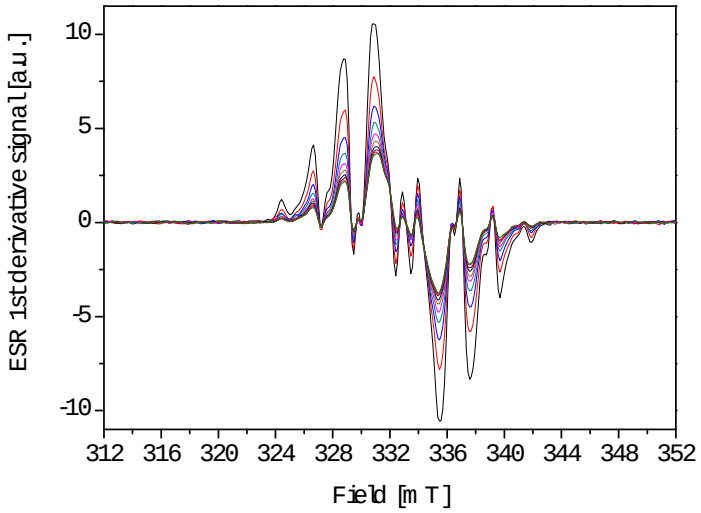

Figure 8.6: First 10 min of decay of the ESR spectrum of electron irradiated PP measured at room temperature.

First attempts at measuring the radical decay were done in air. Even though as the literature suggests oxidative processes do play a role in radical yields and decay processes, it was believed that the process is slow enough that the influence is marginal in the time regions one would be interested in (<15 min). The creation of peroxyl radicals requires that a carbon radical is created first, as the two oxygen atoms attach to the radical site, moving the site of the unpaired electrons foremost to the end oxygen atom, far away from the protons in the molecular chain [174]. In the conversion process of the primary radical it is evident that there is a very slow increase of a sub-structure in the ESR spectrum, however the contribution of the latter to the spectrum on a whole is minimal. Only after a day or longer decaying in air does it becomes clear that the substructure is in fact due to the peroxyl radical. In addition, the peroxyl radicals also decay, albeit at a very slow rate, by a diffusion controlled mechanism of the mobile radical sites [175], so with time these radicals also disappear. The spectrum of the peroxyl radical in PP created after a day decaying in air at room temperature is plotted in figure 8.7. The plot also includes the simulated curve for the same data. The data fits well with following values

$$g_{xx} = 2.03219, \quad g_{yy} = 2.00656 \quad \text{and} \quad g_{zz} = 2.00139$$

where the signal of the peroxyl radical has only contributions from the anisotropic g factor and no hyperfine coupling. The signal is highly anisotropic with an anisotropy of

$$\frac{\Delta g}{\bar{g}} = (1.54 \pm 0.04) \times 10^{-2} \tag{8.4}$$

which would lead to significant broadening at higher fields[3]. This field dependent broadening excludes the radical from any possible DNP based experiments, as it is not to be expected that high

[3] EHBA has the worst g factor anisotropy of those materials discussed in chapter 4 with 6×10^{-3}, however the anisotropy of the peroxyl radical in PP is still a factor $2^{1/2}$ times larger. By comparison the g factor the TEMPO and porphyrexide radicals are around $\sim 4 \times 10^{-3}$

polarisation values can be obtained by its use. In addition to the high g anisotropy there is the immense drawback of very low radical yields. Though the peroxyl radical can be easily identified after prolonged heating, it must be noted that the peroxyl radical itself is not a stable radical and may have an influence on the overall kinetics of the decay. Even if not present in high enough concentrations to be detected in the mixed ESR spectrum, it is possible to conceive that the decay rate of the primary radical is accelerated by the diffusing oxygen. As one would like to identify a specific mechanism that influences the polarisation characteristics of the material, the measurement of the change of structure in air does not help to isolate what these specific parameters may be, so that the decay in an oxygen free environment should take precedence over the measurement of the decay processes in air.

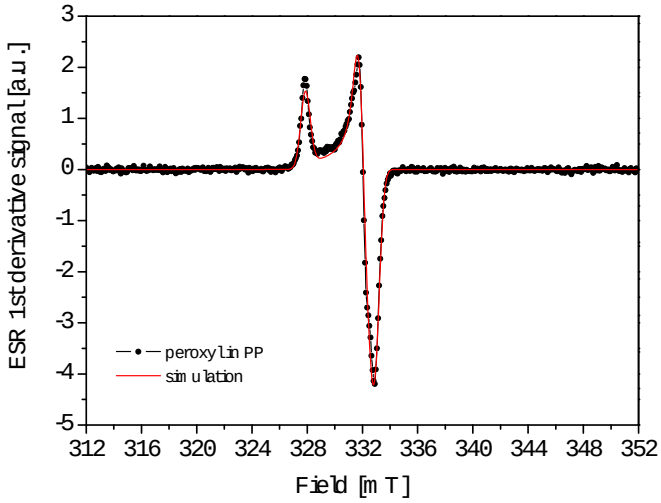

Figure 8.7: ESR of a peroxyl radical in PP taken at 77 K after heating at room temperature.

8.3.1.2 77 K measurement of decay channels

To eradicate any oxygen based influence on the decay character of the radical, the decay was observed for samples heated at room temperature in a nitrogen gas atmosphere. To increase the sensitivity, samples were measured under liquid nitrogen, where here the automation of measurement, that was possible at room temperature, had to be forfeited. The samples were heated for an allotted time and then once again frozen in liquid nitrogen. If one was to repeat this process in the incrementation of the room temperature measurement, the decay rate of the reaction would be shifted to longer times as the heating of the sample material is not immediate, bringing in a small constant error per measurement and effectively shortening the actual period of decay. As it is difficult to judge how long the sample takes to acquire room temperature, the better option is to start afresh for each heating period with a new sample, assuming that as the samples are from the same irradiation batch they all have the same initial spin concentration. In this manner all samples have the same initial thermalisation period and the decay curve only gets shifted by a small amount, not influencing the overall decay rate. This method was employed for various time periods of heating and gave highly reproducible results for all samples.

Figure 8.8 shows an example of a curve of the total radical concentration versus time, measured in this fashion for a PP12 sample, where the error bars have been omitted for reasons of clarity. The heating of the sample leads to a significant drop from the initial spin density followed by a region in which the decay is slowed. This fits well with the observations made by Gvozdic et al. [162], as detailed

in section 7.2. There does not seem to be any discernible difference in the decay rates of our sample materials, with the radicals in PP12, PP250 and PP580 samples all decaying at similar rates and having similar asymptotic end values. For a fixed temperature the decay is determined by the initial local distribution of the radicals and the diffusion mechanism along the molecular structures, so from this point of view one wouldn't expect the materials to show any major differences in their decays as 1) the material compositions are very similar, as determined by DSC 2) the initial concentration of the radicals is similar, as determined by ESR and 3) the diffusion mechanism and the associated rate constants would not be expected to vary, as they are solely dependent on the interaction mechanisms determined by the molecular structure of the material (and temperature).

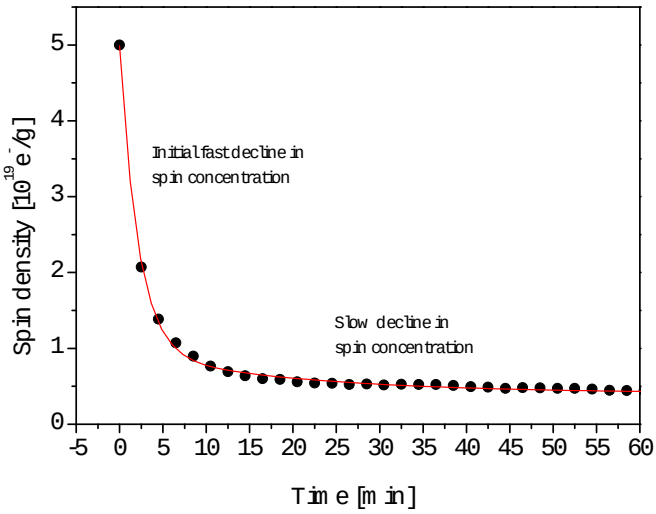

Figure 8.8: Decay of the spin density in irradiated PP caused by heating of sample in nitrogen.

Even after the warming of the sample, the fitting of the line of centre of the transitional lines gives an average peak separation of the main components of (2.3 ± 0.05) mT. Overall the total ESR signal width decreases with time, which is an indication of loss in the number of radicals, whilst maintaining the same governing ESR structure. This will be presented with the helium irradiation results in the next section for the samples that were used for later polarisation. As the alkyl radical is the only radical present in the PP sample, even after the heating of the sample materials, any polarisation characteristics that are measured can be attributed to this radical. To see how the polarisation of the samples changed after heating, samples were heated in the manner described above for periods of 2.5, 5 and 10 mins and subsequently polarised. The values of the spin density were checked by ESR measurements and cross-checked with the decay curves and gave good agreement. The spin densities of the samples used for polarisation were

$$(2.1 \pm 0.2) \times 10^{19}\,\mathrm{e^-/g} \quad (1.2 \pm 0.1) \times 10^{19}\,\mathrm{e^-/g} \quad \text{and} \quad (0.8 \pm 0.1) \times 10^{19}\,\mathrm{e^-/g}$$

in the order of 2.5, 5 and 10 mins heating periods, respectively.

8.4 ESR of PE/PP irradiated in helium by electrons at the LINAC2

Figure 8.9: Irradiated PE and PP pellets.

The continuation of the irradiation programme at the LINAC2 included a widening of the scope of materials and for the first time it was also possible to irradiate the PE materials HDPE, LDPE and LLDPE, as well as the PP materials. For reasons of comparison all materials were first irradiated with the same dose of 2.8 mC incident charge of electrons, which calculates to a dose 7.3×10^{14} e^-/cm^2, over the allocated temperature region. The dose reduction in comparison to the argon irradiations is due to the fact that the evaluation of the polarisation characteristics showed that the nuclear relaxation of the PP samples was particularly fast. To counteract this phenomena lower doses were used to reduce the spin concentration produced in the irradiation process. After irradiation the irradiated polymers are easily distinguished, with the PP samples being green in colour in contrast to the PE samples that showed a bright orange colouring. The intensity of the colouring lessened somewhat after exposure to light, but the bleaching did not lead to any loss of the spin density of the materials, a process that has also been seen in other irradiated target materials, e.g., ammonia.

As with the PP samples in the previous irradiations it was evident that the major differences in the spin densities of the materials, lies in the differences of the base polymer and not any other material characteristic, such as the material density or the molecular weight. The materials of the polymer group of a single temperature batch are almost identical and thus the average of all sample materials of that batch were taken as the corresponding spin density of the whole material at that temperature. For clarification, this means that near equal spin densities were created in the group of PE materials: LDPE, HDPE and LLDPE and also in the PP group: PP12, PP250 and PP580, so there is no inner group distinction. In terms of crystalline and amorphous content of the polymers it follows that there is no preferential region within the polymer for the creation of the primary radicals. This is to be expected for high energy electron interactions with the polymer material, where in principle the crystalline/amorphous regions would be expected to show only very minimal differences, as the overall density differences in the materials are small and it is the density of the overall material that determines the number of interactional centres.

It is evident though that the radical production mechanism in PP is much more effective than in PE and the yield of radicals we have measured were around 40% higher over the irradiated temperature range, though there is no reason to believe that this can be generalised for all temperatures, as the radical yield is expected to be highly temperature dependent, as well as being dependent on the type of irradiating beam. However, the tendency of PP to produce higher yields than PE has been reported in the literature for UV-irradiation at a temperature of 77 K by Rånby and Yoshida [176] and the 30% greater yields of PP over PE when irradiated in vacuum at 77 K by γ-irradiation measured by Carlsson et al. [177] are also consistent with the results of our electron beam irradiations.

As figure 8.10 shows, for both materials there is a drop over the analysed temperature range in the radical yield to higher temperatures, highlighting the problem of creating stable radicals in sufficient quantities at higher temperatures. This is most likely due to the temperature dependent recombination process of the primary alkyl radicals during irradiation. At low temperatures one creates the primary alkyl radicals that are then stabilised by the lack of thermal energy of the system. At higher temperatures the mobility of the radicals is increased, increasing the decay rate of the radicals. The analysis of the

ESR spectra of both the PE and PP irradiated materials shows that at all of the irradiation temperatures the alkyl radicals are the dominant radical in all spectra: These radicals were described in section 7.1.1 and section 7.1.2. Once again the eight peak structure of the PP radical is evident, with the same splitting as determined for the previous samples. In the ESR spectrum of PE radical (shown in figure 8.11) we see the main six peaks with an average separation of (3.1 ± 0.1) mT. The substructure that is visible in the peaks is due to the non-equivalence of the α and β protons. The substructure does not have any particular relevance for our studies, as the signal is still purely a hyperfine split spectrum and can be approximated by a six peak structure sufficiently well. Due to the larger peak separation in PE, but the reduced number of peaks, the outer peak spacing of the PE and PP radical are very similar (3.1×5 mT=15.5 mT for PE and $2.2 \times 7 = 15.4$ mT for PP).

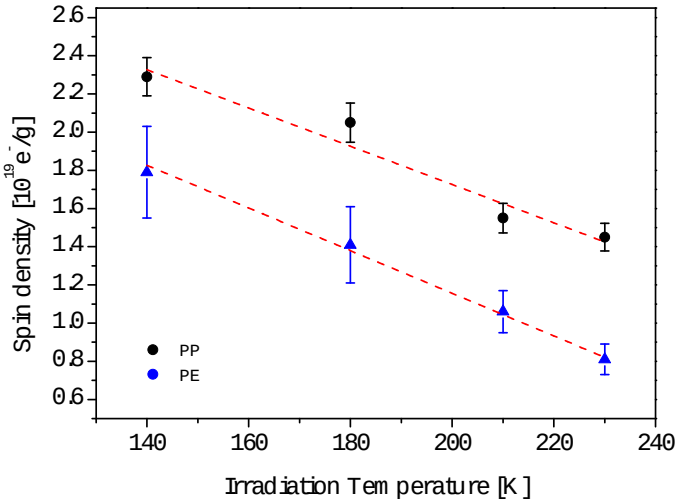

Figure 8.10: The dependence of the irradiation temperature of the total radical concentration in electron beam irradiated PE and PP.

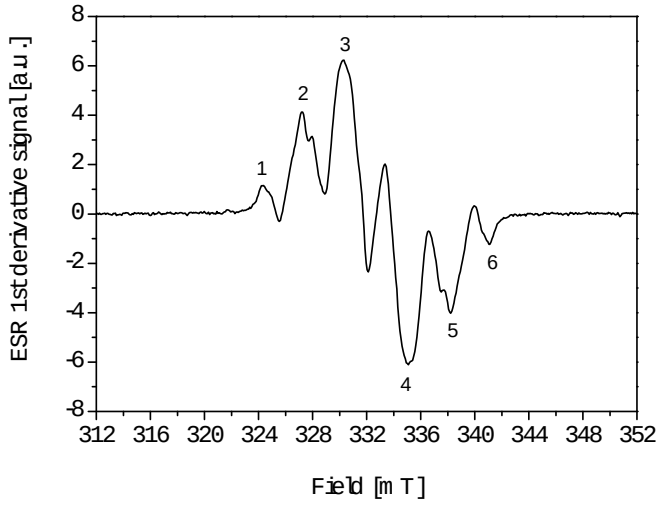

Figure 8.11: 1st derivative ESR spectrum of the electron beam irradiated PE.

After the initial polarisation tests further irradiations were conducted at higher doses, those doses consisting of multiples of the initial dose. Whereas preliminary tests at 140 K showed linearity of the spin concentration with dose, that was no longer the situation for the higher temperatures. For the PP samples an irradiation of double the initial dose only gave ~ 80% of the value obtained by doubling the initial spin density. By the same calculation at a temperature of 210 K a tripling of the initial dose only gave ~ 70% of the calculated linear values. For the PE samples roughly the same ratios applied, so that even though both doses were not linear with the increase of dose they nevertheless maintained the yield ratio of 40% higher radical yields in the PP materials. Though saturation effects can play a role in irradiation processes, the data suggests that is more an effect of elevated temperature and would go in line with the observation made for the temperature dependent drop in the single dose measurements of the spin density. This highlights how important it is to have beam stability, as the time of the actual irradiation would influence the yield of the radicals created. Additionally, it also shows the importance of lowering the temperature immediately after the irradiation period to maintain the stability of the created radicals. The spin densities of the materials that were later polarised for the 180 K irradiation of double dose corresponding to 5.6 mC of charge injection were

$$(3.4 \pm 0.2) \times 10^{19} e^-/g \text{ for PP} \qquad \text{and} \qquad (2.4 \pm 0.2) \times 10^{19} e^-/g \text{ for PE}$$

and for the 210 K irradiation of triple dose corresponding to 8.4 mC of charge injection

$$(3.6 \pm 0.3) \times 10^{19} e^-/g \text{ for PP} \qquad \text{and} \qquad (2.1 \pm 0.2) \times 10^{19} e^-/g \text{ for PE.}$$

The linewidths of the samples are comparable to those previously obtained and will be discussed in the chapter summary 8.6, however a remark in advance is that at higher temperatures we see a reduction of the linewidths, which can be attributed solely to the reduction in the radical concentration.

8.5 Conversion process of alkyl- to allyl-type radicals in PE

The results of the polarisation tests of heated PP samples (see section 10.2) showed that the heating of PP samples leads to an increase in the polarisation values. Obviously, this invites one to propose that the same positive effect can be achieved by the heating of PE samples. As tempting as this idea may be, in reality the situation is slightly more complicated than is the case for PP. It was shown that the PP radical remains the same radical type throughout the heating period. This is not the case for PE materials that exhibit a conversion process from the alkyl-type radical to an allyl-type radical when heated at room temperature. If one were to see an enhancement of the polarisation, it is much more difficult to determine which radical is producing the positive effect. For this purpose one would like to isolate the radical in the material, i.e., only have one or the other radical.

It is possible to produce the alkyl radicals directly by irradiation, but to produce the allyl type radical (see figure 8.12), as described in section 7.1.1, a heat treatment of the samples after the irradiation is needed, where the primarily created radical (the alkyl) is completely converted at room temperature to the more stable secondary radical. The heating process follows the same procedures outlined in section 8.3.1.2, where the PE samples were heated for up to $1^{1/2}$ h. The heating of samples allows for an easier and more controlled mechanism to create the allyl radical than the high dose, high temperature irradiations, described in the literature, as the irradiation at an elevated temperature will always be accompanied by an unproportionally large net loss of the paramagnetic centres. As some DNP theories predict that a radical with a narrower linewidth should have better polarisation capabilities (see section 2.3.4), the allyl radical would seem to be a highly interesting prospect for future research. In

addition to the alkyl radical, because, as figure 8.13 shows, the linewidth of the allyl radical is narrower still than that of the alkyl radical.

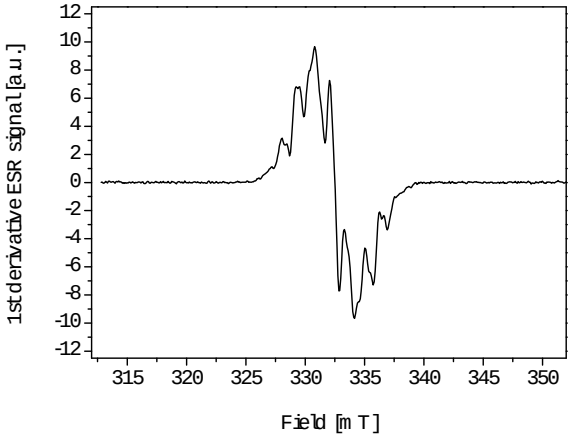

Figure 8.12: 1st derivative ESR signal of the allyl radical in PE.

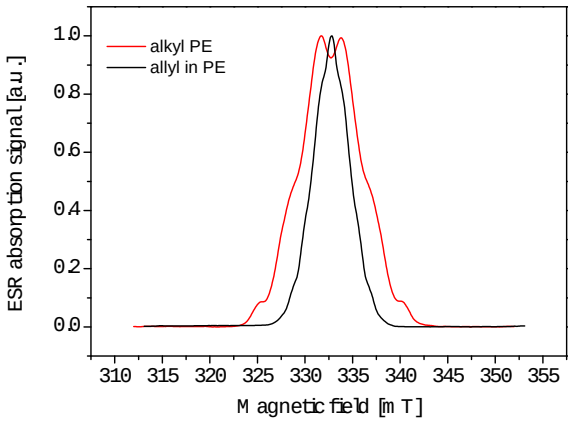

Figure 8.13: Absorption ESR spectrum of the alkyl and allyl radical in PE.

A common method to analyse the conversion of the alkyl radical to the allyl radical is to monitor the height of the outer wing peak in the ESR spectrum of the alkyl, as this has no overlap with the ESR spectrum of allyl radical [144]. Though this is not particularly difficult it does come with an inherent error, as it assumes that the lines are rather narrow, which is not the case for highly irradiated materials. The outer peaks can be fitted easily in the absorption spectrum and as we know the relative structure of the rest of the ESR signal, the alkyl components can be reconstructed. If one then subtracts the alkyl contribution from the whole of the absorption spectrum one gets the contribution of the allyl radical. The conversion process is illustrated in figure 8.14. Here we can see the total spin density decay, which is easily measured by CW-ESR. The alkyl decay, as determined by the above described process, fits well with the diffusion based equation postulated by Johnson and given by equation 7.1. The allyl radical sees an initial build-up to a maximum value before then decaying, also.

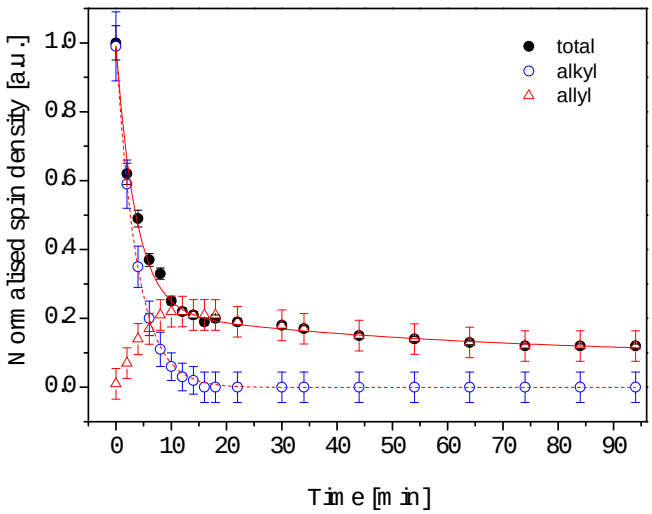

Figure 8.14: Alkyl radical decay and the build-up and subsequent decay of the allyl radical.

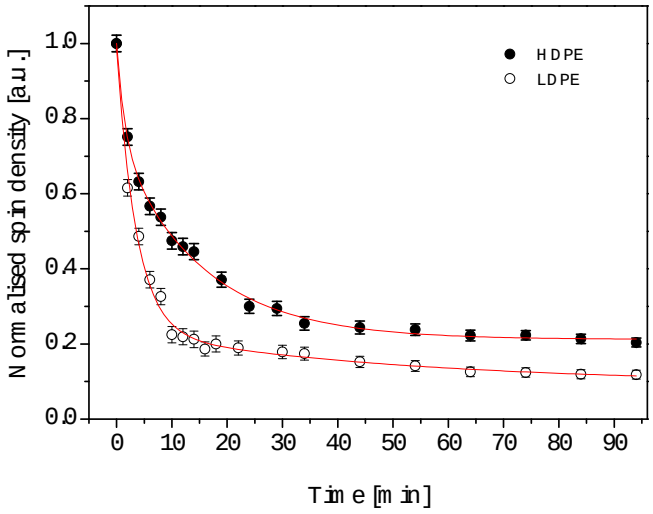

Figure 8.15: Decay of spin concentration of HDPE and LDPE.

If one considers that the decay mechanisms are diffusion based then it would be expected that the decay in the HDPE samples would be slower, as they have a higher crystalline content. The radicals in the amorphous phase of the polymer decay faster, so the decay in LDPE should be faster, also. This can be verified by our decay measurements. An example of the decay process is given in figure 8.15 for a HDPE and LDPE sample that have been irradiated (and heat treated) under the same conditions. Apart from the differences in the total decay rates the graph also shows another interesting characteristic of the samples. Though the prolonging radicals are decaying at approximately the same rate, the extrapolation of these curves does not go to zero, but to a material specific value, with the HDPE samples showing higher values of the residual radial.

The decay curves of HDPE and LDPE always converge to a fixed ratio, which is determined by the initial fraction of the free radicals created in the crystalline regions of the polymer and the initial dose. This is evident in the fact that the allyl concentration in HDPE is higher than that of the LDPE and that the amount of allyl remaining in the material is linear with the initial dose for both materials The values of the final spin density are plotted versus the initial density for both materials in figure 8.16. If one takes the ratio of the slopes of the linear fits one obtains the value $0.21/0.35 \approx 60\%$. Furthermore if one considers the ratios of the values of the crystallinity, as determined in chapter 5, we get $42\%/70\% \approx 60\%$, so the data gives a strong indication that the crystallinity is the determining factor in the quantity of the residual radical. As the purpose was to illustrate the process the errors have not been discussed in any detail, but if the aim of future research was to study the polarisation characteristics of the allyl radical, then the heating of the sample would provide a method with which these could be produced. Due to the high numbers of radicals that are persistent in the HDPE sample the obvious advice would be to chose a highly crystalline PE material.

To see how this calculates to actual irradiation time, and determine the practicability of such an irradiation, one could assume a linearity in the radical production for the dose, which is most definitely not true due to the radical saturation characteristics of the polymer. For every $1 \times 10^{19}\,e^-/g$ created within the material of HDPE $\approx 0.35 \times 10^{19}\,e^-/g$ are left after heating. Due to the higher yield production lower temperatures would probably be preferred, e.g., at 140 K. At this temperature $1.8 \times 10^{19}\,e^-/g$ were produced in $\sim 2^{1/2}$ h at the LINAC2, so to produce, lets say, a typical spin density of $2 \times 10^{19}\,e^-/g$ of allyl radicals, one must first produce $2/0.35 \times 10^{19}\,e^-/g \approx 6 \times 10^{19}\,e^-/g$ alkyl radicals, which then calculates to

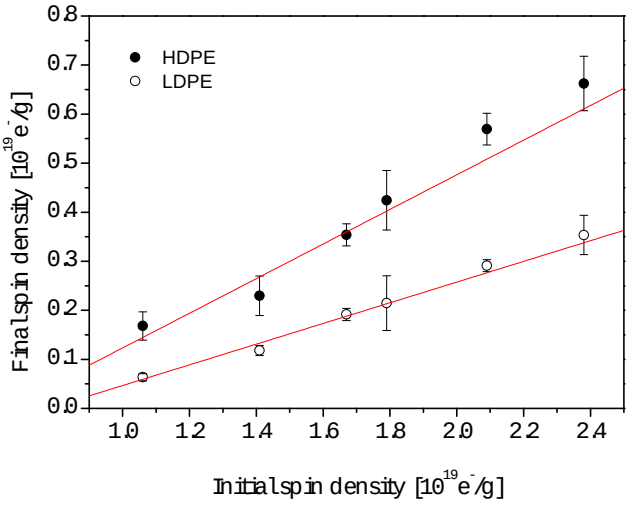

Figure 8.16: The relationship of the initial and final spin densities in HDPE and LDPE.

a total irradiation time of $6/1.8 \times 2.5\,\text{h} \approx 8\,\text{h}$. In practice one would likely have to irradiate stepwise as to avoid saturation effects. This would entail the irradiation, a heat treatment and then further irradiations, repeating the previous steps, until the desired spin concentration is reached. However, one must also consider that at high level irradiation doses there is also the possibility to create another radical in PE called the polyenyl radical, this is discussed in the appendix A.1. This additional radical may be a hindering factor in the creation of allyl radical in sufficiently high concentrations.

A concluding remark: An attempt was made to polarise the allyl radical in the highest doped HDPE sample. However, the polarisation build-up of the sample was far too slow. The continual build up of the polarisation signal was observed for two days and then the attempts were stopped. In principle a slow material is not automatically an exclusion criteria, but the inability to take a decent TE signal is, as the polarisation can not otherwise be evaluated. The conclusion is that the radical concentration of allyl was too low and thus irradiations to higher doses must be conducted to achieve higher concentrations.

8.6 Summary of ESR evaluation

All irradiations produced radicals that are identified in the literature, and were discussed in chapter 7, as being of the alkyl type. This was independent of the projectile type, but also of the irradiation temperature. For the PP samples an octet structure with an average peak separation of 2.2 mT and for the PE samples the sextet structure with an average peak separation of 3.1 mT are the clear identifiers of the radicals produced in the interaction of the projectiles with the medium. The ESR signals of all materials are very symmetric. The assumption is that all signal structures can be described by inhomogeneous broadening caused by hyperfine splitting and that the g anisotropy is very small. Regarding the mentioned structure, it could be shown that even after heating the PP samples at room temperature in an oxygen free atmosphere the alkyl type radical is still the dominant radical in the material, as identified in the ESR spectra. If other radicals are present there is no marked influence on the overall ESR structure and it can be safely assumed that the polarisation characteristics that were subsequently measured can be attributed to the primary radical.

As was desired, based on previous experience of the concentrations needed for efficient DNP, all irradiation programmes produced spin densities $\propto 10^{19}$ e$^-$/g in all PE and PP materials. A major difference in the actual numbers of radicals produced in PE and PP is evident, with the PP materials containing 40% more radicals than the PE materials when irradiated at the same temperature and to the same dose. However, no influence of the molecular weight in PP, or the density in PE, on the radical numbers produced was measured, so that it seems the crystallinity does not have an influence on the amount of radicals that are produced within the materials. This suggests that the radicals are produced throughout the polymer materials, independent of material composition, i.e, in the amorphous and crystalline phase.

The signal width in X-band of both the PE and PP materials are similar and large in contrast to the signals obtained from chemically doped butanol, but it is the comparison with the widths at higher fields that are more relevant. If we assume that the signals obtained arise solely from the hyperfine action, or if at least there is a contribution due to the anisotropic g factor that it is small enough that it can be neglected, then the signal width at higher fields remains the same, though for the discussed chemically doped materials all have a g factor anisotropy that becomes relevant at higher fields. The predicted ESR signal width of the polymer samples at 2.5 T is only about 50% of the EHBA-Cr(V) doped samples. In a way this is the worse comparison to make, because the broadening is unproportionally large in comparison to the other common target materials: For the porphyrexide and TEMPO doped samples of butanol the signal width of the irradiated polymer samples are about a third larger.

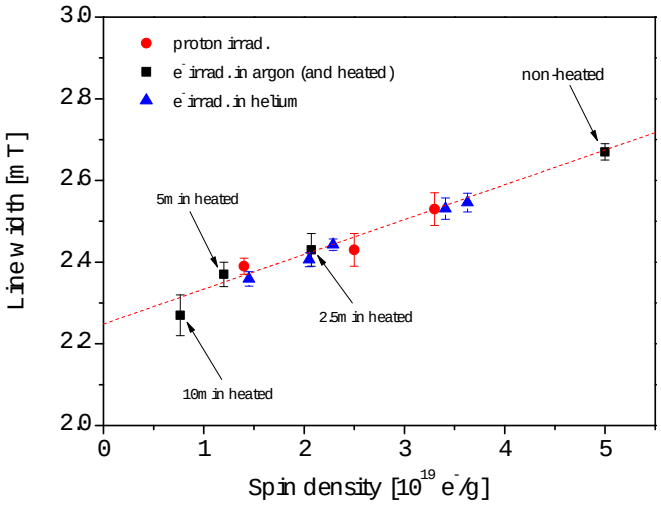

Figure 8.17: The relationship of the linewidth on the spin density in irradiated PP samples.

At higher temperatures we see a reduction of the linewidths of the PP material, which can be attributed solely to the reduction in the radical concentration. To put this into perspective we can plot all the linewidths of the PP samples in one graph, and we see that there is indeed a relationship between the individual linewidths and the spin density of the material, where for the heated samples only those that were used for later polarisation are included. As long as the lines are predominantly homogeneously broadened by the dipolar interactions due to the electrons one would expect this linear relationship. For our sample material with spin densities in the order of 10^{19} e$^-$/g this is most certainly the case. Though the linewidth does not give us access to any material specific parameters that could help to optimise the polarisation characteristics, it is a pointer that the overall characteristics of the irradiated materials fit into a broader picture. However, here we must be slightly cautious as it has been shown that small spin density clusters in highly irradiated solids give the same broadening as a homogeneous distribution of

the same amount of radicals [178]. This means that the unsaturated CW-ESR technique can be used to quantify the overall spin density of materials, but it does not tell us anything about spacial distribution of these radical sites. Access to this type of information can only be accessed by advanced pulsed ESR methods, that were unavailable to us at the time of this study.

This broad comparison of the linewidths does not make sense for the PE samples, because of the reduced amount of data points, and the above made observations certainly won't apply for annealed PE samples. As was detailed in the previous section heated samples of PE show a conversion from an alkyl to an allyl radical. Nevertheless, the small reduction of the linewidth for the higher temperatures is noticeable. In the PE materials there is a conversion process involved in the annealing process and thus the end linewidth does not have anything to to with the initial linewidth as they do arise exclusively from the same radical. Similarly, this also applies to the PP samples when heated in air, as here we see an influence of peroxyl radicals of the ESR structure.

Lastly, for an estimate of the effectiveness of the radical creation of the protons on the foils (this includes the mechanism and the procedure) we can compare the yield of created spin densities to the amount of incident protons. Using the values obtained from the calculations provided in section 6.3 it can be calculated that for a 25 mg piece of foil, depending on the irradiation time, between $(3.5 - 8.3) \times 10^{17}$ unpaired electrons were created within a single piece of foil. These amounts of electrons were created by $(1.1 - 3.4) \times 10^{14}$ protons. This means on average approximately 3000 unpaired electrons were created per incident proton. We can compare this to the proton irradiation dose and spin densities of the 1970s CERN irradiations (also see section 6.3). Here we have $\sim$ 5000 unpaired electrons created for every incident proton, so that the results are certainly comparable. However, the CERN irradiations were at much higher energies and the irradiated material was ammonia, which is known to be extremely radiation hard, making it difficult to judge whether the obtained values for the polymer are reasonable.

We can also compare this, e.g., to the lowest temperature electron irradiation in liquid argon. A quick calculation shows that a charge of 4.2 mC incident irradiation consists of 2.6×10^{16} electrons. Theses create spin densities in the order of $5{\times}10^{19}$ e^-/g in a target material container holding approximately 50 g of polymer material. This means that for every incident electron approximately 10^5 unpaired electrons are created within the material. This value is significantly higher than those in the proton irradiations. Due to the completely different systematics, specifically the temperature, one cannot say that the electron irradiations are per se more efficient than the proton irradiations, a conclusion the numbers however do seem to suggest in this case.

CHAPTER 9

Helium refrigerator test facility

ESR spectroscopy in X-band and DSC crystallinity measurements were used to classify the sample materials. The final and most important analysis, especially in regard to the FOM as mentioned in section 4.4, is the determination of the polarisation characteristics of the materials. Before the results of these measurements are presented in the next chapter, a short introduction into the apparatus and the procedures will be given. The chapter starts with the basic components of a solid state polarised target, before moving onto the working principle of a helium refrigerator, i.e., how does one get to cryogenic temperatures experimentally. Concluding the chapter the measuring principle of the polarisation determination by NMR will be presented.

9.1 Polarised target system

The absolute minimal setup needed for thermal polarisation, as described in section 3.1, consists of a refrigerator, with an incorporated vacuum system that is needed to cool to very low temperatures, and a magnet: Greater nuclear polarisation is achieved at lower temperatures and higher fields. However, boundaries are set by the experimental implementation of the polarised target. Increasing the magnetic field does increase the polarisation, but the bending radius of charged particles, potentially created as products in the collision of the incoming particles in the field of the nucleus, are then reduced, making the detection and the tracking a much more difficult task. This effectively limits these types of high field experiments to neutral particles, e.g., neutrons or gammas. The lowering of the temperature always comes with the understanding that in particle scattering experiments some energy from the beam will be deposited in the target material and must be cooled away. However, the cooling power of a refrigerator drops exponentially with temperature [179], highly restricting the base temperature that can be achieved with a particle beam, which practically limits low temperature experiments to low intensity beams. Experiments using statically polarised targets are extremely rare, but do exist. A magnetic field of 10 T and at a temperature of 10 mK still only produces proton polarisations of ~50% in most known target materials and the samples can take 2-6 months to reach full polarisation [180]. Higher polarisation can be achieved using DNP at low temperatures, but at, by comparison, moderate magnetic fields and at much faster rates of polarisation.

One of the test facilities in the Polarized Target group's laboratory in Bonn consists of a ^{4}He refrigerator with an operating temperature of around 1 K and a solenoidal superconducting magnet producing a magnetic field of 2.5 T with a field homogeneity of $\Delta B/B = 5 \times 10^{-5}$ [181] over the test material

volume. We use DNP to reach high polarisation values by microwave irradiation. The Larmor condition for the transitions of the electronic states, dictated by the magnetic field strength, calls for a microwave source that drives the DNP process producing microwaves with a frequency in the vicinity of 70 GHz. The microwave source that was used can produce microwaves in the frequency range of 69.63 GHz to 70.23 GHz with a maximum output power of ~150 mW. The polarisation is determined using an NMR system based on the evaluation of the susceptibility of the NMR-coil that surrounds the polarised target material. As the thermal equilibrium polarisation signal is used as a calibration for the dynamically enhanced signals, the temperature of the thermal bath within the cavity containing the target material must be known to high precision. The refrigerator uses a temperature monitoring system based on the measurement of the electronic resistance of a variety of strategically placed resistors. The thermometry of our system is assessed using a cryogenic resistance bridge, the *AVS-47 AC Resistance Bridge* produced by *Rv Elektroniikka Oy Picowatt* [182]. The refrigerator is equipped with a multitude of resistance elements, all using a four-wire resistance configuration: For the high temperature measurements we find it sufficient to use PT100 resistors. These become less sensitive at lower temperatures as they have positive temperature coefficients. For lower temperatures we use carbon based resistors with negative temperature coefficients, and especially where the exact temperature is needed we use calibrated resistors of the type *Cernox*® (Zirconium Oxy-Nitride) produced by *Lakeshore* [183].

9.2 Working principle - helium as a refrigerant

Since helium was first successfully liquidised by Kamerlingh-Onnes in 1908 [184], helium has become the principle cryogenic refrigerant for the cooling of superconducting magnets and is used in particle physics experiments requiring low base temperatures in a variety of different refrigerator systems. Helium is one of the lightest elements, actually the lightest noble gas, and the Van der Waals force between the atoms is very small. The lighter the element, the greater the influence of quantum mechanical effects, which in this case reduce the distance dependent interatomic forces even further: The ground state energy is given by $E_0 = \hbar^2/2mV^{2/3}$, where m is the atomic mass and V is the atomic volume, and is quite large for helium, due to the light mass of the helium atom. The ground state energy is also positive, corresponding to a repulsive force which balances the attractive forces between the atoms. The consequence is that helium can remain in a gaseous state even down to very low temperatures. Under normal atmospheric pressure standard helium liquidises at 4.2 K, but due to its lack of a triple point (solid/liquid/vapour coexistence) it does not solidify when the pressure is dropped further, but can remain liquid down to $T \to 0$ K.

The basic principle of a helium refrigerator is to lower the vapour pressure above the liquid phase of the helium, resulting in a drop of temperature. The decisive point is that if one knows the pressure of the vapour directly above over the liquid phase to high precision one could calculate the temperature. An empirical equation giving the relation of temperature and the saturated vapour pressure is given by Preston for the ITS 90 scale [185]:

$$T = \sum_{i=0}^{9} A_i \left(\frac{\ln(P) - B}{C} \right)^i , \tag{9.1}$$

where P is the pressure in units of Pascals and A_i, B and C are coefficients particular to the two helium isotopes (summarized in appendix A.3). Equation 9.1 is valid down to 0.65 K for ^{3}He and down to 1.25 K for ^{4}He. Below 1.25 K the equation that describes the pressure-temperature relation for ^{4}He is

given by Donnelly and Barenghi [186] as

$$\ln(P) = i_0 - \frac{L_0}{RT} + \frac{5}{2}\ln(T) \tag{9.2}$$

where P is the pressure in units of Pascals, $L_0 = 559.83\,\mathrm{J/mol}$ is the latent heat of evaporation at absolute zero, $i_0 = 12.2440$ is a scaling constant and $R = 8.314510\,\mathrm{J/(K\,mol)}$ is the molar gas constant.

Using the equations 9.1 and 9.2 the relation between pressure and temperature of the two helium isotopes have been plotted in figure 9.1 for the temperature range of 0.5 K to 2 K. The lower binding energy of ^{3}He results in a higher vapour pressure, meaning that 1) the pumping speed needed to reach the same temperature of, e.g., 1 K, is significantly less for ^{3}He than for ^{4}He and more relevantly 2) for the same end pressure, determined by the pumping capability of the system, the temperature reached with ^{3}He is lower than that achieved at the same pressure with ^{4}He. ^{3}He is a very rare isotope and has the distinct disadvantage of being very expensive, a reason why ^{3}He is only used in highly isolated systems where the ^{3}He can be recirculated. The minimum continuous temperature that can practically be achieved in this manner is nevertheless still limited to around 300 mK for ^{3}He [179]. For our ^{4}He setup experience has shown that in stable operation the pressure of the helium vapour over the liquid phase reaches the lower 10^{-1} mBar region (~ 10 Pa) resulting in a minimum temperature in the region of 960 mK. The pressure and the temperature can be further reduced by reducing the helium flow into the refrigerator and thus reducing the back-stream of helium. This so-called single shot mode is not suitable to measure samples over a prolonged period of time, especially if the build-up and relaxation times are quite long, as was often the case with the polymer samples we analysed. Though the pressure does indeed give a good indication of the temperature, standard pressure gauges usually do not give values to the very high precision needed for the calibration of the NMR signals. For this reason, a separate independent high precision temperature measurement is necessary.

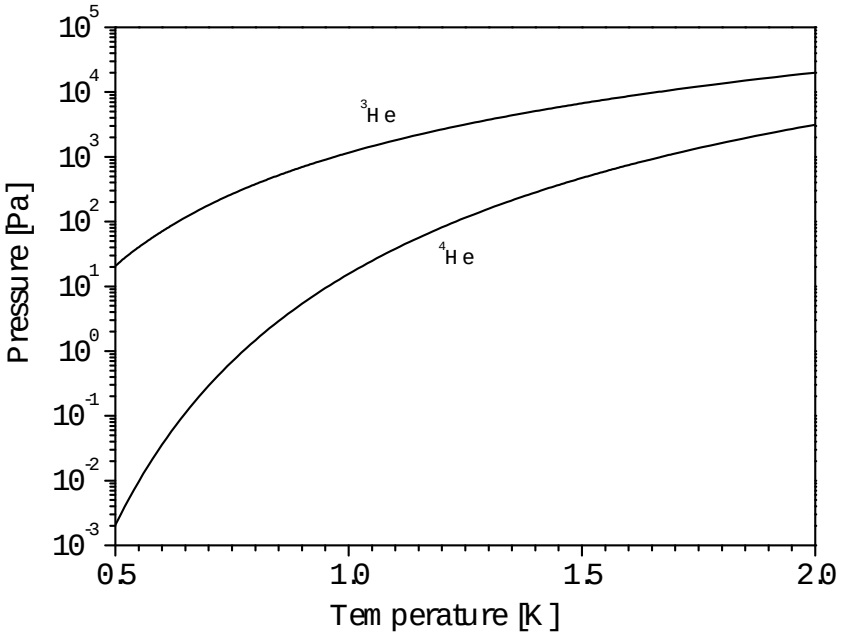

Figure 9.1: Relationship of the pressure and the temperature for the saturated helium vapour of the isotopes ^{3}He and ^{4}He.

If one wishes to achieve extremely low temperatures one can use a dilution refrigerator which utilizes the phase separation at 870 mK of a ^{3}He/^{4}He mixture into a highly concentrated ^{3}He rich phase and a ^{3}He poor phase. By pumping over the dilute phase the ^{3}He molecules are extracted above the liquid, driving the ^{3}He molecules of the rich phase through the phase boundary into the dilute phase, which is an endothermic process, removing heat from mixing chamber walls [187]. As the eventual aim would be to use a polymer target in a ^{3}He/^{4}He dilution refrigerator at very low temperatures, all potential materials must also be tested under these conditions. However an extensive measuring programme, including the changing of many samples and cooling them, is cumbersome and time consuming in a dilution refrigerator in comparison to the measurement at 1 K in the simpler ^{4}He refrigerator. A measurement at a temperature of 1 K still gives an impression of the performance capabilities or potential drawbacks of materials and though one cannot fully deduce the behaviour of the material at lower temperatures from such a measurement some general conclusions can still be made. The polarisation and relaxation characteristics of all irradiated samples were measured under similar conditions in the ^{4}He refrigerator.

9.3 Practical considerations for the operation of a helium refrigerator

Some of the more important components of a ^{4}He refrigerator are illustrated in figure 9.2. How a refrigerator of this type practically works is best explained by the path of helium through the system. The helium is fed into the refrigerator via a vacuum insulated rigid liquid helium transfer line. The liquid helium first arrives at the separator. Just as the name implies the job of the separator is the separation of the incoming helium into its liquid and gaseous phase. The separator is pumped independently from the rest of the refrigerator with a small pump of 100 m^3/h pumping speed, with the aim of extracting the gaseous vapour. The back-stream from the separator is then used to cool the outer heat shield via a coupling to a heat exchanger. After the initial pre-cooling of the system the separator temperature in operation is approximately 4 K. Once the separator is cold enough, a level of liquid helium is maintained ensuring that only liquid is fed into the cavity, which helps the overall pressure stability of the system.

In the cool down period the helium can be routed directly into the cavity via a bypass (not illustrated on the schematic), allowing for an overall faster cooling of the system. However this is ill advised in typical running operation, as the helium that leaves the separator flows through an additional heat exchanger, which is used to cool an inner heat shield, before finally arriving in the cavity containing the sample material with the incorporated NMR coil. The bypass is then only used when filling the cavity with helium as it otherwise only creates a surplus helium flow into the cavity which would increase the pressure and temperature as well as failing to cool the inner heat shield.

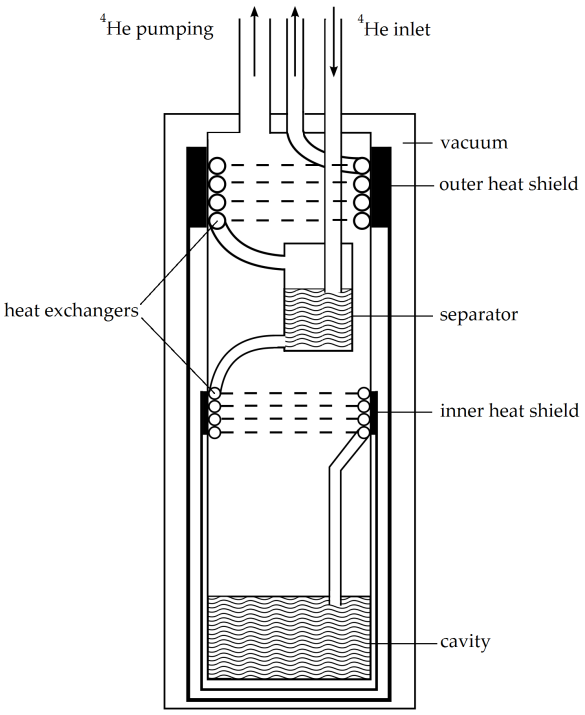

Figure 9.2: Schematic of a helium refrigerator.

The idea is to regulate the flow into the separator such that a steady level of helium in the separator and cavity are maintained, i.e., the amount of helium pumped off as vapour is compensated by the incoming liquid.

If one considers the working point temperature of the refrigerator one must assess all possible heat sources with the aim of minimisation where possible. A stable operation of the refrigerator is only possible if the refrigerator can produce compensating cooling power. As previously mentioned an experiment with beam will always have an inherent heat source given the beam/target material interaction. Another of the main source arises due to the manner in which the target materials are polarised. Any irradiation with microwaves will naturally lead to heating in the cavity, whether this is heating due to the microwave/target material interaction or due to the microwave/cavity walls interaction is irrelevant. In the so-called "frozen-spin mode", used presently in the ^{3}He/^{4}He dilution refrigerator for the Crystal Barrel Detector, the polarisation is built-up to high values and then the microwaves are switched off and the polarisation is allowed to relax at lower temperatures, but because of the polarisation relaxation the build-up of polarisation with microwaves must be routinely "refreshed". The test measurements in the ^{4}He refrigerator are similar in the sense that the build-up of the polarisation is done with microwaves, obviously without external beam, and once the maximum polarisation is reached the microwaves are switched off and the polarisation decay is then monitored. By simply reducing the microwave power by attenuation the heat load on the refrigerator can be greatly reduced.

Another source of heat input comes in the form of thermal radiation. Along the refrigerator the input is reduced by copper baffles, which are discs with numerous little holes to allow cooling by the flow of helium gas back-stream. Within the refrigerator there are two heat shields: The inner and outer heat shield. For a grey body of surface A at a temperature T has a total power emittance of:

$$P = \epsilon \cdot \sigma \cdot AT^4 \tag{9.3}$$

with the emissivity ϵ<1 and the Stefan Boltzmann constant $\sigma = 5.67 \times 10^{-8}$ W/(m^{2}K^4). To minimise the heat input into the refrigerator one must ensure that 1) the heat shields are as cold as possible and 2) the emissivity is as low as possible. The cooling of the heat shields is regulated by the helium flow in the refrigerator. The heat shields consist of a copper base material, coated in a very thin, highly polished gold coating to ensure a low emissivity.

To stop heat transport by gas interaction between the refrigerator walls, the system as a whole is thermally insulated from room temperature by pumping to a high vacuum with turbo-molecular pumps. The cold walls of the refrigerator act as a cryo-pump, extracting energy from the residual gas molecules, further reducing the pressure and thus the transport of energy from the outer to inner surfaces of the vacuum jacket, as less molecules are available for the transport of energy, and those lesser numbers of molecules also have lower kinetic energies. Maintaining a good thermal insulating vacuum is usually quite simple and the heat input from thermal conduction of this type can normally be neglected.

The last heat source to be discussed is that arising from heat conduction into the system by solid connections from room temperature to the cooled cavity bath. The structural materials of the actual refrigerator are chosen with a compromise between low thermal conductivity and structural stability in mind. Where more stability is necessary stainless steel is used, opting for thin walled and tubed structures where possible. An option is also to hinder thermal conduction by the insertion of materials with low thermal conductivity, e.g., standard polymer types, within the carrying structure. The purpose of the refrigerator is not just limited to cooling, i.e., the additional components of the polarised target must also have their place in the apparatus. The NMR system, the microwave supply line and the electronic connections for the thermal resistors are all inevitable heat sources.

In section 9.2 it was shown that the relation of pressure and temperature for helium can be given by empirical equations. The theory that describes the phase transition of a material is given by Clausius-Clapeyron [188], [189]. For the pressure-temperature relation the line separating two phases is known as the coexistence curve:

$$\frac{\mathrm{d}p}{\mathrm{d}T_{gas}} = \frac{S_{\mathrm{gas}} - S_{\mathrm{liquid}}}{V_{\mathrm{gas}} - V_{\mathrm{liquid}}}, \tag{9.4}$$

with V giving the molar volumes and S giving the entropy of the gas and liquid phases. This equation can be used to derive the cooling power $\dot{Q}$ of a refrigerator system that is dependent on the end pressure p (or temperature) and the pumping speed of the pumping station $\dot{V}$:

$$\dot{Q} = \frac{L(T)}{p_0 V_0} \cdot p \cdot \dot{V}, \tag{9.5}$$

with $p_0 = 10^5$ Pa and $V_0 = 22.710980 \times 10^{-3}$ m^3 being standard pressure and molar volume at 273.15 K. A full derivation, highlighting the many simplifications and assumptions that are made, is given in the diploma thesis of Harmsen [190]. At a temperature of 1 K ($p = 15.58$ Pa) the cooling power of our refrigerator can then be calculated for the values of the latent heat $L(T) = 80.22$ J/mol [186] and the pumping speed $\dot{V} = 1000$ m^3/h of the pumps. This calculates to 152 mW cooling power and considering the base temperatures we can achieve, one would have to assume that concerning the above made considerations, that we are getting the most out of the system and have little (or no) extra cooling capability, especially if one further considers that realistically the pumping speed will be lower due to the conductance dependence of the molecular flow on the bellows, transition pieces and surface areas of the guidance pipes.

9.4 Detection of polarisation - nuclear magnetic resonance

The next section follows along the lines of the explanation of the NMR specific determination of the polarisation given by Goertz, Meyer and Reicherz [191]. Though the following summary is in no way extensive, a brief flavour of the underlying principle of the measurement will be given here.

To measure the polarisation of the samples in a magnetic field one uses the principle of Nuclear Magnetic Resonance (NMR). The sample material is surrounded by a coil (for protons often just a single loop of uncoated cooper wire) which is placed so that a magnetic field is created perpendicular to the field direction of the external magnet. By connecting the coil in series to a capacitive element, an LC-oscillating circuit is created that can be tuned to the Larmor frequency of the nuclei by $\omega_0 = 1/\sqrt{LC}$. By the application of an oscillating RF field with a frequency that is close to the nuclear Larmor frequency of the protons in the material, one can achieve a change in the numbers of protons in each of the occupational levels by a reorientation of a minor proportion of the proton spins. The underlying idea of the NMR measurement is that the polarisation of the material has an influence on the electronic characteristics of the coil system.

The susceptibility of a system is defined as the proportionality constant between the magnetisation and a constant applied magnetic field B_0 with a permeability μ_0:

$$M_z = \chi H_0 = \chi \frac{1}{\mu_0} B_0. \tag{9.6}$$

In the same manner that the susceptibility is defined for a static external field, one can also define the susceptibility for an oscillating magnetic field B_1, by the splitting of the susceptibility into a real and a complex part:

$$\chi(\omega) = \chi'(\omega) - \mathrm{i}\chi''(\omega), \tag{9.7}$$

where $\chi'(\omega)$ is the dispersive and $\chi''(\omega)$ is the absorptive part of the susceptibility. The magnetisation of the sample material causes a change in the inductance of the coil:

$$L(\omega) = L_0(1 + 4\pi\eta\chi(\omega)) \tag{9.8}$$

which changes in the impedance of the coil:

$$Z(\omega) = R + \mathrm{i}\omega L(\omega) = \underbrace{R + \omega L_0 \cdot 4\pi\eta\chi''(\omega)}_{\mathrm{Z_R}} + \underbrace{\mathrm{i}\omega L_0(1 + 4\pi\eta\chi'(\omega))}_{\mathrm{Z_L}}, \tag{9.9}$$

where L_0 is the inductivity of the empty coil, η is the filling factor, giving a distribution function of the coil and target material volume, and R is the ohmic resistance of the coil. The filling factor is constant during the measurement of a sample and its direct influence goes into the calibration, i.e., it does not need to be calculated from first principles. The impedance can then be split into a real part, corresponding to the ohmic resistance of the coil and the imaginary part, corresponding to the inductive resistance. The average power loss/gain in the coil in terms of the susceptibility can then be given for the coil current I_C as:

$$P_\mathrm{C} = \frac{1}{2} I_C^2 (Z_\mathrm{R} - R) = \frac{1}{2} I_C^2 \omega L_0 4\pi\eta\chi''(\omega). \tag{9.10}$$

The power loss/gain is proportional to the absorptive part of the susceptibility, which is proportional to the magnetisation of the sample material, so the energy loss in the coil is caused by the change in occupational densities of the Zeeman populations. By integration over the whole frequency range one then obtains the polarisation measured as the area of the absorptive part of the spin susceptibility $\chi''(\omega)$ [192]:

$$P = C \int_0^\infty \chi''(\omega)\,\mathrm{d}\omega \propto A, \tag{9.11}$$

where C is a proportionality constant dependent on the filling factor η and the inductivity of the coil L_0, and A is the area of the absorption signal. For a spin 1/2 particle like the proton the thermal equilibrium polarisation can be written as:

$$P_\mathrm{TE} = \tanh\left(\frac{g\mu B}{2k_\mathrm{B}T}\right) = C \int_{\omega_0 - \Delta\omega/2}^{\omega_0 + \Delta\omega/2} \chi''(\omega)\,\mathrm{d}\omega \propto A_\mathrm{TE} \tag{9.12}$$

where ω_0 is the Larmor frequency and $\Delta\omega$ is the width of the frequency sweep. The calibration constant C is then calculated by the polarisation of the thermal equilibrium signal at the temperature T and applied external magnetic field B. The polarisation of the TE signal, calculated with the Brillouin function (equation 9.12), can then be used to calibrate the polarisation signals by comparison of the integrated areas of the absorption peaks:

$$P_\mathrm{dyn} = P_\mathrm{TE} \cdot \frac{A_\mathrm{dyn}}{A_\mathrm{TE}}. \tag{9.13}$$

Shown in figure 9.3 is a comparison of a TE and dynamic nuclear polarisation signal. The main figure is for the signal taken for a HDPE sample irradiated at 210 K by 2.8 mC of incident charge at ~17% polarisation with the TE signal seen as a small wiggle beneath the large signal. The inset shows an amplified section for the TE signal at approximately 0.25% polarisation. In this case the integrated area of the dynamically polarised signal is approximately 70x larger than the area of the TE signal. To obtain and fit the absorption signal one selects a window for ramping over the central frequency which gives an adequate zero-line for the fitting of the absorption peak to a Gaussian function. In the case of our samples we selected a window width of 512 kHz, corresponding to a 512 channel readout, giving a 1 kHz/channel sweep for all samples. As the TE signals are rather small a method must be employed to increase the signal-to-noise ratio (S/N-ratio). To do so the frequency is not ramped just once over the specified range, but done so repeatedly. The reason is quite simple: For a number n sweeps the signals can be added in each of the channels, resulting in a signal that is n times higher. By adding within the channels the signal noise also increases, but due to the statistical nature of its source, the noise only increases by a factor of $\sqrt{n}$, resulting in an overall improvement of the S/N-ratio by a factor of $n/\sqrt{n} = \sqrt{n}$. In all measurements the sweep number was maintained at $n = 100$ for the TE signals and reduced to $n = 50$ for the dynamically enhanced signals.

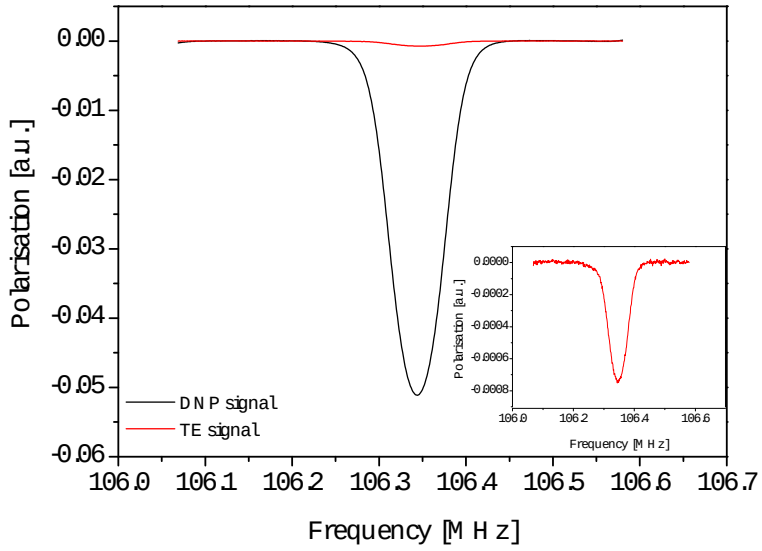

Figure 9.3: Comparison of the TE and dynamic polarisation NMR signal in HDPE.

CHAPTER 10

Nuclear polarisation and relaxation of PE/PP

Test measurements of the polarisation characteristics of the materials were conducted in a helium-refrigerator at temperatures around 1 K in a magnetic field of 2.5 T. The two main characteristics of interest for target materials are the relaxation time and the maximum obtained polarisation values. The typical method of analysing the polarisation characteristics is as follows:

- Determine the TE signal for the calibration of the NMR-spectrometer in the static magnetic field
- Determine the optimal frequency for DNP by varying the frequency of the microwaves
- Build up to max. positive polarisation with the optimal microwave frequency
- Relax from positive maximum polarisation (to TE-signal if time permits) by switching off the microwave source and thus stopping the DNP process
- Repeat previous steps for negative polarisation

To clarify the use of terminology, positive polarisation is defined as giving an NMR signal in the same direction as the thermal equilibrium signal, whereas negative polarisation gives a signal in the opposing direction. The build-up and decay of nuclear polarisation is described in the literature [44], [193]. Though not explicitly measured for our samples the build-up is given by the equation

$$\frac{\mathrm{d}P_\mathrm{n}(t)}{\mathrm{d}t} = W(P_0 - P_\mathrm{n}(t)) - \frac{P_\mathrm{n}(t) - P_\mathrm{TE}}{T_{1\mathrm{n}}} \tag{10.1}$$

where P_0 and P_TE are the thermal equilibrium polarisations of the electrons and the protons, respectively, and W is the growth rate constant of the proton polarisation and $T_{1\mathrm{n}}$ the nuclear relaxation time. Solving this equation gives the time dependence of the polarisation in the build-up period

$$P_\mathrm{n}(t) = \frac{W}{W + T_{1\mathrm{n}}^{-1}}(P_0 - P_\mathrm{TE})\left(1 - \exp^{-\left(W + T_{1\mathrm{n}}^{-1}\right)t}\right) + P_\mathrm{TE}. \tag{10.2}$$

The relaxation of the nuclear polarisation from any arbitrary polarisation value is given by the equation

$$P_\mathrm{n}(t) = P_\mathrm{n}(0)\exp^{-t/T_{1\mathrm{n}}} + P_\mathrm{TE} \tag{10.3}$$

with $P_\mathrm{n}(0)$, the start value of polarisation from which the nuclear polarisation is allowed to relax.

10.1 Proton irradiations of foils in vacuum

A foil material posed a new challenge for the use as a solid state polarised target, because the classically used materials are in pellet or crystal form and can be irradiated in bulk, providing ample material for the polarisation tests. The standard target material container can be filled with sample materials and an adequate NMR coil placed either through or around the target material. As the NMR detection is sensitive to the volume distribution of the material enclosed within the field of the NMR coil (this is the filling factor mentioned in section 9.4), then a foil poses a problem in the sense that the filling factor is quite poor for our standard sample holders, leading to a poor signal detection. One way too then increase the detection sensitivity is to reduce the distance of the coil from the material, i.e., use a smaller container, another improvement is to increase the number of windings of the detection coil, of which both methods were employed.

The new target material container (shown in figure 10.1) consisted of a perforated polytetrafluoroethylene (PTFE) tube of 23 mm length, 9 mm inner diameter and a wall thickness of 0.5 mm and an NMR coil made of 4 windings of uncoated copper wire. The loading and sealing of the tube was done under liquid nitrogen: The foil material was cut into strips and placed within the tube, between the windings of the NMR coil, and the tube was then finally sealed on either side by PFTE tape used as a bung. The tube was then placed within the "old" target container, which was then filled and packed with quartz (SiO_2) beads of 2 mm diameter to hinder the tube moving around within the cavity. The preferred use of the standard container was because it could be easily secured to the cryostat insert without any modifications.

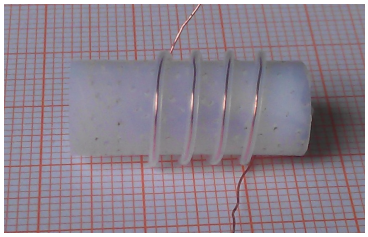

Figure 10.1: Target holder with NMR coil for the proton irradiated foils.

The relaxation time of all samples of the study was calculated from the average of multiple relaxation processes, including the relaxation from both positive and negative values of polarisation. In principle, the relaxation curves in figure 10.2 show the expected behaviour of the increased relaxation time for lower doses, though due to the lack of data points it is hard to say what the exact relationship between dose and relaxation time is. Though there are no surprises for the relaxation curves the polarisation data did turn up something unexpected. The polarisation curves showed that, accompanying the drop in relaxation time, the maximum polarisation values were increased to higher doses. This is shown in figure 10.3 and tabulated with the relaxation times in table A.2 in the appendix A.4. Under other circumstances one would increase the dose further to see if one can find the optimal dose, however this encouraging effect is diminished by the complete lack of adequate negative polarisation values, only achieving on average about a fifth of the values obtained for the positive direction. This is in contradiction to expectation, as one would presume the signals to be symmetrical, achieving very similar values in both polarisation directions. As the polarisation is linked to the electronic structure of the radical and the signal seen in the ESR spectrum seems to be very symmetrical, one would assume this to reflect on the polarisation structure. A deeper understanding of this problem would shed some light on feasibility of use of these materials as one may be able to control this problem. However, as of yet no concrete explanation can be given. Nevertheless, this observation has also been made for other polymers, with researchers also reporting problems with polarisation asymmetries measured for irradiated polymers [18]. On top of the unknown source of the asymmetry one can see that the overall polarisation is not particularly large in the first place, which is especially the case in the negative polarisation direction. Even in the positive polarisation direction the maximum enhancement in only in the order of twenty times higher than the thermal equilibrium polarisation. Common target materials tested under similar conditions show at least double these values.

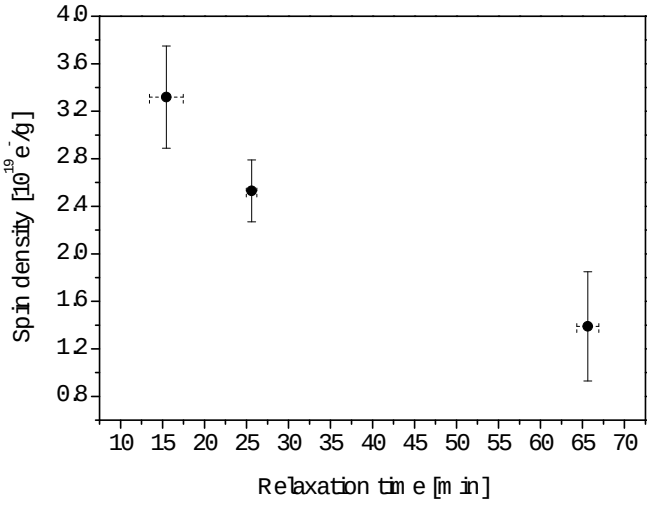

Figure 10.2: Relaxation times of the proton irradiated PP foils in dependence of the spin density.

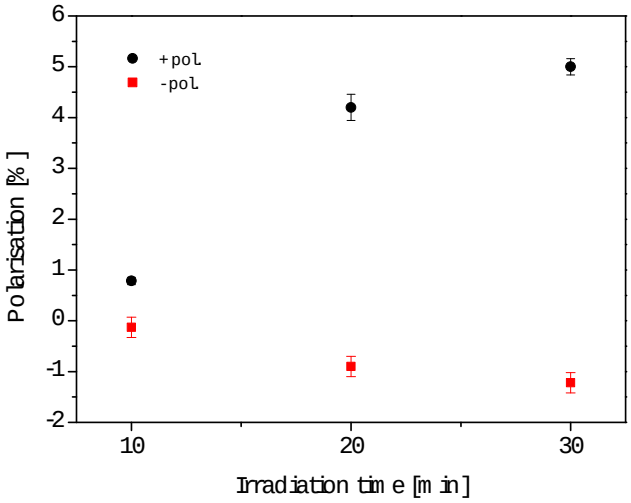

Figure 10.3: Polarisation for the proton beam irradiated PP foils versus time of irradiation.

Without a doubt, the proton irradiations posed more questions than they answered. The low polarisations could be a result of the irradiation temperature. Here one has the uncertainty of the actual temperature at irradiation, as well as the problem that the temperature could not be measured directly on the foils in addition to the lack of temperature control. The problem of the polarisation asymmetry could be an intrinsic property of the PP material, i.e., the radical created, however it may also be a property arising from the irradiation process with protons. On top of these unanswered issues comes the lack of a bulk preparation method, adding to the large systematic errors. It was decided to switch from the proton beam irradiations and focus as per usual on the electron beam irradiations at LINAC1. It was hoped at that time that irradiations under different conditions might shed some light on the underlying problems, or at least show whether the asymmetries may be a result of the the irradiation process with protons.

10.2 LINAC1 - Electron irradiations in argon

10.2.1 Samples as irradiated

Due to the maintenance of the cryostat in our laboratory at the time of irradiations, initial polarisation measurements were conducted in the laboratory of the Polarized Target group of the Bochum university. The group in Bochum, with which the Bonn group has a long standing working relationship, offered their help and expertise and it was possible to measure the polarisation characteristics of the irradiated PP in their ^{4}He refrigerator. The first batches of PP were analysed in their "SOPHIE"-cryostat, described in detail in the work of Harmsen [190]. This cryostat works on the same basic principles described in section 9.2 and also operates at a temperature in the vicinity of 1 K with a 2.5 T magnetic field. To check the reproducibility of the measured polarisation characteristics and to eliminate systematic errors when comparing results the samples were subsequently re-evaluated in Bonn in our cryostat and results were in very good agreement with those obtained in the Bochum laboratory.

As with previous measurements a crude frequency curve of the sample was taken, with the aim of gaining a first basic impression of the frequency dependency of the polarisation. To this end the frequency was varied from 69.7 GHz - 70.3 GHz in 50 MHz steps and the maximum polarisation for each frequency was determined (see figure 10.4). The ideal frequency for positive polarization was in the vicinity of 69.8 GHz, compared to the 70.2 GHz for negative polarization[1], thus resulting in an immense frequency difference of ~400 MHz in comparison to the 300 MHz commonly seen for chemically doped butanol. The ideal frequency was later found by fine tuning the frequency around these core values and monitoring the effect on the polarisation. For subsequent measurements the values previously determined were used and fine tuned in the individual measurement. No stand out difference in the frequency curves of the various PP samples could be found, all exhibiting the same large frequency width. Based on this rudimentary frequency curve alone, one can already see that the asymmetry problem encountered in the previous measurement no longer seems to carry the same weight. Even though a slight asymmetry can be seen it is in no way comparable to those seen for the proton beam irradiations.

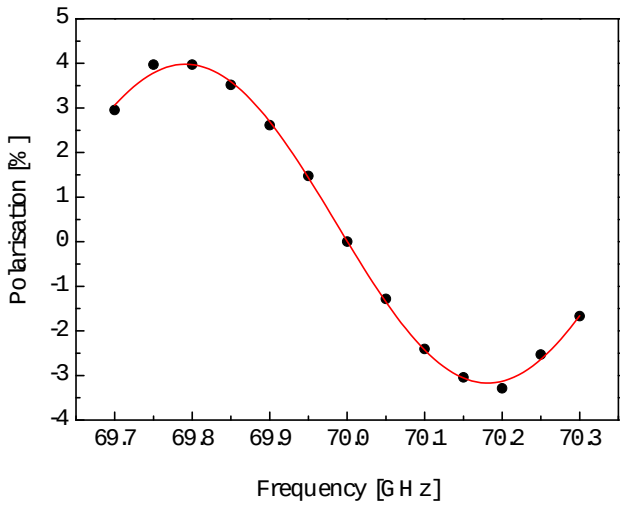

Figure 10.4: Frequency curve of the irradiated PP580 sample.

[1] These values are similar to those obtained for the proton beam irradiated materials.

The build-up of polarisation in the samples was extremely fast. Between switching the microwaves on and the next NMR sweep the maximum polarisation is more or less already established, so the build-up is somewhat shorter than a minute. The relaxation of the polarisation signal was measured after turning off the microwave source, but maintaining the magnetic field. All relaxation curves can be fit by a first order exponential decay, an example of a representative curve is given in figure 10.5. The relaxation time of all the sample materials was comparable with

$$(132 \pm 10)\,\mathrm{s}, \qquad (116 \pm 10)\,\mathrm{s} \qquad \text{and} \qquad (122 \pm 10)\,\mathrm{s}$$

for the PP12, PP250 and PP580 materials, respectively. The maximum measured values of the polarisation for the samples were

$$+4\%/-3.3\%, \qquad +3.8\%/-3.2\% \qquad \text{and} \qquad +3.7\%/-3.1\%$$

in the same order each with an absolute error of 0.2%. The first impression is that the molecular weight of the samples had insignificant influence on the polarisation values that were achieved. However the polarisation values are still quite low, having an enhancement of sixteen times on the thermal equilibrium polarisation. This may be due to the spin density of the material being too high, as the same coupling of the electron and nuclear spins that allows for an effective build-up of polarisation by DNP, also offers a mechanism for the nuclear spins to relax when the microwave field is switched off. This is effectively seen in consequence by the very fast build-up and relaxation times.

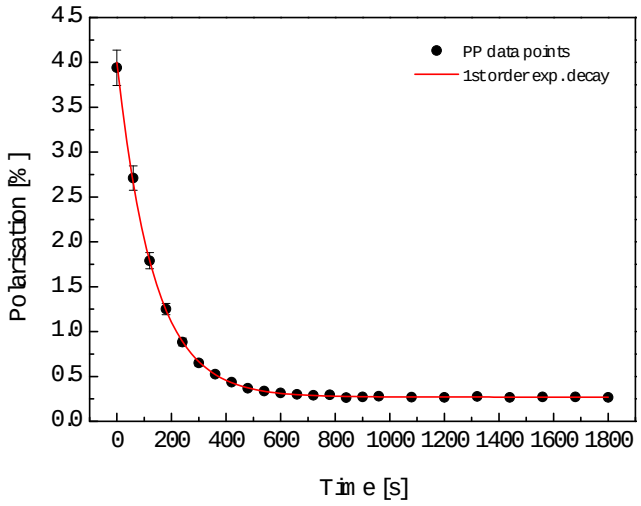

Figure 10.5: Example of relaxation in PP12 from the positive maximum polarisation to the TE polarisation.

Though the asymmetry is still noticeable, the negative polarisation value manages about 80% of the maximum values obtained in the positive direction, which is an obvious improvement on the asymmetries seen in the proton beam irradiations. These values seem to indicate that the vast asymmetry seen in the polarisations may lie in the systematics of the irradiation. From this standpoint the decisive factor would seem to be the difference in the beams. Though temperature dependent effects can not be fully excluded, as the irradiation also took place at different temperatures. The two main temperature implementations that are seen to affect the polarisation characteristics are the irradiation temperature, and possibly also the annealing of the sample materials at temperatures higher than the irradiation temperature. As the irradiation cryostat is designed to cool the samples in liquid argon there is no way to use this cryostat for the irradiations at other temperatures. Irradiations at various temperatures took place in

the helium gas cooled cryostat and will be discussed in section 10.3. For the samples irradiated in argon there is the option to heat the samples to room temperature and determine whether this heating has an effect on the polarisation and relaxation times.

10.2.2 Heated samples

At the time of the measurement it was not possible to conduct further irradiations at additional temperatures or at lower doses, therefore the effect of heating on the polarisation characteristics was examined. As mentioned in the previous section the spin density was believed to be too high and in section 8.3.1.2 it was shown that the heating of the sample reduces the number of radicals drastically, whilst retaining the same radical type. However one must be cautious with the conclusions from this type of experiment, because though the "active" radical is still of the same type, there are likely to be other influences playing a role other than the pure number reduction of the radicals to more favourable amounts, e.g., a change in the local distribution of the radicals.

The samples were heated for 2.5, 5 and 10 min in nitrogen, but already in these short periods of heating the change to the polarisation characteristics was remarkable. At first tests showed that the characteristics of the sample had changed, new frequency curves were taken for the heated samples. This proved more and more difficult with increasing heating time, as the "reaction" of the polarisation to a change in microwave frequency was slower and slower. It became clear that the heating of the sample in this time range does not change the frequency dependence of the polarisation and ultimately analogous frequency curves to those of the pre-heated samples were obtained. Once again it was not possible to find marked differences in the behaviour of the different PP materials. All samples reacted in the same manner and showed minor differences that can be attributed to small systematic errors alone. The complete results are summarized in tabulated form in table A.3 in the appendix A.5.

Whereas the relaxation of the irradiated samples was in the region of minutes, the heated samples showed extremely long relaxation times ranging up to the region of hours, so an extremely fast sample material had been gradually converted into an extremely slow sample material (see figure 10.6). This influence of the heating on the relaxation time is particularly apparent when the relaxation curves are plotted in the same diagram, as shown in figure 10.7, where four typical curves are presented for the different heating times.

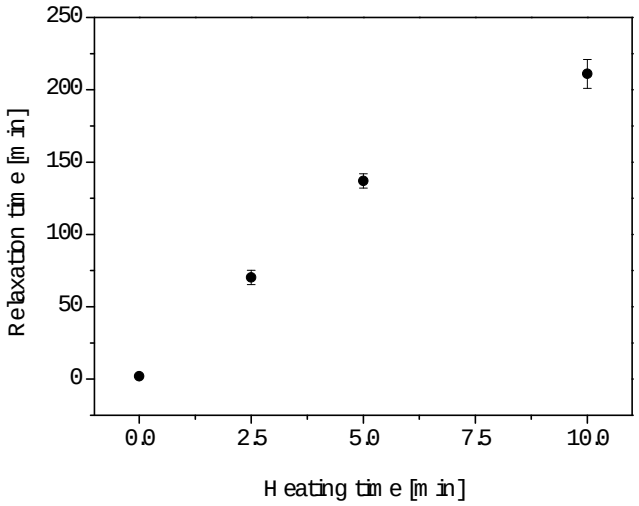

Figure 10.6: Relaxation times of irradiated PP after heat treatment at room temperature for 0, 2.5, 5 and 10 min.

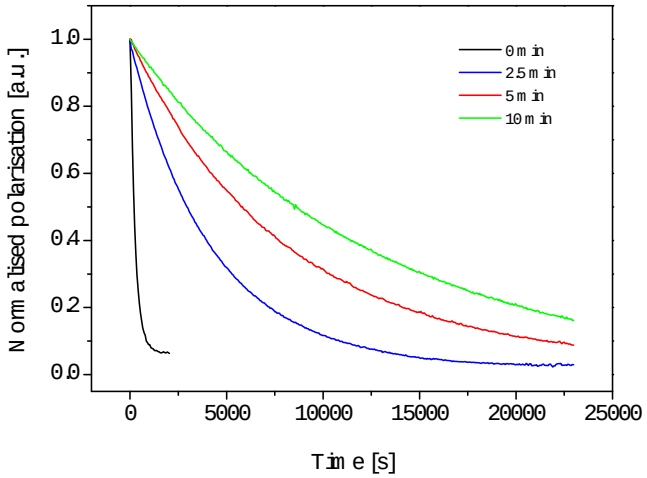

Figure 10.7: Relaxation behaviour of PP, where samples have been heated for 0, 2.5, 5 and 10 min.

The polarisation values of the irradiated materials were not very impressive at all. However, the polarisation values of the heated samples increased with heating time to values that were very promising. Where the initial polarisation of the PP samples was in the region of ~4%, with additional heating this could be increased to around ~14% (see figure 10.8). The polarisation of the heated samples show a steady increase of the maximum obtained values with heating time, but the difference between the sample heated for 5 min and 10 min is minimal and it it is not to be expected that much higher values could be obtained by additional heating. The main problem with the polarisation characteristics, once again, are apparent when one has a look at the negative polarisation of the materials, as the positive and negative values do not coincide. The inherent asymmetry of polarisation seems to be influenced by the time of heating. Even though the negative polarisation values increase with heating time, they do not seem to do so to the same degree as the positive values. For the relative polarisations we have measured 84% for the irradiated sample and 50%, 38% and 33% for the heating periods of 2.5 min, 5 min and 10 min. So in summary the heating of electron beam irradiated PP leads to longer relaxation rates and higher positive polarisation values, at the cost of an increased asymmetry of polarisation values, with the asymmetry already seen in the non-heated sample, but becoming larger for longer heating times.

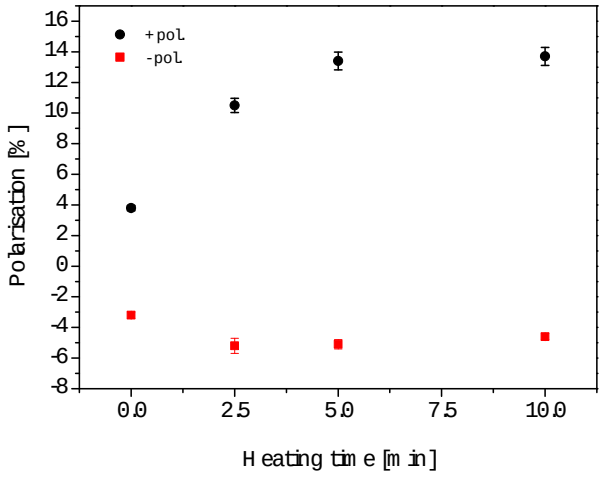

Figure 10.8: Polarisation of irradiated PP after heat treatment.

10.3 LINAC2 - Electron irradiations in helium

It was shown for the PP material that a heat treatment at room temperature increased the maximum values of the polarisation, as well as increasing the relaxation times. This positive effect may also be obtained by irradiating the materials above a material dependent specific temperature. In this way the "reorganisation" of the electronic structure can be obtained directly during the irradiation. In 20 min the change of the heated samples was more or less completed by the transition of the primary radical, created by the initial irradiation, into a quasi-stable state. In the case of the irradiation the same (or a similar) radical can be created over a period of a few hours in a much more controlled way. To find the optimal temperature of irradiation a wide range cryostat was used, which allows for a regulated temperature between 90 K and room temperature [131],[132].

Based on the observations of the decay regions of the radicals in polymers made by investigators in the past it is to be expected that the polarisation characteristics of the materials will be influenced by the mobility of the radicals during the creation process. The tendency of the samples to improved polarisation values after heating also indicates that a warmer irradiation temperatures is likely to produce more favourable results than irradiations at lower temperatures. The polymer samples were irradiated at temperatures of 140 K, 180 K, 210 K and 230 K with an incident accumulated charge of 2.8 mC, where for the first time in this study PE was added to the scope of the investigation. At a temperature of 140 K the radicals in both irradiated PE and PP are stable. It is only above a temperature of 155 K that a decay of the primary radical can be seen in PE [155] and in PP the radicals are stable up until a temperature of 170 K [149]. At temperatures of 180 K and higher the radicals in both sample materials are no longer stabilised and decay and rearrangement processes can start to take place. However, as described in part 8.4, even at these elevated temperatures the same type of radical is created in either material. As the PP samples had shown no molecular weight effects on polarisation, be that in the initial irradiation in argon or in the subsequent measurement on heating, as well as showing no differences in ESR structure or radical yield, it was decided to reduce the analysis of the materials to just one type of PP, so in all further accounts the characteristics of the PP the discussion is of the randomly chosen PP580 material.

10.3.1 NMR and polarisation curve comparison

When analysing material the NMR signal is used to determine the polarisation and though the signal does not give an indication of the polarisation characteristics of the material it is distinct for the individual materials.The NMR signal of PE/PP are extremely similar. For reference two NMR curves for dynamically enhanced polarisation signals are shown in figure 10.9. Both materials show a broader NMR signal than most commonly used target materials with a Gaussian lineshape with a FWHM of ~70 KHz, where doped butanol samples exhibit a narrower 50 kHz linewidth, regardless of the doping radical as the NMR signal is determined by the base material and not the dopant. The similarity of the NMR signal does not carry over to the polarisation characteristics of the materials, as will be detailed in the following sections. Though this is not surprising if one considers that the polarisation capabilities of the irradiated base materials are essentially determined by the different radicals that are created in the irradiation process.

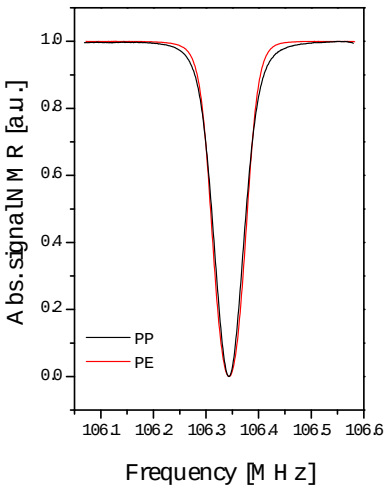

Figure 10.9: Comparison of the NMR signal for DNP enhanced polarisation signals of PE and PP

The frequency at which the maximum and minimum polarisation values were obtained are independent of material type and have a spacing of ~420 MHz. One has to conclude that the frequency dependency of the polarisation, in terms of the optimized frequency for the polarisation, is independent of the projectile type, i.e., protons or electrons, and is not influenced by a subsequent heating of the sample materials, or by the irradiation temperature in the range of 87 K to 210 K. This backs the observation that the radical type is maintained as no conversion processes are evident in the ESR structure.

The highly irradiated materials of PP gave a slight hint of some interesting underlying structure, so for reasons of comparison the most irradiated sample of HDPE and PP580 were then analysed with greater precision. The frequency dependency of the polarisation was checked by slowly ramping the microwave frequency from 69.65 GHz to 70.3 GHz in 10 MHz steps. For these highly irradiated materials a comparison of the curves is shown in figure 10.10. In the lower frequency ranges the polarisation curves follow the same general progression. This is not the case for the higher frequencies, where the asymmetry of the PP sample is once again visible. Especially the frequency curve of PP shows a distinct substructure, the frequency curves of the PE samples on the other hand show no such dominant substructure and were quite smooth. Nevertheless, at closer inspection one can also see a very slight peak-like structure in these curves. The frequency curve of the PE samples also have a broad plateau of ~ 80 MHz width in the positive polarisation direction, which is the broadening from the overlay of two of the underlying peaks.

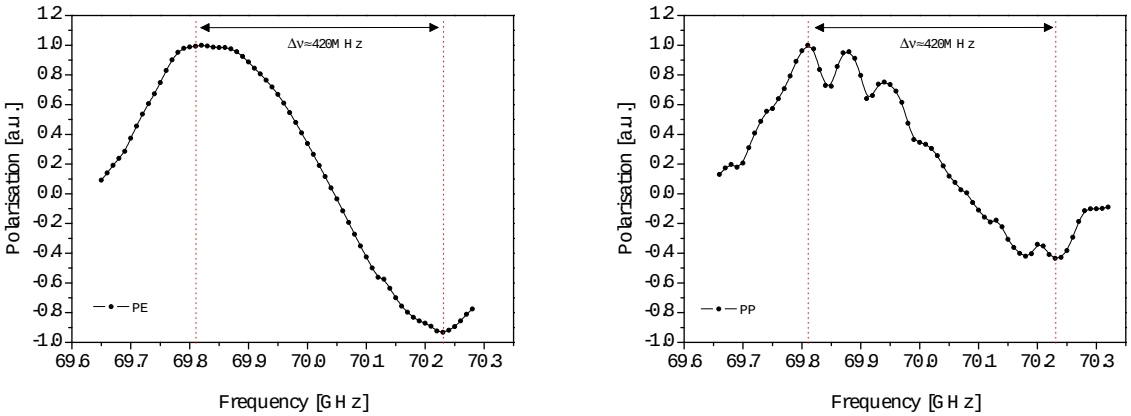

Figure 10.10: Comparison of the frequency dependency for the polarisation of PE and PP.

The polarisation curve is the reaction of the nuclear polarisation to the irradiation of the microwaves and reflects on the coupling of the nuclear system to the electronic system of the radicals within the material. Though this means that the polarisation curve is not synonymous with the ESR curve, it does however indicate how the polarisation of the material reacts to the underlying ESR structure. The natural assumption would then be that the structure one sees in the frequency curve is a direct result of the ESR structure and in this case would be given by the hyperfine splitting. The obvious peak structure in the frequency curve of the PP samples has an average splitting in the region of (60 ± 2) MHz, counting 8 peaks having a total of (420 ± 10) MHz separation. This is equivalent to a field splitting of (2.14 ± 0.07) mT and coincides with the values determined by the ESR measurements in X-band of (2.2 ± 0.1) mT[2]. The best values of polarisation coincide with the outermost peak structures of the radicals. We can reverse engineer this from the perspective of the outer peak separation in X-band

[2] This is under the assumption that the g factor is very close to the value of the free electron. Our field calibration gave an isotropic g factor of $2.0025 \pm (5 \times 10^{-5})$. The g value of hydrocarbon alkyl radicals are usually in the range of 2.0025-2.0028 [194].

(15.4 ± 0.1 mT). This is the equivalent of 432 ± 2 MHz and fits with the observations made in V-band. This also substantiates the claim of a very small g anisotropy as no additional structure is evident and the broadening of the polarisation curve at 2.5 T can be related to the structure seen in the X-band ESR. The PE curve exhibits unresolved components and thus it is not possible to do the same peak analysis. From the rough estimation of the peak positions one would certainly be justified in proposing that the same mechanisms in PE are involved as in PP, so that the frequency curve is the same mirror of the ESR structure dominated by the hyperfine splitting. The outer peak positions of the PE and PP radicals observed in X-band ESR are also in similar positions, mentioned in section 8.4, and the PE curve has many unresolved components and an overall linewidth that is similar to that PP. Then it is probably not at all surprising that the frequency curves follow similar progressions if the broadening mechanisms of both materials are predominantly hyperfine splitting in origin.

10.3.2 Relaxation characteristics

Due to the simultaneous irradiation of the polymer materials it was possible to compare the polarisation characteristics of PE and PP directly, as both had experienced exactly the same experimental conditions. Perhaps one of the standout differences of the materials was the radical yields, which can be considered to have a direct influence on the relaxation characteristics of the samples. The biggest distinction is that the PP samples were much faster in build-up and relaxation times, but the PE samples polarised to higher values. Whereas the slowest sample of PP had a relaxation time of 45 min the fastest PE sample had a relaxation time of over $2^{1/4}$ h. Another general trend for both materials was that the relaxation times became longer for higher irradiation temperatures. Of the four temperatures chosen for the irradiations only the samples of three lowest temperature irradiations were actually tested, as the relaxation times of the PE samples became increasingly long, making the measurement of the sample that had been irradiated at a temperature of 230 K highly unpractical.

A summary of the relaxation times of the PP and PE samples is given in figures 10.11 and 10.12. The different samples of PE show similarity in terms of their relaxation characteristics. Though the relaxation times for the HDPE samples were slightly higher than those measured in LDPE the deviation is not such that one could say that there are outstanding molecular influences at work and the measured values of the relaxation times for the LLDPE samples were situated somewhere between those of the LDPE and HDPE, so that there is no clear indication that the relaxation time is influenced by the density (or the crystallinity) of the PE samples. The relaxation rate in PP on the other hand is significantly faster and results in an approximately twenty-five times faster sample material. The two factors that could explain this are 1) the differences in the spin density of the materials for the same irradiation dose and 2) the differences in the coupling of the unpaired electrons to the nuclear systems.

To put this into perspective we can consider how the polarisation mechanism would effect the relaxation time. The solid effect involves the coupling of two spins, so that the relaxation rate is predicted to be linear to the spin density of the paramagnetic centres [44]. Both thermal mixing and the cross effect are described by three spin processes, involving two electrons and the nucleus. This inherently means that the relaxation rate of the samples is expected to increase with the square of the radical concentration [193]. One can assume that one of the latter processes describes the polarisation mechanism in these polymers. It follows that for the PP samples that show a higher spin concentration of about 40% more than PE for the same irradiation dose, it would thus be expected that the relaxation rate would increase, at least in theory, by a factor of approximately two for the equivalent radical. So in terms of the radical concentration being the dominant factor in the differing relaxation characteristics, this factor can be ruled out.

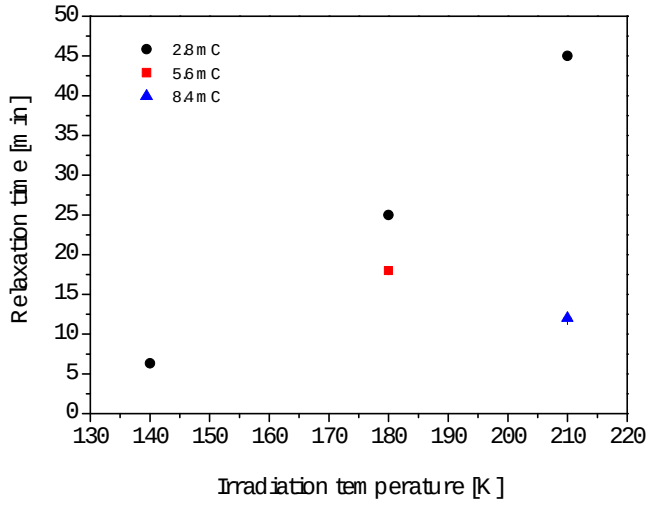

Figure 10.11: Relaxation results of PP electron irradiated in helium.

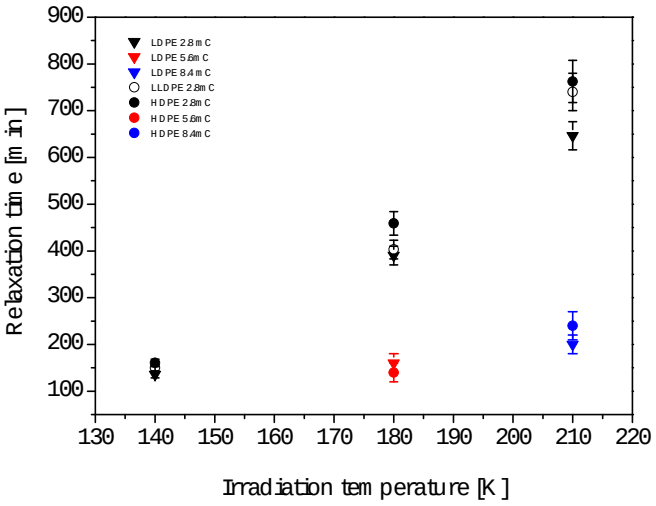

Figure 10.12: Relaxation results of PE electron irradiated in helium.

The measurement of the characteristics of the materials gave results that were very encouraging, especially in regards to the polarisation values that were obtained. This will be discussed shortly. However, the relaxation times of the PE materials were exceptionally long and faster samples would have a benefit at lower temperatures, as it is to be expected that these times would increase further when the temperature is reduced. To create faster materials it is necessary to create more unpaired electrons within the materials, which effectively means irradiating to higher doses. For the PP material the irradiation in argon at the LINAC1 had created a greater spin density within the material and this is evident if we compare the relaxation times to those obtained in this irradiation cycle. To see if the same effect could be achieved in the PE materials, HDPE and LDPE were irradiated at a temperature of 180 K and at 210 K to higher doses. For comparison the PP580 was also irradiated in the same batch. In all cases the desired effect was achieved, with the relaxation rate increasing.

10.3.3 Polarisation characteristics

The polarisation of all samples were measured and is presented in figures 10.13, 10.14,10.15 and 10.16 for the sample materials LDPE, HDPE, LLDPE and PP580, respectively. The total results of the LINAC2 irradiation programme are also given in the tables A.4, A.5, A.6 and A.7 in the appendix A.6. These tables include the polarisation values, the asymmetry value and the relaxation times that were measured for our samples. The data shows conclusively that all sample polarisations benefited from an increased irradiation temperature, with the polarisation values increasing with a shift to elevated temperatures. In terms of the maximum reached polarisation values the PE materials were clearly more successful with the maximum values trending towards 20%, whereas the values measured in PP did not even reach 10%.

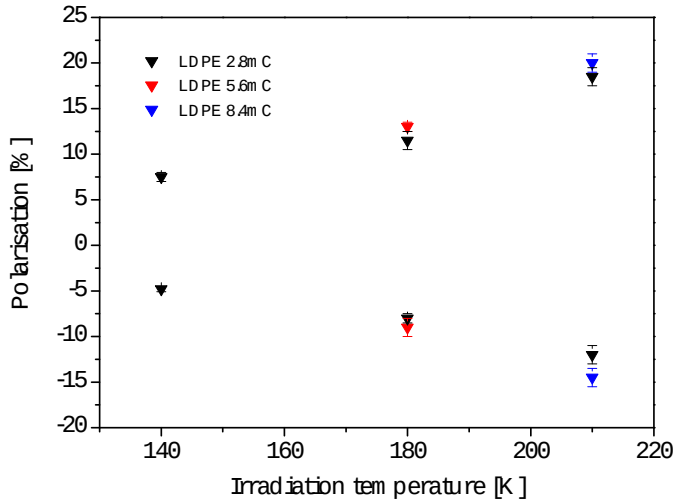

Figure 10.13: Polarisation results for the polarisation of electron irradiated LDPE.

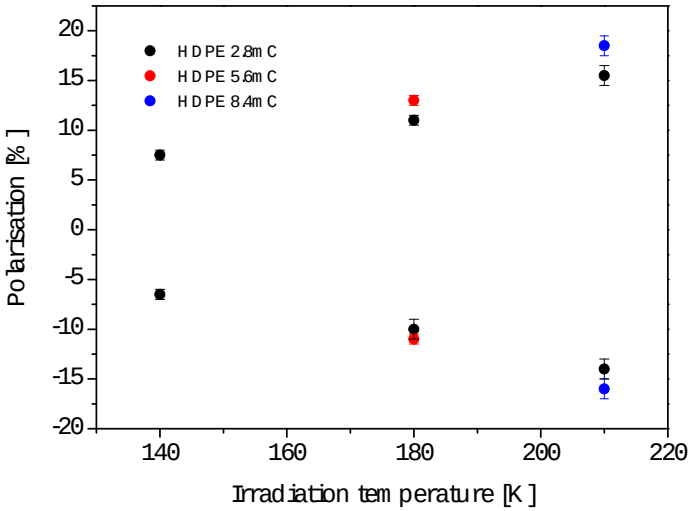

Figure 10.14: Polarisation results for the polarisation of electron irradiated HDPE.

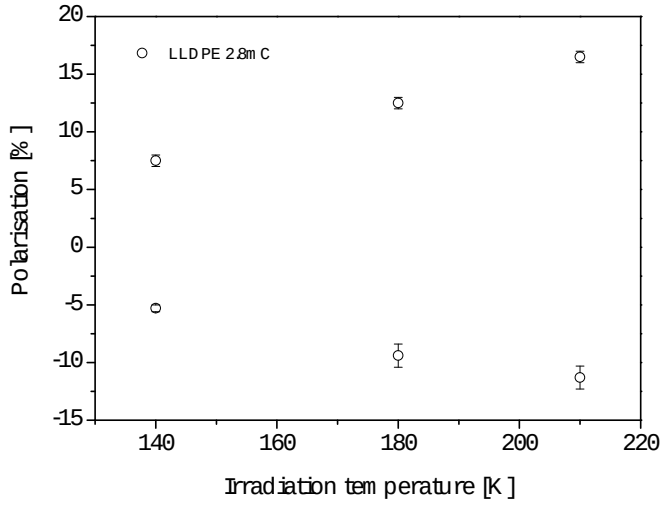

Figure 10.15: Polarisation results for the polarisation of electron irradiated LLDPE.

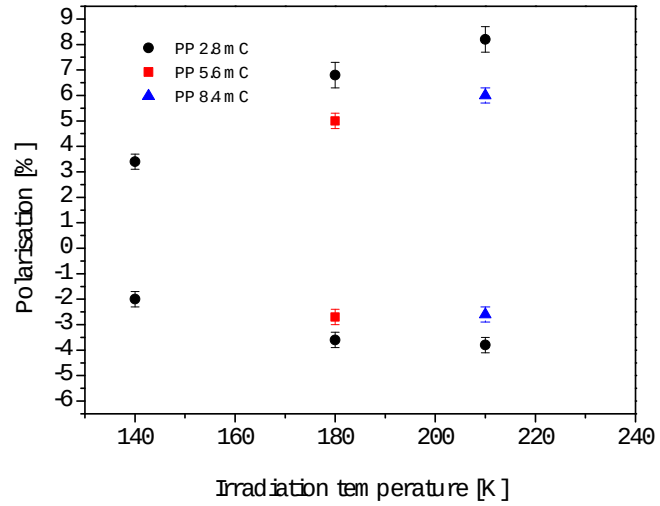

Figure 10.16: Polarisation results for the polarisation of electron irradiated PP.

Though still most prominent in the PP samples, the PE samples also show the asymmetries observed in all previous irradiations. The asymmetries in PE are smaller, but the asymmetry seems to vary for the different material densities, but no correlation could be seen between the irradiation temperature and the asymmetries that were measured. This means that the asymmetry in the polarisation values in PE is not dependent on the irradiation temperature for this selected range. The HDPE samples showed the best symmetry of polarisation values, with polarisations in the negative direction still making up to approximately 85% of the those measured in the positive direction. The negative polarisation values obtained for LDPE and LLDPE on the other hand only managed (60-70) % on the positive polarisation values. The only discernable difference between the samples is the fraction crystallinity: LDPE and LLDPE are predominately amorphous materials, whereas HDPE is highly crystalline, resulting in the different densities, but how this would translate to an asymmetry in the polarisation values cannot be answered at this point. The asymmetry of polarisation values of PP does however show a temperature dependence.

Much like the heated samples, where long heating led to a depression in the negative polarisation values, irradiations at higher temperatures also influence the negative polarisation to a greater extent.

These observations could lead one to conclude that the crystallinity is the defining factor, however the crystallinity of the material does not change at different irradiation temperatures and the asymmetry gets worse for PP at higher temperatures, but not for PE. So one would think that the radical itself could likely be the culprit. In reality the solution is probably to be found in the temperature dependent mobility of the radicals and the molecular environment that surrounds them. Without fully understanding the mechanisms causing these asymmetries, no definitive answer as to how to remedy it, if at all even possible, can be provided. In addition there is really no way of predicting whether the problems that are evident at a temperature of 1 K will be the same at experimental temperatures of 200 mK and lower, and conclusive measurements at these temperatures have to be performed.

In principle the irradiation results were quite satisfactory, especially for the higher temperature irradiations, with polarisation results surpassing the polarisation of our doped butanol samples measured under similar conditions. The commonly employed chemically doped samples all exhibit much faster build-up and relaxation times. So, though this may not be a criteria that must be fulfilled, especially with an eye to the future and the use of a continuous-mode dilution cryostat [195],[196], [197], where in practice the build-up and relaxation times are only relevant for the change in polarisation orientation, this could still be a decisive factor. This was the basis for the idea to irradiate to higher doses. As irradiations at higher temperatures gave the better results in terms of maximum polarisation it was decided to irradiate at these temperatures.The hope was that the temperature dependent polarisation results could be replicated but in faster times.

If one considers that the yield of the radicals drops at higher temperatures, then one would expect that to get equivalent spin densities, higher doses must be chosen for the higher irradiation temperatures. To this end, double the initial dose was given to the PP580, LDPE and HDPE samples at a temperature of 180 K and triple the initial dose at a temperature of 210 K. If one considers the ratios of the initial and the new spin concentrations for PE at the temperatures of the double dose (2.4/1.4) and of the triple dose (2.1/1.1) one can predict the resulting relaxation times, by the same argument used in the previous section. This calculates to a reduction of the relaxation time to only 35% of the value measured for the lower dose at 180 K and to 25% of that measured at 210 K. Within error these values do actually fit those measured. Perhaps more importantly, the maximum polarisation values are not significantly different to those previously obtained for the same irradiation temperatures, achieving the desired effect of creating faster samples but maintaining the higher polarisation characteristic, at least for PE.

The PP materials also became faster, however this has an adverse effect on the polarisation. The values of the polarisation drop slightly, meaning that we lost about a quarter on the maximum values. So where the higher dose irradiations improved the polarisation characteristics of the PE samples the same does not apply to the PP samples. If one considers that the PP samples relax too fast, and the higher polarisation values were obtained for lower spin concentrations, be that by heating or by the increased temperature of irradiation, then a possible way to increase the polarisation values further in PP may be to go to lower doses than covered in this irradiation programme. Whether the desired increase can also be achieved in PP remains to be seen.

10.4 Polarisation summary and discussion

Though the data has come from a variety of different setups, it is important to try and find some common ground, where certain characteristics can be attributed to specific parameters of the experimental setup and contribute to a coherent overall picture. Here the important differences in the setups are the use of protons or electrons, the temperature of irradiation and whether the samples were annealed post irradiation. The influences of these parameters lie in the characterisation of the relaxation times, polarisation values, and in this individual case, the asymmetry of the positive and negative polarisation values. The basis for a valid comparison is the identification of the radical types. Here, the ESR measurements were not only used to quantify the spin densities but also to check that the assumption of identical radicals was well founded.

For simplicity we can start with the similarities. The CW-NMR measurement showed very similar NMR signals for the PE and PP materials. This is not surprising as the chemical shifts associated with different functional groups are very small in the first place (ppm) and even if the molecules are not structurally equivalent the broadening of the NMR signals in the solid state is known to smear out any substructure [198]. For this reason chemical shifts are measured in highly diluted systems in the liquid state. The nuclear interaction in our polymers arises from the dipole-dipole coupling of the protons, so that the presence of many non equivalent protons [3] in the local environment leads to a significant overlap of the underlying spectra. Both materials are hydrocarbons that have similar densities and similar molecular distributions which explains the similarity in the broad NMR spectra.

For all of the PP materials it could be shown that regardless of the irradiation projectile the same radical type was produced. But also, that for the range of the irradiation temperatures investigated there was no influence on the radical type that was generated, even after heat treatment at room temperature. It is concluded that throughout the whole study the polarisation of the same radical was analysed. This was verified by the analysis of the ESR spectra presented in chapter 8. The radical in PP is assigned to the alkyl radical I presented in figure 7.2 and described in the section 7.1.2. Though the PE materials were introduced later into the study and thus were only irradiated in the helium cryostat, the same conclusions can be drawn with regards to the temperature dependent production for all types of PE that were used. The radicals produced in PE could be identified as the alkyl radical shown in figure 7.1 and described in the section 7.1.1. Though not explicitly irradiated in the proton irradiation programme, there is no reason to believe that this would have led to a different radical type [120]. It was shown that there is a direct connection between the ESR structure seen in X-band and the frequency curves in the V-band measurement of the polarisation dependency on the frequency. Due to the more extensive broadening of the PE samples the peaks arising from the hyperfine interaction cannot be clearly identified due to the unresolved components, though a hint of their presence is seen in the frequency curves. The case for the hyperfine splitting in the PP samples on the other hand is much more apparent. Both curves exhibit a broad frequency curve when measured in V-band, with the difference of the maximum polarisation values being separated by approximately 420 MHz. The similarity of the frequency curves for PE and PP is a reflection of the similar widths of the ESR signals and the fact that the broadening is fundamentally caused by the hyperfine splitting. From this standpoint the comparison of the materials is certainly valid.

Though not as obvious at first glance as the above mentioned characteristics, the dependent behaviour of the relaxation rate on the spin density also shows similarities. A summary of all the relaxation rates in dependence of the spin density of the PP materials is presented in figure 10.17. Here the relaxation rate is

[3] The non equivalence of the protons in the solid state comes from the different orientations of the molecules to the external magnetic field.

plotted versus the square of the spin density. The relaxation rates of the PP samples irradiated under the same conditions gave the same relaxation times, irrespective of the molecular weight of the samples. The linear fit is on all data points through the (0,0) origin, but excludes the two data points that are notably not in the linear region. These two data points belong to the 140K irradiation in helium by electrons and the 87K irradiation in argon by the same projectile, so that the irradiations at the lowest irradiation temperatures do not fit the overall scheme. Somewhat unexpected is the fact that the protons fit into the same picture painted by the electron irradiations and even though the temperature was measured as being below the supposed decay threshold, it still looks like it fits the scheme of the higher temperature irradiations. It is imaginable that the proton irradiations at 120 K create local pockets of heat, meaning that the base temperature of the polymer is a lower temperature, than locally in the interactional vicinity of the material the temperature, where the temperature is much higher than that measured externally for the bulk material. This can be understood in terms of the high LET of protons in polymer materials, as protons deposit their energy in compact ionisation tracks, as described in section 6.2.

Though the PE irradiations in total provided less comparative data points, due to the fact that the PE samples were only introduced in the last data taking cycle in the helium cryostat, it was found that the density of the PE samples did not influence the relaxation rates of the material. The data also shows that the low temperature irradiations at 140 K do not fit into the broad scheme of the irradiations when the square of the spin density is plotted versus the measured relaxation times, see figure 10.18 [4]. This does imply that the radio-chemistry of both materials at an irradiation temperature below 140 K is different from those of the irradiations above this temperature and must be treated separately, as the underlying polarisation mechanisms may vary. For the low temperature irradiations the relaxation rate of the samples may be considered as being too fast, when considered in the overall scheme, so that the relaxation rate would somehow correspond to a higher spin density. However, as was shown in section 8.4, the ESR linewidth correlates with the spin density for all samples, so that the only difference can be that the radicals are on average closer together in the low temperature irradiations, as the linewidth as determined in the ESR is not that sensitive to spin density distributions[5]. In this regards it would certainly be interesting to irradiate materials at lower temperatures to see whether the separation into the two temperature regions with regards to the relaxation characteristics can be corroborated. The extension of the temperature range to higher temperatures would certainly also provide additional information. However, here one has the problem that above a specific thermal threshold the alkyl radicals in PE will start converting into allyl radicals, so that one can no longer be sure which radical is influencing the polarisation characteristics. If one wishes to optimise the polymer for polarisation enhancement, then this is surely an effect one would aim to avoid. The question is which temperature regime is more favourable.

Generally it was found that the nuclear relaxation of the PP samples was in the order of 15-20 times faster than PE when irradiated under the same conditions and to the same dose. Initially one might conclude that this is due to the higher radical production in the PP materials, but in a more thorough examination this proposition no longer holds. We have a wide range of irradiation temperatures and produced spin densities, and as it was shown that at the higher irradiation temperature the relaxation times of the materials are solely dependent on spin densities, this means that a direct comparison of the materials at similar spin densities can be made. Taking this into account one finds that even for the case of similar spin concentrations the PP samples are in the region of ten times faster than the PE samples, so that one can confidently state that the PP samples are comprehensively faster than the PE samples.

[4] In this figure the allocation of the temperatures and doses corresponds to the positions of the helium irradiation data points in the PP figure.

[5] See e.g. Wyard [178]

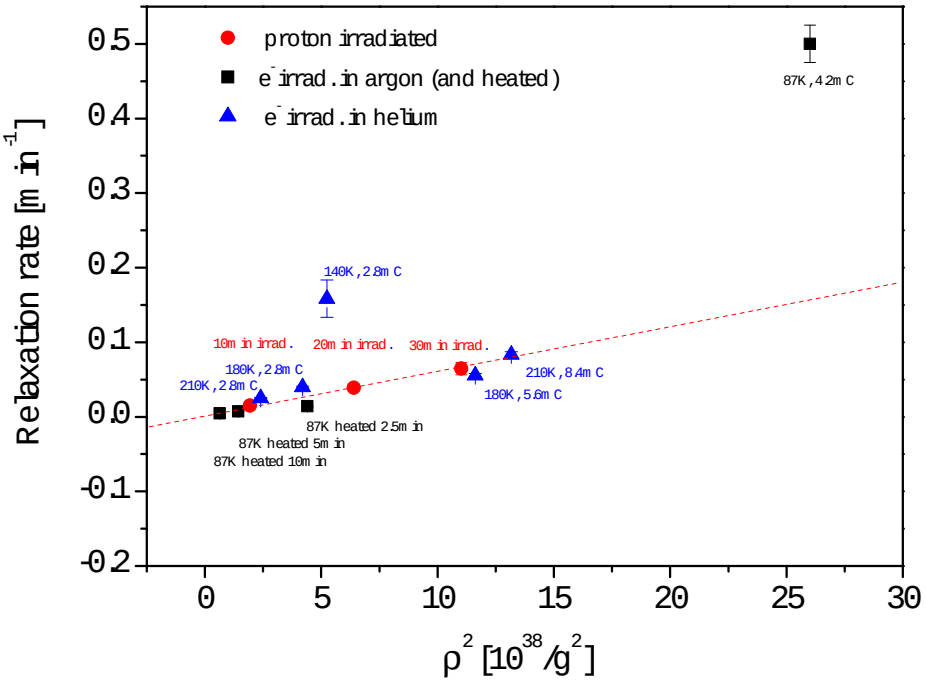

Figure 10.17: The relationship of the relaxation rate on the square of the spin density of irradiated PP materials.

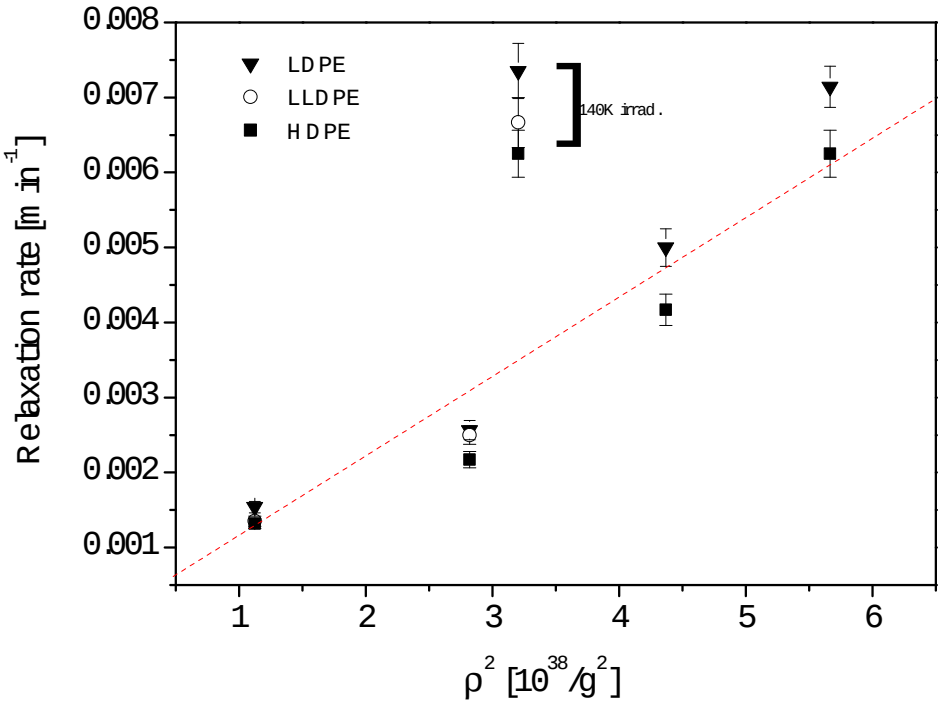

Figure 10.18: The relationship of the relaxation rate on the square of the spin density of irradiated PE materials.

We found that the relaxation rate in all PP materials was not influenced by the differences in the molecular weight, and that the differences in the densities of the PE materials also did not result in any measurable differences in the nuclear relaxation. PP12, PP250 and PP580 make up a distinct group, in regard to the relaxation characteristics, HDPE, LDPE and LLDPE make up another. In terms of the relaxation characteristics the constituents of the groups are indistinguishable, yet the same does not apply broadly to the polarisation characteristics.

Evidently, a higher temperature irradiation does increase the polarisation for all materials. Even so we must be slightly cautious as the relaxation rate also decreased for the same parameters and can, as was previously shown, be directly related to the spin density of the materials. Thus, though it may seem that the higher temperature irradiations produce higher polarisation values, the argument that lower spin densities are the cause may also be valid. The drop in the spin density causes slower samples that polarise to higher values than those measured for samples irradiated to the same dose, but at a lower temperature. For the polymer materials it could be suggested that lower doses than those expected from the irradiation of other common target materials produce better results in terms of higher polarisation values. In the same manner this would then apply to the heated PP samples, where we also see a considerable drop in the spin concentration accompanied by an increase of the polarisation values, but not necessarily to heated PE samples, due to the conversion processes initiated by the heat process, though this later point has not been verified. However, an argument against this is that the higher dose irradiations at 180 K and 210 K in PE also gave similarly high polarisation values, as those measured for the lower doses at the same temperature. These samples were significantly faster, but still managed to reach the high polarisation values, so that the spin density relationship cannot be the only contribution to the polarisation characteristics and one would have to assume an irradiation temperature effect in the radical creation process.

Across the board the polarisation values of the PE samples were higher than those of PP. There are many ways to compare the samples, some making more sense than others. Comparing the samples for the same irradiation doses doesn't really tell us much, as we already know that the spin densities of PP were higher than PE and that the relaxation rates of PP were also much higher. Comparing the polarisation for similar spin densities probably makes slightly more sense. However, even here we have the problem that we know the coupling of the spin systems is vastly different, evidenced in the differences in the relaxation times. Likely the better way to compare the materials is by the comparison of samples with similar relaxation times. Here we have the problem that the fastest PE sample is still much larger than the slowest PP sample, making a direct comparison in this manner impossible. Notwithstanding the lack of a tangible comparative method, the observation that we obtained higher polarisations in the PE materials is obviously still correct.

The major differences in the materials is in the ability of the material to build up to negative polarisation values. The directional dependence of the polarisation was first noticed in the proton irradiations for PP. The asymmetries however were still present in the electron beam irradiated materials, so that the proton irradiations as such could be excluded as the source of the problem. Though that being said the asymmetries were largest in these samples. Here, as above, one has to assume a temperature effect, since higher irradiation temperatures led to larger asymmetries as does prolonged heating. Though the proton irradiations do not fit exactly into this scheme, if one accepts the increased local temperature postulation, then the assumption of a temperature effect is still valid. The question is how the temperature can influence the radical configuration in such a manner that these asymmetries can occur.

For the PP samples that were analysed no differences in the relaxation or polarisation behaviour could be found for PP12, PP250 and PP580, each material performing in the same way, whilst the PE materials did show some differences in the asymmetries. In the positive direction all materials built up to equivalent values. However, as discussed, the LLDPE and LDPE materials showed larger

discrepancies than the HDPE samples for the negative direction, but still not as large as those measured in PP. The influence of the temperature on the asymmetry was not as clear in PE as for the PP materials, where the asymmetries in the PE samples were seemingly not influenced by the irradiation temperature, maintaining the same asymmetry values over the temperature range of the irradiations. The reason for the asymmetries could not be established and thus no reason can be given at this point as to the varied response of the materials to different irradiation temperatures.

The question is whether one can find examples of materials that have similar characteristics, that might help to explain the asymmetries that we see. A search of different radical types and configurations show that the biradicals show some similar traits. An argument for the biradical association is that asymmetries similar to those we have observed are notable for many of the well known biradicals, presently the focus of research in bio-chemistry and other applications. Some examples are bTbk (62%), TOTAPOL and BTUrea (both 84%), B2TE (80%), for which it has been suggested that the asymmetry is a result of the flexibility of the tether between the unpaired electron sites and of the orientation of these sites to each other in a magnetic field [199]. The different orientations of the principal axes of the radicals leads to greater difference in the g factors and hyperfine influence on the ESR spectrum although this may not be obvious in X-band. One must consider that if the excitation bandwidth is small in relation to the inhomogeneous width of the ESR spectrum and thus only a small portion of the ESR spectrum can be saturated, then only a small portion of the spectrum can be excited and may correspond to individual pairings of molecular orientations. The cross effect is generally accepted as being the polarisation mechanism that determines the polarisation behaviour at high fields. Depending on whether there are more electron pairings corresponding to the matching condition on the high or low field side of the ESR spectrum, this results in an asymmetry on the low or high field, respectively. However, it must be emphasised that it is not clear how this would cause the differences in asymmetries in the polymer materials, especially the differences observed for HDPE and LDPE, and those observed by the heating of PP. A conjectural mechanism is that the orientation of the individual radical in the pairs is influenced by the structural configuration of the polymer and by the molecular motion, that in turn is influenced by the temperature. This would mean that more rigid structures, implying highly crystallinity, maintain the original orientation of the pairs as created. If this orientation is favourable the asymmetries are minimised. If however the mobility of the chains is higher, implying lower crystallinity, then the resulting orientation of the radical is somewhat randomised, resulting in a greater spread of the energy dependencies and the g factors. Even if the g factor asymmetry is small and the spread lies within that of the hyperfine coupling, this still leads to an asymmetry in the energy transitions and thus in the polarisation structure, even if this is not apparent in X-band ESR spectrum, or for that matter in the the V-band structure. In this case a high chain mobility due to a lower crystallinity produces the same effect as the heating of a sample material.

It has also been shown that the polarisation of biradicals is highly dependent on the inter-spatial separation of the unpaired electrons, as determined by the tether used to link the radicals [200], [201], so that the distance matching of the radicals is the optimisation process in the polarisation enhancement. In polymers the tether is basically the molecular backbone, so that the optimisation of the inter-spatial distance of the radicals can be controlled by the irradiation temperature. Nunome at al. showed that similar radical concentrations of irradiated PE had differing ESR saturation characteristics, depending on the temperature of the irradiation [202]. As the overall concentration was maintained, the average spatial separation of the unpaired electrons must differ and was related to the thermal diffusion of the extracted hydrogen atom, before the subsequent extraction of the second hydrogen atom can occur. This means that polymers irradiated at higher temperatures should have larger average inter-spatial distances, an effect that can be used to match the distance separation of the pairs created in the irradiation process to maximise the polarisation, assuming that they are not already too far apart at very low temperatures. Due

to the local confinement, which comes from the creation process of the radicals in pairs, the alkyl radicals can be considered as a type of biradical system, for which the two unpaired electrons are spatially concentrated. Whether these unpaired electrons are situated on the same molecule, or on adjacent chains is irrelevant.

The second thermal process influencing the distance between the alkyl radicals in the polymers, is the diffusion of the radical pairs after irradiation by heating, or during irradiation at elevated temperatures. Seguchi and Tamura calculated the diffusion constants for an isotropic diffusion of alkyl radicals in polyethylene [167]. Their calculations showed the relationship of $-\ln(D) \propto 1/T$, with D being the diffusion constant and T being the temperature of the polymer. The problem is that their study was for significantly higher temperatures than the irradiation temperatures of this study. The general correlation of the diffusion and temperature is plausible, even at much lower temperatures. However it has been shown that different decay regions exist in polymeric materials, so that one needs to know the diffusion/temperature relationship at the exact temperature of irradiation. Seguchi and Tamura give the diffusion constant of the alkyl radicals in PE as $3 \times 10^{-18}\,\mathrm{cm^2/s}$ at 20 °C. Ichikawa et al. used pulsed ESR methods to determine the inter-spacial distance of the alkyl pairs when irradiated at 77 K [203]. Their measurements showed the pairs had an average separation of $3.5 \pm 0.4\,\mathrm{nm}$[6], so that one would have to assume that the dominant mechanism in the spatial separation of the alkyl pairs is the irradiation temperature, as reasoned by Nunome et al., as the diffusion at low temperatures is expected to be slower than that measured by Seguchi and Tamura at room temperature.

Experiments with biradicals also show a strong correlation of the relaxation times of the electrons and the nuclei on the maximum achieved polarisation values, with the tendency towards higher polarisation values for materials with longer relaxation times (T_{1e}, T_{2e} and T_{1n}) [47]. This is certainly the case for the comparison of PE and PP, as well as for the increase of the irradiation temperatures. In addition it has been shown that for some biradicals with long relaxation times the maximum polarisation that can be achieved is less sensitive to the radical concentration. An example of this is given by Hu et al. where varying the spin concentrations from the high $10^{18}\,\mathrm{e^-/g}$ to the mid $10^{19}\,\mathrm{e^-/g}$ had little effect on the maximum polarisation values that were achieved [201]. In a sense this was also the case for the PE materials, where similar polarisation results where obtained for materials of differing doses. Here, once again, it can be postulated that the irradiation temperature determines the inter-spatial distance of the alkyl radicals which influences the polarisation to a greater degree than the dose.

The analogy of the paired radicals in the polymers to the biradicals is particularly interesting if one considers the maximum polarisation values that are obtained in the biradical doped nuclear systems. Biradicals based on the tethering of two TEMPO radicals, have shown polarisations much in the excess of those observed for the same radical in singular form. The researchers at PSI showed, that depending on the concentration of the radicals, up to eleven times higher polarisations for the biradical could be achieved, for samples measured under similar conditions to our test facility, with optimized polarisations still being obtained for concentrations similar to our standard sample of TEMPO [204]. Examples of the characteristic of higher polarisation values for the biradical configuration with regards to their monoradical components are manifold [199], [200], [201], [47].

Lastly, the polarisation mechanism will be discussed. To distinguish between the polarisation mechanisms experimentally one can compare the homogeneous broadened ESR linewidth δ with the inhomogeneous broadened linewidth Δ, as well as with the nuclear Larmor frequency ν_n [201]. For the solid effect (SE) to work the condition of $\delta, \Delta < \nu_n$ must hold. To distinguish between the other two effects, with $\Delta > \nu_n$, one must then consider whether the ESR line is predominately homogeneously broadened,

[6] This distance is in the order of magnitude of the typical biradical systems previously mentioned, where average distances are in the lower nanometer region [199].

i.e., $\Delta \approx \delta$ (TM), or whether the line is mainly inhomogeneously broadened, i.e., $\Delta > \delta$ (CE). If one looks at the frequency curve of the polymer samples (see figure 10.10), eliminating the SE as the polarising mechanism of the polymers is quite straight forward. For the SE to apply the frequencies used to obtain the maximum polarisation values should be separated by the frequency of $2\nu_p = 212.9\,\text{MHz}$ at a magnetic field of 2.5 T, corresponding to the coupled electronic and the proton Larmor frequencies at $\nu_e \pm \nu_p$. However the separation of the maxima observed is twice the predicted value for the SE. Assuming that the g factor anisotropy is negligible, as it seems to be, the field independent hyperfine interaction is the dominant broadening mechanism and Δ at 2.5 T should be very similar to the frequency width as measured in X-band. So one can certainly say with confidence that $\nu_p < \Delta$ and the SE mechanism can be excluded. This is also clear-cut in the relationship between the square of the spin density and the relaxation rate. For the polarisation theories discussed in section 3.2 the dependence of the relaxation rate on the square of the radical concentrations for the higher temperature irradiations is indicative of a two electron process, meaning that thermal mixing or the cross effect would be the polarisation mechanism that determines the polarisation behaviour observed.

However, disentangling the thermal mixing and the cross effect is not that simple. In the case of a homogeneous line, the broadening is largely determined by the electron-electron dipolar coupling, but the hyperfine structure is an inhomogeneous broadening mechanism, so that thermal mixing cannot apply to the whole ESR spectrum. However the spin equalisation of the electronic states may be fast enough that a strong dipolar coupling makes thermal mixing possible for small proportions of the ESR spectrum [46].

The spin–spin relaxation that results in the homogeneous broadening of the ESR line is independent of temperature and the external magnetic field, and is caused by random fluctuations in the fields of neighbouring spins. This means that the electronic relaxation time T_{2e} is dependent on the spin concentration. Ichikawa et al. used spin echo methods to determine the spin-spin relaxation dependence on the radical concentration in PE [203]. In their work they provide an empirically obtained equation with which the T_{2e} value can be calculated. For spin densities in the order of $10^{19}e^-/g$ the evaluation of this equation gives a spin-spin relaxation rate of $\sim 2\,\text{MHz}$. After the argon irradiation programme it was possible to measure relaxation times of the PP samples by pulsed ESR methods. These measurements were done in the laboratory of Prof. Dr. O. Schiemann of the Institut für Physikalische Chemie at the Bonn university, under the supervision of Dr. Hideto Matsuoka. These measurements gave relaxation values of the samples in the area of 500 ns, corresponding to 2 MHz in frequency units. As the values of PE and PP correspond to each other, and the radical concentrations are in the same magnitude, one can estimate that the homogeneous part of the ESR linewidth is $\delta \approx 2\,\text{MHz}$ for all sample materials.

The total linewidth, determined by the FWHM of the ESR spectrum in X-band, is approximately 7 mT, corresponding to a frequency width of 200 MHz. As the signal is hyperfine broadened and the signal seen in the frequency curve spectrum can be related to the ESR spectrum seen in X-band, the linewidth of the ESR spectrum in V-band should also have a frequency width of $\Delta = 200\,\text{MHz}$. From this point of view that would mean that by the allocation $\delta << \nu_n < \Delta$, and by the experimental distinction given by Hu et al. [201], it would follow that the cross effect is the dominant polarising mechanism in the polymer materials. Due to the creation process of the radicals in pairs, it is conceivable that the CE is the polarising mechanism in the polymers, as has also been shown for many biradicals. If this is the case the broader signal of the polymers, compared to those of the doped butanol samples, becomes less problematic, as the energy matching condition of the radical pairs determines the polarisation capabilities of the materials to a greater extent than the total ESR width. This is in contrast to the case for TM where the minimisation of the ESR linewidth in needed to achieve a common spin temperature, as described in section 2.3.4.

All in all the results from the different irradiation programmes do fit into a broader picture. Though the proton irradiations were hampered by systematic problems, especially the lack of a bulk preparation, these irradiations also fit into the scheme. However, the opportunity of the irradiations now available again at the LINAC2 are more promising, due to the ability to use our irradiation cryostats that were designed for this exact purpose. Also in turn, the analysis clearly shows the relationship of the nuclear relaxation on created unpaired electrons. This direct correlation does not transfer automatically to the polarisation values. Temperature effects play a large role in the irradiations and on the polarisation characteristics. Heating and irradiations at higher temperatures all show a shift to higher polarisation values. To sum up, the PP samples are faster than the PE samples, but PE polarises to higher values. It was discussed how the polarisation characteristics of the polymers are similar to those of biradicals and it was proposed that this is due to the creation process in pairs of the alkyl type radicals. It was also shown that the ESR characteristics of the polymers lead to the interpretation that the cross effect is the dominate polarisation mechanism in the polymers, as is the case for the biradical systems.

CHAPTER 11

Summary and Outlook

Polarised target experiments place very specific demands on the target materials that can be used. In addition to high densities and high dilution factors, among many other material characteristics, the ability of the material to reach very high polarisation values is paramount. Polymer materials have been discussed as potential candidates to replace the commonly used alcohol and diol based target materials, predominately due to the ability to form them to any desired geometry, fitting the requirements of the experiment. The additional advantages of polymers was discussed, with respect to the figure of merit of the materials. It was shown that the polymer materials of polypropylene (PP) and polyethylene (PE) could provide improvements in many of the defining characteristics of a solid state polarised target. Though admittedly being only slight improvements for most of these parameters, seen as a whole the polymers have potential to exceed the commonly used target materials in their performance capabilities.

Polarised targets use a process called dynamic nuclear polarisation to build up to high polarisation values. This process necessitates the introduction of unpaired electrons into the material structure. Many possibilities to do this are available. However, this study focussed on the method of irradiation, creating paramagnetic centres in the form of structural defects in the molecular structure of the polymers. The irradiation programmes of this study consisted of proton irradiations at the Helmholtz-Institut für Strahlen- und Kernphysik and electron irradiations at the Physics Institute, all of which are situated in Bonn. These irradiation programmes provided the opportunity to test different irradiation environments, temperatures and projectiles and their influence on the radical structure and the polarisation characteristics of PE and PP.

The polymers show a wide variety of possible radicals that can be created in the irradiation process, including alkyl-, allyl- and polyenyl-type radicals, in addition to those created in oxidative processes such as peroxyl radicals. Over the temperature ranges of 87 K to 210 K it was shown by ESR spectroscopy that the material specific radical yield drops with temperature, but that the radical created at lower temperatures is qualitatively the same radical that is created at the higher temperatures, where the radicals in PE and PP differ due to the differences in their molecular structures. The irradiation of the materials in batches allows the direct comparison of the materials and it appears that the defining characteristics of the materials, those being the density in the case of PE and the molecular weight in the case of PP, have no influence on the the spin densities that are created in the irradiation process. All samples of PE in a single batch had the same spin densities and all samples in the PP batches also had the same spin densities, where the yields of PP are $\sim 40\%$ higher than for PE over the range of 140 K to 210 K, when irradiated in helium gas by electrons to the same dose.

For PP the radical created in the proton irradiations at 120 K in vacuum by ~ 13 MeV protons does not differ from that created at temperatures between 87 K to 210 K by electrons with end energies of ~ 20 MeV. The PP radical in all cases can be identified by a prominent octet in the ESR spectrum, whereas the PE radical appears as a sextet, with minimal substructure. The polarisation characteristics that are observed can thus be attributed to these uniquely identified primary alkyl radicals created in the irradiation process. With an eye to future research, a heat treatment method at room temperature was presented which shows how it is possible to create the allyl-type radical in PE, which exhibits, from a polarised target perspective, many interesting characteristics, foremost a room temperature stability. It was also shown that the crystallinity of the material should be chosen as high as possible to maximise the conversion process of the alkyl to allyl radicals, as the allyl radical remains as a persistent radical in the crystalline region of the polymer after heating at room temperature.

The optimised frequencies to obtain the maximum values of polarisation was very similar in all samples, regardless of being PE or PP materials, so that no obvious differences in the frequency curve positions of maximum and minimum polarisation could be seen. These positions are separated by a frequency width of ~ 420 MHz at a magnetic field of 2.5 T, which is significantly larger than the nuclear Larmor frequency of the protons. The structure of the frequency curves can be related to the hyperfine splitting structure, as evident in the ESR spectrum in X-band, so that the ESR signal is predominately inhomogeneously broadened. The equivalence of the frequency curves can be explained by the very similar total widths of the ESR signals, each determined predominantly by the hyperfine structure.

For both PE and PP the electron irradiation at higher temperatures causes a lengthening of the nuclear relaxation time, effectively making the samples slower. This can be directly related to the decrease in the spin density of the materials. The relaxation rate of the sample materials was shown to be linear with the square of the spin density of the unpaired electrons that are created in the irradiation process, with the exception of those sample materials that were irradiated at temperatures below 140 K. The proton irradiations at 120 K fit into this scheme if one accepts that the local heat input is larger due to the large linear energy transfer of protons in polymers. The relationship fits well with the predictions made by theoretical models of dynamic nuclear polarisation, but does suggest that two temperature regions must be defined and that the lower temperature irradiations are qualitatively different from the higher temperature irradiations. The heating of the PP samples at room temperature has an effect on the relaxation, where longer heating causes the relaxation rate to decrease, but also with the same relationship on the spin density as above described. So though there is a large temperature influence on the relaxation characteristics, these can be related to the spin density of the materials, with lower spin densities making for slower nuclear relaxation. The relaxation rate in the PP materials was in the region of 15-20 times faster than that of PE for the same irradiation doses. The spin concentration for PP is higher when compared to PE at the same dose, so naturally this relates to the faster relaxation times, but a comparison of similar spin concentrations still shows that PP relaxes approximately ten times faster.

The increase of the irradiation temperature from 140 K to 210 K led to a significant improvement of the polarisation values. Here the polarisation values obtained for the PE samples were larger than those obtained for the PP samples. Where the highest values obtained in PE were in the region of 20%, those measured for PP were ~ 8.5%, though the factor of improvement was similar in both cases, where the 87 K and 140 K irradiations gave polarisations in the vicinity of 4% for PP samples, and the 140 K irradiations gave results of 7.5% for PE. Roughly, this means that the polarisation enhancement was improved by a factor of two in both cases. Where the relaxation time is influenced by the spin concentration of the materials, the same direct correlation cannot be seen for the polarisation values. Though the relaxation rate decreases and the polarisation increases in the same manner for higher irradiation temperatures, this

cannot be a direct influence of the spin concentration, as it was shown that irradiation to higher doses at elevated temperatures also gave much improved results in the polarisation, similar to those obtained at the same temperature but at lower doses. This shows that at least for these temperatures and doses, the maximum polarisation values were more influenced by the irradiation temperature than the dose, hinting at a temperature dependent effect of the interactional mechanism in the creation process of the radicals. A temperature effect was also seen in samples of PP that were heat treated for short times at room temperature post irradiation. The polarisation of the materials grew for longer heating periods, with maximum values of $\sim 14\%$. These were the highest polarisation values measured for PP in this work.

Throughout this study the materials showed problems with the asymmetry of polarisation values, where the negative values were never measured as being as high as the positive values. This is particularly the case for the PP material, where the asymmetry is more pronounced and the worst asymmetry was measured for the proton irradiated materials. Here it was possible to show that the asymmetry was influenced by the temperature. This was shown by the heating of samples at room temperature where the asymmetry got worse the longer the samples were heated. Also, there was a marked effect caused by the irradiation temperature, here it was also the case that the asymmetry got worse the higher the irradiation temperature was. This is especially disappointing as the polarisation values in both cases were improved. No such temperature effect was notable for the PE samples. Both the LDPE and HDPE materials showed asymmetries, however these were not dependent on the temperature, with the same asymmetry measured for all irradiation temperatures. There were however differences in the asymmetries measured, where the difference in the positive and negative values were more prominent in the LDPE samples. The source of this asymmetry could not be determined and remains a topic for future research.

The study has produced some promising results, and will hopefully provide a good basis for the continuation of future research in this direction. However, many questions remain unanswered, first and foremost the source of the polarisation asymmetries seen in all sample materials. If this question can be answered it will provide the opportunity to possibly influence this characteristic and optimise for better performance. No matter how high the end polarisation becomes, the unequal distribution of polarisation values is unquestionably a major problem.

Overall the results of the proton irradiations were not significantly different to those of the electron irradiations and seen as a whole the results are consistent with each other. However due to the problem that only foils can be irradiated, this method lacks the bulk production method provided by the electron beam irradiations at the ELSA facility, where the irradiation temperature regulation of the samples is also much more reliable. With this in mind future irradiations are best conducted at ELSA, where the modifications to the beamline and the irradiation setup now allow for the continuation of irradiation programmes with the LINAC2. The continuation of the irradiation programme should incorporate higher irradiation temperatures and also dose variations, as the most obvious takeaway from this work is that the elevated temperatures greatly improved the polarisation values that could be reached.

The polarisation values that were measured are very comparable to those values obtained for the commonly used target materials. The main problem here is that there is no way of predicting how this will translate to polarisation values at typically experimental solid state polarised target setups where temperatures are below 200 mK. The polarisation characteristics of these samples must be analysed at these temperatures if they are to prove viable substitutions for the targets materials currently used.

And finally, the measured polarisation characteristics can be attributed to very specific radicals that were created in the irradiation process. Polymers are unique systems in which it is possible to create a wide variety of different radicals. In addition the radical creation process is particularly important due to the macromolecular structure of the polymer, which is once again unique with regards to the currently used target materials. As it is the radicals that drive the polarisation process, the study of the polarisation characteristics of the base polymer should be expanded to include them. A full and systematic analysis of the irradiation characteristics of the polymer would include a full analysis of the radical production for all radicals (alkyl, allyl, linear polyenyl, cyclic polyenes, scission products, etc.). Polymers remain an interesting prospective target material for future double polarisation experiments.

APPENDIX A

Apppendix

A.1 Polymers irradiated to high dosages

High levels of irradiation have been known to produce singlets in the ESR spectra of polymers, attributed to the polyenyl-type radical, illustrated for PE in figure 7.1, when irradiation is at room temperature and in vacuum by a ^{60}Co or by an electron source. At these high levels of irradiation the crystallinity of the sample materials is completely diminished due to the large amount of structural reconfiguration and it would be expected that the end product would not resemble the initial product in any of its critical physical and chemical properties. At a threshold dose in the region of $\sim 10^3$ Mrad the PE radical, in particular, gives a very narrow ESR signal with a peak to peak width of 2.6 mT in the X-band ESR spectrum and is highly stable, even at room temperature [205]. With a further increase of dose the line width of theses singlets converge asymptotically to a material specific value, e.g., 1.7 mT for PE and 2.7 mT for PP and it has been reported that the phenomena has been observed in a wide variety of polymers, including PS, PTFE and PVC, among others [206]. Assuming that the width of this signals is dominated by the hyperfine structure and that the signal does not broaden notably at higher fields, it would make these radicals potentionally very interesting for DNP applications.

The viability of such irradiations can be judged on the following calculation. The standard dose in the LINAC2 irradiations of this study was 2.8 mC incident electron charge, that being the equivalent to 0.73×10^{15} e$^-$/cm^2. The calculations for the average energy deposit of a single electron for our 23 MeV setup is well known, see e.g., [132]. The NIST ESTAR software [119] gives the stopping of PE/PP at this energy as 2.51 MeV cm^2/g, which calculates to $\sim$5 MeV energy deposit per electron on average. Using the charge deposit one can then calculate the total number of electrons incident on the target material and thus the resulting energy deposition. As the target container holds approximately 55 g of material, this results in a dose of 270 J/g, or 27 Mrad. This means 1 Mrad is equivalent to 2.7×10^{13} e$^-$/cm^2. To reach a $\sim 10^3$ Mrad dose one would have to irradiate for approximately 100 h, assuming that the standard dose used is obtained in around $2^{1/2}$ h and even then one doesn't know what spin densities will be produced in the material.

Grishina and Bakh irradiated samples of PE at room temperature and in vacuum to a dose of 10^3 Mrad, resulting in a spin concentration of $\sim 10^{19}$ e$^-$/g. The free radical concentration was attributed solely to the polyenyl radical, showing that it is possible to create, in number at least, the structural defects we anticipate to be needed for DNP [207]. When increasing the dose further to $>6 \times 10^3$ Mrad the singlet width was further reduced to only 0.75 mT. This secondary reduction in line width is explained as the

conversion of linear polyenic groups to cyclic polyene groups.

The importance of the increase of double bond concentration lies in the stabilisation of the radical migration. Irradiation creates additional double bonds in the carbon chains which can be extended by higher doses of irradiation. Double bond production in the polymer materials is not proportional to the initial vinylene concentration, as detected by the analysis of UV absorption spectra by Fallgater and Dole [143], so that the diene production does not necessitate the pre-existence of vinylene groups. In the case of irradiated PE and PP this would mean that the allyl and polyenyl free radical can be created by irradiation at room temperature at an adequately high dose, as the number of unsaturated chemical bonds would then increase with the dose. Though this sounds extremely intriguing these high doses of irradiation for the larger batch irradiations needed to produce enough material for the targets for scattering experiments as carried out at present may be difficult, but not impossible.

A.2 Mechano-radicals in polymers

An alternative method to chemical doping and irradiation is the mechanical destruction of the polymer chains by a macroscopic fracture mechanism, e.g., sawing, milling or pulling [208]. As with the irradiated polymers, the products are highly reactivate and must be processed at low temperatures, typically by immersion in liquid nitrogen. Direct evidence of a chain-type destruction was shown in the ESR spectra of the machined molecules of PE and PP by Kawashima et al. [209]: The observed ESR spectra of the mechanically fractured polymers differ significantly from those obtained from the irradiated polymers and can be assigned to the C–C scission type radical (see figure A.1), a conclusion that is substantially backed by the observed decrease in the molecular weight of the polymers.

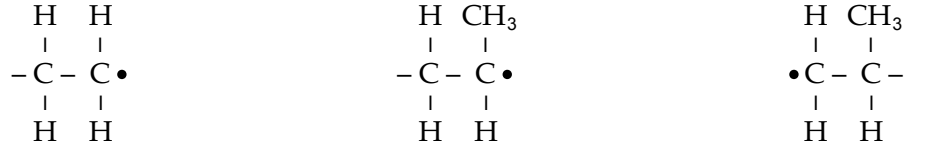

Radical in PE. Radical in PP. Radical in PP.

Figure A.1: Radicals created in PE and PP by the scission of the carbon backbone.

It has been shown that for organic compounds with low molecular weight it is not possible to produce these types of radicals, making mechano-radicals unique to polymeric materials. In lower weight molecules the shear stress on the molecules results only in the fracture of the intermolecular van der Waals' bonds, but not the covalent bonds between the atoms. In longer chained polymers the chains are effectively bent until broken. A lower bound on the molecular size, below which mechanical fracture is no longer possible, was given by Sakaguchi and Sohma for PE [210]: Their experiments determined a minimum degree of polymerization between 70 and 100. This would produce radicals concentrations in PE and PP of $\sim 10^{20}\,\mathrm{e^-/g}$, which is presumably more than sufficient for DNP. However, regardless of the overall material radical density that can be produced, the main disadvantage of the procedure would be that the samples are then in powdered form and this would greatly reduce the filling factor of the materials.

Whether or not these radicals can be used for polarisation by DNP is certainly worthy of consideration, however one thing to keep in mind is that the fracture mechanism creates the radicals in pairs. For a homogeneous material like PE this results in twice the amount of the same radical-type, however in a heterogeneous material such as PP this results in two types of radicals, both of which may have completely different polarisation characteristics.

A.3 Helium Vapour Coefficients for the ITS90 scale

The lowering of the vapour pressure above a liquid helium bath results in a drop in temperature of the liquid. The temperature/pressure relationship is well studied and documented for both helium isotopes and is summarized by the ITS90 scale [185]. The empirical equation is written as:

$$T = \sum_{i=0}^{9} A_i \left(\frac{\ln(P) - B}{C} \right)^i , \tag{A.1}$$

where P is the pressure in units of Pascals and A_i, B and C are coefficients, summarized in the table below.

Coefficients	^{3}He (0.65 K to 3.2 K)	^{4}He (1.25 K to 2.1768 K)	^{4}He (2.1768 K to 5 K)
A_0	1.053477	1.392408	3.146631
A_1	0.980106	0.527153	1.357655
A_2	0.676380	0.166756	0.413923
A_3	0.372692	0.050988	0.091159
A_4	0.151656	0.026514	0.016349
A_5	-0.002263	0.001975	0.001826
A_6	0.006596	-0.017976	-0.004325
A_7	0.088966	0.005409	-0.004973
A_8	-0.004770	0.013259	0
A_9	-0.054943	0	0
B	7.3	5.6	10.3
C	4.3	2.9	1.9

Table A.1: Coefficients for the calculation of the temperature in dependence of the vapor pressure of helium defined by the ITS 90 standards for temperatures 0.65 K to 5 K [185].

A.4 Tabulated results of the polarisation characteristics of the proton irradiations

Irrad. time [min]	ρ [10^{19} e$^-$/g]	$\Delta\rho$ [10^{19} e$^-$/g]	$P_n(+)$ [%]	$P_n(-)$[%]	Relax. time [min]
10	1.4	0.5	0.8 ± 0.1	-0.13 ± 0.2	66 ± 1
20	2.5	0.3	4.2 ± 0.3	-0.9 ± 0.2	26 ± 1
30	3.3	0.4	5.0 ± 0.2	-1.2 ± 0.2	15 ± 2

Table A.2: Polarisation and relaxation results of the irradiation of PP foils in vacuum.

A.5 Tabulated results of the polarisation characteristics of the LINAC1 electron irradiations

Heating time [min]	$P_n(+)$ [%]	$P_n(-)$[%]	$P_n(-)/P_n(+)$ [%]	Relax. time [min]
0	3.8 ± 0.2	-3.2 ± 0.2	84 ± 2	2 ± 0.1
2.5	10.5 ± 0.5	-5.2 ± 0.5	50 ± 2	70 ± 5
5	13.4 ± 0.6	-5.1 ± 0.3	38 ± 2	137 ± 5
10	13.7 ± 0.6	-4.6 ± 0.2	33 ± 2	211 ± 10

Table A.3: Polarisation and relaxation results of the heated PP samples.

A.6 Tabulated results of the polarisation characteristics of the LINAC2 electron irradiations

Irrad. temp. [K]	Incident charge [mC]	$P_n(+)$ [%]	$P_n(-)$[%]	$P_n(-)/P_n(+)$ [%]	Relax. time [min]
140	2.8	7.5 ± 0.5	−4.8 ± 0.3	65 ± 2	140 ± 10
180	2.8	11.5 ± 1	−8 ± 0.5	70 ± 2	390 ± 20
210	2.8	18.5±1	−12 ± 1	66 ± 2	650 ± 30
180	5.6	13 ± 0.5	−9 ± 1	72 ± 2	140 ± 20
210	8.4	20 ± 1	−14.5 ± 1	60 ± 2	200 ± 20

Table A.4: Summary of the polarisation and relaxation results of the LDPE samples irradiated in helium at various temperatures and doses.

Irrad. temp. [K]	Incident charge [mC]	$P_n(+)$ [%]	$P_n(-)$[%]	$P_n(-)/P_n(+)$ [%]	Relax. time [min]
140	2.8	7.5 ± 0.5	−6.5 ± 0.5	86 ± 2	160 ± 10
180	2.8	11 ± 0.5	−10 ± 1	90 ± 2	460 ± 25
210	2.8	15.5 ± 1	−14 ± 1	90 ± 2	760 ± 45
180	5.6	13 ± 0.5	−11 ± 0.5	85 ± 2	160 ± 20
210	8.4	18.5 ± 1	−16 ± 1	86 ± 2	240 ± 30

Table A.5: Summary of the polarisation and relaxation results of the HDPE samples irradiated in helium at various temperatures and doses.

Irrad. temp. [K]	Incident charge [mC]	$P_n(+)$ [%]	$P_n(-)$[%]	$P_n(-)/P_n(+)$ [%]	Relax. time [min]
140	2.8	7.5 ± 0.5	−5.3 ± 0.3	70 ± 2	150 ± 10
180	2.8	12.5 ± 0.5	−9.4 ± 1	75 ± 2	400 ± 20
210	2.8	16.5 ± 0.5	−11.3 ± 1	68 ± 2	740 ± 40

Table A.6: Summary of the polarisation and relaxation results of the LLDPE samples irradiated in helium at various temperatures and doses.

Irrad. temp. [K]	Incident charge [mC]	$P_n(+)$ [%]	$P_n(-)$[%]	$P_n(-)/P_n(+)$ [%]	Relax. time [min]
140	2.8	3.4 ± 0.3	−2 ± 0.3	60 ± 2	6 ± 1
180	2.8	6.8 ± 0.5	3.6 ± 0.3	53 ± 2	25 ± 2
210	2.8	8.2 ± 0.5	−3.8 ± 0.3	47 ± 2	45 ± 4
180	5.6	5 ± 0.3	−2.7 ± 0.3	54 ± 2	18 ± 1
210	8.4	6 ± 0.3	−2.6 ± 0.3	43 ± 2	12 ± 1

Table A.7: Summary of the polarisation and relaxation results of the PP samples irradiated in helium at various temperatures and doses.

Bibliography

[1] E. Rutherford, "The scattering of alpha and beta particles by matter and the structure of the atom", *Phil. Mag.* 21 (1911) 669–688.

[2] N. Bohr, "On the constitution of atoms and molecules, Part I.", *Phil. Mag.* 26 (1913) 1–25.

[3] N. Bohr, "On the constitution of atoms and molecules, Part II.", *Phil. Mag.* 26 (1913) 476–502.

[4] J. Chadwick, "Possible existence of a neutron", *Nature* 129 (1932) 312.

[5] M. Gell-Mann, "A schematic model of baryons and mesons", *Phy. Lett.* 8.3 (1964) 214 –215.

[6] G. Zweig, "An SU(3) model for strong interaction symmetry and its breaking. Vers. 1" (1964), CERN-TH-401.

[7] R. Aaij et al., "Observation of $J/\psi p$ resonances consistent with pentaquark states in $\Lambda_b^0 \to J/\psi K^- p$ decays", *Phys. Rev. Lett.* 115.7 (2015) 072001.

[8] L. de Broglie, "Recherches sur la théorie des quanta" (1924), Migration - université en cours d'affectation.

[9] R. Mülhaupt, "Hermann Staudinger and the origin of macromolecular chemistry", *Ang. Chem. Int. Ed.* 43.9 (2004) 1054–1063.

[10] D. Hill, B. Hasher and C. Hwang, "Dynamic polarization of protons in radiation-damaged polyethylene by the solid effect", *Phys. Lett.* 23.1 (1966) 63–64.

[11] M. Borghini et al., "Sizeable proton polarizations in frozen alcohol mixtures", *Proceedings of the international conference on polarized targets and ion sources*, (Saclay, France), CEN, Saclay, 1966 387–391.

[12] E. Rosantsev, *Free nitroxyl radicals*, Plenum Press, 1970.

[13] B. van den Brandt et al., "Dynamic nuclear polarization in thin polymer foils and tubes", *Nucl. Instr. Meth. Phys. Res. A* 356.1 (1995) 36 –38.

[14] B. van den Brandt et al., "Dynamic nuclear polarization in thin polyethylene foils cooled via a superfluid ^{4}He film", *Nucl. Instr. Meth. Phys. Res. A* 381.2-3 (1996) 219–222.

[15] T. Kumada et al., "Dynamic nuclear polarization of high- and low-crystallinity polyethylenes", *Nucl. Instr. Meth. Phys. Res. A* 606.3 (2009) 669 –674.

[16] D. Crabb, "Polarization in radiation-doped butanol and CD_2", *Nucl. Instr. Meth. Phys. Res. A* 526.1-2 (2004) 56–59.

[17] D. Crabb, "Solid polarized targets and applications", *PSTP 2007 - Proceedings of the 12th international workshop on polarized ion sources, targets and polarimetry*, (Upton, New York, USA), AIP Conference Proceedings, 2008 297–306.

[18] L. Wang, "DNP measurements of irradiated deuterated polyethylene", *PSTP2015 - Proceedings of the 16th international workshop on polarized sources, targets and polarimetry*, (Bochum, Germany), Proceedings of Science, 2016.

[19] D. Crabb, "Proton and deuteron polarizations with irradiated materials", *PSTP2005 - Proceedings of the 11th international workshop on polarized sources, targets and polarimetry*, (Osaka, Japan), World Scientific, 2007 54–58.

[20] F. Bloch, "Nuclear induction", *Phys. Rev.* 70.7 and 8 (1946) 460–473.

[21] E Zavoisky, "Paramagnetic absorption in perpendicular and parallel fields for salts, solutions and metals" (1944), PhD thesis - Kazan State University.

[22] E. Zavoisky, "Spin-magnetic resonance in paramagnetics", *Fizicheskiĭ Zhurnal* 9 (1945) 211–245.

[23] W. Gerlach and O. Stern, "Der experimentelle Nachweis der Richtungsquantelung im Magnetfeld", *Zeit. für Phys.* 9 (Dec. 1922) 349–352.

[24] A. Lund, M. Shiotani and S. Shimada, *Principles and applications of ESR spectroscopy*, 1. edition, Springer Netherlands, 2011.

[25] G. Eaton et al., *Quantative EPR*, 1st ed., Springer-Verlag, 2010, chap. 1.7. - The Signal Channel 10–13.

[26] B. Rånby and J. Rabek, *ESR spectroscopy in polymer research*, Springer-Verlag, 1977.

[27] C. Poole and H. Farach, *Handbook of electron spin resonance*, v.2, Springer New York, 1999, chap. 4. - Lineshapes.

[28] A. M. Portis, "Electronic structure of F centers: Saturation of the electron spin resonance", *Phys. Rev.* 91.5 (1953) 1071–1078.

[29] G. Breit and I. I. Rabi, "Measurement of nuclear spin", *Phys. Rev.* 38.11 (1931) 2082–2083.

[30] *CODATA internationally recommended values of the fundamental physical constants*, physics.nist.gov/cuu/Constants/index.html, last visited: 20.12.2016.

[31] S.Wu and H. Dong, "Investigations of the g-factors of Fe+ in MgO and CaO", *Zeit. für Nat. forsch. A* 60.5 (2014) 366–368.

[32] A. Abragam, *Principles of nuclear magnetism*, Oxford Univeristy Press, 1961.

[33] M. Goldman, *Spin temperature and nuclear magnetic resonance*, Oxford University Press, 1970.

[34] M. Borghini, "Spin-temperature model of nuclear dynamic polarization using free radicals", *Phys. Rev. Lett.* 20 (9 1968) 419–421.

[35] A. W. Overhauser, "Polarization of nuclei in metals", *Phys. Rev.* 92 (2 1953) 411–415.

[36] T. R. Carver and C. P. Slichter, "Polarization of nuclear spins in metals", *Phys. Rev.* 92 (1 1953) 212–213.

[37] A. Abragam, "Overhauser effect in nonmetals", *Phys. Rev.* 98 (6 1955) 1729–1735.

[38] A. Abragam and W. G. Proctor, "Spin temperature", *Phys. Rev.* Vol. 109, 1958 1441–1458.

[39] C. Jeffries, *Dynamic nuclear orientation*, Interscience Publishers, 1963.

[40] A. Kessenikh et al., *Sov. Phys. Solid State* 5 (1963) 321–329.

[41] M. Kozhushner and P. B.N., "On the theory of forced dynamic nuclear polarization", *Proceedings ail-union conference on magnetic resonance*, (Moscow, Russia), Radiospektroskopiya Tverdogo Tela, 1967 5–8.

[42] A. Abragam and W. G. Proctor, "Dynamic polarization in atomic nuclei in solids", *C.R. Acad. Sci.* 246 (1958) 2253.

[43] W. Hardy and G. Shapiro, "Effects of radiation damage on proton relaxation time in lanthanum magnesium double nitrate", *Proceedings of the international conference on polarized targets and ion sources*, (Saclay, France), CEN, Saclay, 1966 367–371.

[44] A. Abragam and M.Goldman, "Principles of dynamic nuclear polarisation", *Rep. Prog. Phys.* 41 (1978).

[45] A. G. Redfield, "Nuclear magnetic resonance saturation and rotary saturation in solids", *Phys. Rev.* Vol. 98, 1955 1787–1809.

[46] M. Borghini, "Mechanisms of dynamic nuclear polarization by electron-nucleus dipolar coupling", *Proc. on the 2nd Int. Conf. on Pol. Targets*, 1971.

[47] D. J. Kubicki et al., "Rational design of dinitroxide biradicals for efficient cross-effect dynamic nuclear polarization", *Chem. Sci.* 7 (1 2016) 550–558.

[48] K. Hu et al., "Quantum mechanical theory of dynamic nuclear polarization in solid dielectrics", *J. Chem. Phys.* 134.12 (2011) 125105.

[49] J. Heckmann, *Elektronensprinresonanz polarisierbarer Festkörper-Targetmaterialien bei 2.5 T*, Dissertation, Ruhr University of Bochum, 2004.

[50] J. Heckmann et al., "Electron spin resonance and its implication on the maximum nuclear polarization of deuterated solid target materials", *Phys. Rev. B* 74.13 (2006) 134418.

[51] E. Bunyatova, "Free radicals and polarized targets ", *Proceedings of the 9th international workshop on polarized solid targets and techniques*, (Saclay, France), Nucl. Instr. Meth. Phys. Res. A 526.1-2, 2004 22–27.

[52] M. Haulait-Pirson et al., *Alcohols with water. - (Solubility data series, v. 15)*, ed. by A. Barton, 1st ed., Pergamon Press, 1984.

[53] A. L. Zanocco, A. Y. Canetem. and M. X. Melendez, "A kinetic study of the reaction between 2-p- methoxyphnl-4-phenyl-2-oxazolin-5-one and 2,2,6,6-tetramethyl-1-piperidinyl-n-oxide", *Bol. Soc. Chil. Quim.* 45 (2000) 123–129.

[54] O. Piloty and B. Graf Schwerin, "Ueber die Existenz von Derivaten des vierwertigen Stickstoffs", *Ber. deut. chem. Gesell.* 34.2 (1901) 2354–2367.

[55] M. Perkins, "Acyl nitroxides", *Rev. Chem. Intermediates* 7 (1986) 133–141.

[56] S. Mango, "Early target material research with chemical dopants", *Proceedings of the 9th international workshop on polarized solid targets and techniques*, (Saclay, France), Nucl. Instr. Meth. Phys. Res. A 526.1-2, 2004 1–6.

[57] S. Mango, Ö. Runólfsson and M. Borghini, "A butanol polarized proton target", *Nucl. Instr. Meth.* 72.1 (1969) 45–50.

[58] H. G. Aurich and J. Trösken, "Nitroxide, IX. Darstellung cyclischer Imino-nitroxide und isotop-markierter Porphyrexide. ESR-spektroskopische Untersuchungen zur Struktur des Porphyrexids", *Chem. Ber.* 105.4 (1972).

[59] H. Dutz, "Highlights of polarized solid state target instrumentation", *Proceedings of the 9th international workshop on polarized solid targets and techniques*, (Saclay, France), Nucl. Instr. Meth. Phys. Res. A 526.1-2, 2004 117 –125.

[60] A. Thiel et al., "Double-polarization observable G in neutral-pion photoproduction off the proton", *Euro. Phys. J. A* 53.1 (2017) 8.

[61] O. L. Lebedev and S. N. Kazarnovskii, *Zhur. Obshch. Khim.* 30 (1960) 1631.

[62] C. Keith et al., "The Jefferson Lab frozen spin target", *Nucl. Instr. Meth. Phys. Res. A* 684 (2012) 27–35.

[63] M. Krumpolc and J. Roček, "Synthesis of stable chromium (V) complexes of tertiary hydroxy acids", *J. Amer. Chem. Soc.* 101.12 (1979) 3206–3209.

[64] J. Kyynäräinen, "The SMC polarized target", *Proceedings of the 7th international workshop on polarized target materials and techniques*, (Bad Honnef, Germany), Nucl. Instr. Meth. Phys. Res. A 356.1, 1995 47 –52.

[65] S. Bültmann et al., "Properties of the deuterated target material used by the SMC", *Proceedings of the 7th international workshop on polarized target materials and techniques*, (Bad Honnef, Germany), Nucl. Instr. Meth. Phys. Res. A 356.1, 1995 102 –105.

[66] F Kurdzesau et al., "Dynamic nuclear polarization of small labelled molecules in frozen water-alcohol solutions", *J. of Phys. D* 41.15 (2008) 155506.

[67] T. Niinikoski and J.-M. Rieubland, "Dynamic nuclear polarization in irradiated ammonia below 0.5 K", *Phys. Lett. A* 72.2 (1979) 141 –144.

[68] U. Härtel et al., "Experience with NH_3 as target material for polarized proton targets at the Bonn 2.5 GeV electron synchrotron", *Proceedings of the international symposium high energy physics polarized beams and targets*, (Lausanne), Birkhäuser, 1981 447–450.

[69] W. Meyer et al., "Irradiated ammonia (NH_3) as target material for polarized proton targets", *Nucl. Instr. Meth. Phys. Res.* 215.1 (1983) 65 –69.

[70] W. Meyer, "Ammonia as a polarized solid target material - a review", *Proceedings of the 9th international workshop on polarized solid targets and techniques*, (Saclay, France), Nucl. Instr. Meth. Phys. Res. A 526.1-2, 2004 12–21.

[71] R. Dostert et al., "Dynamic nuclear polarization studies in ammonia at 1 K", *Proceedings of the 4th international workshop on polarized target materials and techniques*, (Bad Honnef, Germany), 1984.

[72] B. Adeva et al., "Measurement of proton and nitrogen polarization in ammonia and a test of equal spin temperature", *Nucl. Instr. Meth. Phys. Res. A* 419.1 (1998) 60–82.

[73] Roinel, Y., Bouffard, V. and Roubeau, P., "Nuclear antiferromagnetism in lithium hydride", *J. Phys. France* 39.10 (1978) 1097–1103.

[74] P. Chaumette et al., "Progress report on polarization of irradiated ^{6}LiD and ^{7}LiH", *AIP Conference Proceedings* 187.2 (1989) 1275–1280.

[75] S. Goertz et al., "Investigations in high temperature irradiated ^{6,7}LiH and ^{6}6LiD, its dynamic nuclear polarization and radiation resistance", *Nuc. Instr. Meth. Phys. Res. Sec. A* 356.1 (1995) 20–28.

[76] F. Pretzel et al., "Properties of lithium hydride-IV", *J. Phys. & Chem. of Solids* 23.4 (1962) 325 –337.

[77] S. Goertz, *Dynamische Kernspin-Polarisation strahlendotierter Lithiumwasserstoffe und deren Verhalten im intensiven Elektronenstrahl*, PhD thesis, Univeristy of Bonn, 1994.

[78] *Goodfellow GmbH.* www.goodfellow.com, last visited: 28.12.2016.

[79] *Sigma-Aldrich Chemie GmbH.* www.sigmaaldrich.com, last visited: 28.12.2016.

[80] R. Windmolders, *An introduction to the evaluation of spin structure functions from experimental data*, Lecture @ 10th Seminaire Rhodanien de Physique : Spin in Physics, 2002.

[81] S. Robinson et al., "Density measurement of solid butanol by γ-ray attenuation", *High Energy Spin Physics*, Springer Berlin Heidelberg, 1991 385–387.

[82] M. Hassaine et al., "Low-temperature thermal and elastoacoustic properties of butanol glasses: Study of position isomerism effects around the boson peak", *Phys. Rev. B* 85.10 (2012) 104206.

[83] G. W. Ehrenstein, *Polymeric materials: Structure, properties, applications*, Hanser Verlag Gmbh Co KG, Munich, 2001, chap. Structure of Polymeric Materials 61–141.

[84] I. Perepechko, *Low-temperature properties of polymers*, Elsevier Science, 2013, chap. Thermal expansion of polymers at low temperatures.

[85] R. Corruccini and J. Gniewek, *Thermal expansion of technical solids at low temperatures*, NBS Monograph 29, US Govt. Print. Office, 1961.

[86] J. L. Zakin, R. Simha and H. C. Hershey, "Low-temperature thermal expansivities of polyethylene, polypropylene, mixtures of polyethylene and polypropylene, and polystyrene", *J. Appl. Poly. Sci.* 10.10 (1966) 1455–1473.

[87] C. Rohlof and H. Dutz, "Effective densities and polarizations of the targets for the GDH-experiments at MAMI and ELSA", *Nucl. Instr. Meth. Phys. Res. A* 526 (2004) 126–131.

[88] A. Raccanelli, R. Krause and H. Dutz, "A finite element model for the thermal transport in solid targets", *AIP Conference Proceedings* 915.1 (2007) 983–986.

[89] M. Berger et al., *XCOM: Photon cross section database (version 1.5). (2010)*, physics.nist.gov/xcom, last visited: 30.03.2017.

[90] D. Hill and M. Krumpolc, "Dynamic polarization in some high-hydrogen glasses", *AIP Conference Proceedings* 95.1 (1983) 479–484.

[91] M. Krumpolc and D. Hill, "Stability of chromium (V) doped target materials contaning borane - ammonia and amines", *Proceedings of the 4$^{\text{th}}$ international workshop on polarized target materials and techniques*, (Bad Honnef, Germany), 1984 94–99.

[92] D. Hill, J. Hill and M. Krumpolc, "Polarization in chemically doped hydrogen rich glasses", *Proceedings of the 4$^{\text{th}}$ international workshop on polarized target materials and techniques*, (Bad Honnef, Germany), 1984 84–93.

[93] E. Bunyatova, "New investigations of organic compounds for targets with polarized hydrogen nuclei", *Proceedings of the 7th international workshop on polarized target materials and techniques*, (Bad Honnef, Germany), Nucl. Instr. Meth. Phys. Res. A 356.1, 1995 29–33.

[94] W. Alewelt, *Technische Thermoplaste. 4. Polyamide*, Kunststoff-Handbuch, Hanser, 1998.

[95] B. Wunderlich, *Thermal analysis of polymeric materials*, 1. edition, Springer Verlag, 2005 780.

[96] C. Frank, *Lecture notes from the Stanford University course on chemical engineering 160/260 - Lecture 16 Morphology of semicrystalline polymers given on February 23, 2001*, web.stanford.edu/class/cheme160/lectures/lecture16.pdf, last visited: 23.01.2017.

[97] C. Carraher, *Seymour/Carraher's polymer chemistry*, 6th ed., Undergraduate chemistry, CRC Press, 2003 43–45.

[98] M. J. Richardson, "Crystallinity determination in polymers and a quantitative comparison for polyethylene", *Brit. Poly. J.* 1.3 (1969) 132–137.

[99] S. Kavesh and J. M. Schultz, "Meaning and measurement of crystallinity in polymers: A Review", *Poly. Eng. & Sci.* 9.6 (1969) 452–460.

[100] *Mettler Toledo GmbH.* www.mt.com/de/de/home.html, last visited: 20.11.2016.

[101] A. P. Gray, "Polymer crystallinity determinations by DSC", *Thermochimica Acta* 1 (1970) 563 –579.

[102] D. Domininghaus, *Kunststoffe - Eigenschaften und Anwendungen*, 7. edition, Springer Verlag, 2008 168.

[103] M. Stadlbauer, *Rheo-kinetics of polymers in extension*, Dissertation, University of Linz, 2001.

[104] G. Natta et al., "Dependence of the melting point of isotactic polypropylenes on their molecular weight and degree of stereospecificity of different catalytic systems", *Macro. Chem.* 70 (1964) 191–205.

[105] H. A. Bethe, "Zur Theorie des Durchgangs schneller Korpuskularstrahlen durch Materie", *Ann. Phys.* 397.3 (1930) 325–400.

[106] H. A. Bethe, "Bremsformel für Elektronen relativistischer Geschwindigkeit", *Zeit. Phys.* 76.5 (1932) 293–299.

[107] F. Bloch, "Zur Bremsung rasch bewegter Teilchen beim Durchgang durch die Materie", *Ann. Phys.* 408.3 (1933) 285–320.

[108] J. F. Ziegler, "The stopping of energetic light ions in elemental matter", *J. Appl. Phys /Rev. Appl. Phys* 85 (1999) 1249–1272.

[109] E. Fermi, "The ionization loss of energy in gases and in condensed materials", *Phys. Rev.* 57.6 (1940) 485–493.

[110] R. Sternheimer, "The density effect for the ionization loss in various materials", *Phys. Rev.* 88.4 (1952) 851–859.

[111] R. Sternheimer, M. Berger and S. Seltzer, "Density effect for the ionization loss of charged particles in various substances", *Atom. Data & Nuc. Data Tab.* 30.2 (1984) 261 –271.

[112] C. Patrignani et al., "The review of particle physics - Ch. 33. Passage of particles through matter", *Chin. Phys. C* 40.100001 (2016).

[113] J. Jackson, *Classical Electrodynamics*, 3rd ed., Walter de Gruyter, 2002, chap. 15. Bremsstrahlung, Methode der virtuellen Quanten, Strahlung beim Beta-Zerfall.

[114] D. Groom, *Atomic and nuclear properties of materials*, pdg.lbl.gov/2016/AtomicNuclearProperties, last visited: 04.03.2017.

[115] W. H. Bragg and R. Kleeman, "XXXIX. On the α particles of radium, and their loss of range in passing through various atoms and molecules", *Phil. Mag., Series 6* 10.57 (1905) 318–340.

[116] A. S. Lodhi and D. Powers, "Energy loss of α particles in gaseous C-H and C-H-F compounds", *Phys. Rev. A* 10.6 (1974) 2131–2140.

[117] G. Both et al., "Density dependence of stopping cross sections measured in liquid ethane", *Phys. Rev. A* 28.6 (1983) 3212–3216.

[118] International Commission on Radiation Units and Measurement (ICRU), *Stopping powers for electrons and positrons*, ICRU Report 37, 1984.

[119] M. Berger et al., *ESTAR, PSTAR, and ASTAR: Computer programs for calculating stopping-power and range tables for electrons, protons, and helium ions (version 1.2.3)*, physics.nist.gov/Star, last visited: 20.12.2016.

[120] A. Charlesby, "Cross-linking of polythene by pile radiation", *Proceedings of the Royal Society of London A: Mat., Phys. & Eng. Sciences* 215.1121 (1952) 187–214.

[121] A. Henglein, *Einführungin die Strahlenchemie*, Verlag Chemie, Weinheim, 1969.

[122] Z. Zagórski, "Dependence of depth-dose curves on the energy spectrum of 5 to 13 MeV electron beams", *Rad. Phys. & Chem. (1977)* 22.3 (1983) 409 –418.

[123] J. Bik et al., "EB radiation crosslinking of elastomers", *Rad. Phys. & Chem.* 67 (2003) 421–423.

[124] Z. Zagórski, "Solid state radiation chemistry-features important in basic research and applications", *Rad. Phys. & Chem.* 56.5-6 (1999) 559 –565.

[125] T. Kumada, Y. Noda and N. Ishikawa, "Dynamic nuclear polarization of electron-beam irradiated polyethylene by pairs of alkyl free radicals", *J. Mag. Res.* 218 (2012) 59 –65.

[126] S. Lehmann, *The Bonn isochronous cyclotron*, www.zyklotron.hiskp.uni-bonn.de/zyklo_e/index.html, last visited: 21.12.2016.

[127] F. Frommberger, *Elektronen-Strecher-Anlage*, www.elsa.physik.uni-bonn.de/index.html, last visited: 28.12.2016.

[128] F. Klarner, *Konzeption, Aufbau und Inbetriebnahmme eines neuen Vorbeschleunigers an ELSA*, Dissertation, Univeristy of Bonn, 2011.

[129] *Bergoz Instrumentation*, www.bergoz.com, last visited: 04.01.2017.

[130] S. Runkel, *Herstellung und Untersuchung von Ammoniakkristallen als polarisiertes Target für das COMPASS-Experiment*, Diploma thesis, Univeristy of Bonn, 2011.

[131] A. Meier, *Entwicklung eines Kryo-Thermostaten hoher Kühlleistung zur Targetpräparation für das COMPASS-Experiment*, Diploma thesis, Ruhr-University of Bochum, 1997.

[132] S. Reeve, *A wide temperature range cryostat for polarised target material preparation*, Diploma thesis, Univeristy of Bonn, 2011.

[133] E. J. Lawton, J. S. Balwit and R. S. Powell, "Paramagnetic-resonance studies of irradiated high-density polyethylene. I. Radical species and the effect of environment on their behavior", *J. Chem. Phys.* 33.2 (1960) 395–404.

[134] A. A. Miller, E. J. Lawton and J. S. Balwit, "Effect of chemical structure of vinyl polymers on crosslinking and degradation by ionizing radiation", *Poly. Sci.* 14.77 (1954) 503–504.

[135] M. Iwasaki and T. Ichikawa, "ESR of radical pairs in irradiated polymers. The $\Delta M = 2$ transitions", *J. Chem. Phys.* 46.7 (1967) 2851–2852.

[136] M. Iwasaki, T. Ichikawa and T. Ohmori, “Pairwise trapping of radicals in irradiated high polymers as studied by electron spin resonance”, *J. Chem. Phys.* 50.5 (1969) 1984–1990.

[137] D. Libby and M. Ormerod, “Electron spin resonance spectrum of stretched polyethylene”, *J. Phys. & Chem. Solids* 18.4 (1961) 316 –319.

[138] R. Salovey and W. A. Yager, “Electron spin resonance of irradiated solution-crystallized polyethylene”, *J. Poly. Sci.* 2.1 (1964) 219–224.

[139] S. Shimada et al., “Anisotropic hyperfine constant in ESR spectrum of irradiated solution grown polyethylene”, *Jap. J. Appl. Phys.* 8.2 (1969) 145–150.

[140] S. Shimada, Y. Hori and H. Kashiwabara, “ESR study on the trapping process of the free radicals in irradiated polyethylene”, *Rad. Phys & Chem.* 19.1 (1982) 33 –39.

[141] S. Ohnishi, S. Sugimoto and I. Nitta, “Temperature dependence of the ESR spectrum of irradiated oriented polyethylene”, *J. Chem. Phys.* 37.6 (1962) 1283–1288.

[142] V. Ivanov, *Radiation chemistry of polymers*, 1st ed., VSP, 1992, chap. 3. Radiationchemical transformations of polymers.

[143] M. B. Fallgatter and M. Dole, “The radiation chemistry of polyethylene. VII. Polyene formation”, *J. Phys. Chem.* 68.7 (1964) 1988–1997.

[144] D. C. Waterman and M. Dole, “Radiation chemistry of polyethylene. X. Kinetics of the conversion of alkyl to allyl free radicals”, *J. Phys. Chem.* 74.9 (1970) 1913–1922.

[145] W. Y. Wen, D. R. Johnson and M. Dole, “Second-order diffusion-controlled reaction. Decay of allyl free radicals in irradiated polyethylene”, *J. Phys. Chem.* 78.18 (1974) 1798–1804.

[146] H. C. Lefkovits, J. Fain and F. A. Matsen, “Complete π-electron treatment of allyl radical and allyl ion”, *J. Chem. Phys.* 23.9 (1955) 1690–1692.

[147] H. Fischer and K.-H. Hellwege, “Elektronenspinresonanz-Untersuchungen an bestrahltem Polypropylen”, *J. Poly. Sci.* 56.163 (1962) 33–45.

[148] D. Libby, M. Ormerod and A. Charlesby, “Electron spin resonance spectra of some polymers irradiated at 77 K”, *Polymer* 1 (1960) 212 –218.

[149] L. Forrestal and W.G.Hodgson, “Electron spin resonance studies of irradiated polypropylene”, *J. Poly. Sci.* 2 (1964) 1275–1280.

[150] B. R. Loy, “Electron spin resonance of polypropylene”, *J. Poly. Sci. A* 1.7 (1963) 2251–2259.

[151] P. B. Ayscough and S. Munari, “The room temperature ESR spectrum of irradiated polypropylene: A reinterpretation”, *J. Poly. Sci. B* 4.7 (1966) 503–506.

[152] N. Kusumoto, “ESR studies of polypropylene with different stereospecificities”, *J. Poly. Sci. C* 23.2 (1968) 837–853.

[153] T. Ooi et al., “ESR study of γ-irradiated isotactic and atactic polypropylene”, *Polymer* 16.7 (1975) 510–514.

[154] B. R. Loy, “Electron spin resonance studies of free radical decay in gamma-irradiated polyethylene”, *Poly. Sci.* 44.144 (1960) 341–347.

[155] F. Cracco, A. J. Arvia and M. Dole, “ESR studies of free radical decay in irradiated polyethylene”, *J. Chem. Phys.* 37.10 (1962) 2449–2457.

[156] S. Nara, H. Kashiwabara and J. Sohma, "Configurations of the free radicals in irradiated polypropylene and the relation of their decay reactions to the molecular motion", *J. Poly. Sci. A2* 5.5 (1967) 929–938.

[157] A. Charlesby, D. Libby and M. G. Ormerod, "Radiation damage in polyethylene as studied by electron spin resonance", *Proceedings of the Royal Society of London A: Mathematical, Physical and Engineering Sciences* 262.1309 (1961) 207–218.

[158] D. R. Johnson, W. Y. Wen and M. Dole, "Radiation chemistry of polyethylene. XII. Alkyl radical decay and amorphous content", *J. Phys. Chem.* 77.18 (1973) 2174–2179.

[159] Y. Zhao et al., "ESR study of free radicals in UHMW-PE fiber irradiated by gamma rays", *Rad. Phys. & Chem.* 79.4 (2010) 429 –433.

[160] M. Jahan et al., "A study of long-lived free radicals in gamma-irradiated medical grade polyethylene", *Rad. Phys. & Chem.* 62.1 (2001) 141 –144.

[161] V. Milinchuk et al., "Formation and recombination of free radicals on γ-irradiation of polypropylene - I.", *Poly. Sci.U.S.S.R.* 4.4 (1963) 679 –683.

[162] N. Gvozdic et al., "Kinetics of free radical decay reactions in irradiated isotactic polypropylene", *J. Phys. Chem.* 85.11 (1981) 1563–1569.

[163] T. M. Deas, H. H. Hofer and M. Dole, "Solubility of hydrogen in polyethylene by a semimicro method", *Macromolecules* 5.2 (1972) 223–226.

[164] P. J. Butiagin, "The decay of free radicals in polymer media", *Chemical transformations of polymers*, Butterworth-Heinemann, 1972 57 –76.

[165] Y. S. Lebelev, *Kinet. Katal.* 8 (1967) 245–250.

[166] T. Waite, "Bimolecular Reaction Rates in Solids and Liquids", *J. Chem. Phys.* 32 (1960) 21–23.

[167] T. Seguchi and N. Tamura, "Mechanism of decay of alkyl radicals in irradiated polyethylene on exposure to air as studied by electron spin resonance", *J. Phys. Chem* 77.1 (1973) 40–44.

[168] F. H. Winslow et al., "Autoxidation of semicrystalline polyethylene", *Poly. Eng. & Sci.* 6.3 (1966) 273–278, ISSN: 1548-2634.

[169] M. Plückthun et al., "Polarization measurements of TEMPO-doped butanol targets", *Nucl. Instr. Meth. Phys. Res. A* 400.1 (1997) 133 –136.

[170] R. Aasa and tore Vänngård, "EPR signal intensity and powder shapes: A reexamination", *J. Mag. Res. (1969)* 19.3 (1975) 308 –315.

[171] F. Schneider and M. Plato, 1st ed., Thiemig Taschenbücher, 1971 162.

[172] P. M. McKee, "Radiation Damage Effects in Polarized Deuterated Ammonia", *AIP Conference Proceedings* 675.1 (2003) 919–923.

[173] S Bültmann et al., "A study of lithium deuteride as a material for a polarized target", *Nuclear Instruments and Methods in Physics Research Section A: Accelerators, Spectrometers, Detectors and Associated Equipment* 425.1-2 (1999) 23 –36.

[174] H. Fischer, K.-H. Hellwege and P. Neudörfl, "Elektronenspinresonanz-Untersuchungen an Peroxydradikalen in bestrahltem Polypropylen", *J. Poly. Sci. A* 1.6 (1963) 2109–2117.

[175] H. Kashiwabara, S. Shimada and Y. Hori, "Nature of peroxy radicals in polypropylene", *Int. J. Rad. App. & Instr. C.* 37.3 (1991) 511–515.

[176] B. Rånby and H. Yoshida, "Electron spin resonance studies of polyethylene and polypropylene irradiated by ultraviolet light", *J. Poly. Sci. C* 12.1 (1966) 263–276.

[177] D. J. Carlsson, S. Chmela and J. Lacoste, "On the structures and yields of the first peroxyl radicals in γ-irradiated polyolefins", *Macromolecules* 23.23 (1990) 4934–4938.

[178] S. J. Wyard, "The dipolar broadening of electron spin resonance lines in irradiated solids", *Proc. Phys. Soc.* 86.3 (1965) 587–593.

[179] G. Ventura and L. Risegari, "Cryoliquids", *The art of cryogenics*, Elsevier, 2008 37 –54.

[180] C. Keith, "Polarized solid targets: Recent progress and future prospects", *PSTP2009 - Proceedings of the 13th international workshop on polarized sources, targets and polarimetry*, (Ferrara, Italy), World Scientific, 2011 113–122.

[181] H. Dutz, *Aufbau und Test des Bonner 'Frozen Spin Targets'*, Diploma thesis, Univeristy of Bonn, 1989.

[182] *RV-Elektroniikka Oy Picowatt*, www.picowatt.fi, last visited: 12.03.2017.

[183] *Lake Shore Cryotronics, Inc.* www.lakeshore.com, last visited: 12.03.2017.

[184] H. Kamerlingh Onnes, *The liquefaction of helium: Communication no. 108 from the Physical Laboratory at Leiden*, 1908.

[185] H. Preston-Thomas, "The international temperature scale of 1990 (ITS-90)", *Metrologia* 27 (1990) 3–10.

[186] R. J. Donnelly and C. F. Barenghi, "The observed properties of liquid helium at the saturated vapor pressure", *J. Phys & Chem. Ref. Data* 27.6 (1998) 1217–1274.

[187] F. Pobell, "The ^{3}He-^{4}He dilution refrigerator", *Matter and methods at low temperatures*, Springer Verlag, 1996 120–156.

[188] M. Clapeyron, "Mémoire sur la puissance motrice de la chaleur", *Journal de l' École polytechnique* 23 (1834) 153–190.

[189] R. Clausius, "Über die bewegende Kraft der Wärme und die Gesetze, welche sich daraus für die Wärmelehre selbst ableiten lassen", *Ann. Phys.* 155 (1850) 500–524.

[190] J. Harmsen, *Ein ^{4}He-Verdampfer-Kryostat zur Entwickelung polarisierter Festkörpertargets*, Diploma thesis, Ruhr Univeristy of Bochum, 1997.

[191] S. Goertz, W. Meyer and G. Reicherz, "Polarized H, D and ^{3}He targets for particle physics experiments", *Prog. Part. & Nuc. Phys.* 49.2 (2002) 403 –489.

[192] G. Court et al., "A high precision Q-meter for the measurement of proton polarization in polarised targets", *Nucl. Instr. Meth. Phys. Res. A* 324.3 (1993) 433–440.

[193] D. Wollan, "Dynamic nuclear polarization with an inhomogeneously broadened ESR line. I. Theory", *Phys. Rev. B* 13 (9 1976) 3671–3685.

[194] F. Gerson and W. Huber, "Taking and analyzing ESR spectra", *Electron spin resonance spectroscopy of organic radicals*, Wiley-VCH Verlag GmbH & Co. KGaA, 2004 97–165.

[195] S. Runkel et al., "CFD-Simulations of a 4π-continuous-mode dilution refrigerator for the CB-ELSA experiment", *PoS* PSTP2015 (2015) 018.

[196] M. Bornstein et al., "Development of a thin, internal superconducting polarisation magnet for the Polarised Target", *PoS* PSTP2015 (2015) 006.

[197] M. Bornstein et al., "A thin, superconducting magnet for the Polarized Target", Talk held in the target session of the 22nd International Spin Symposium, 2016.

[198] J. S. Waugh, "NMR Spectroscopy in solids - a historical perspective", *Anal. Chem.* 65.17 (1993) 725A–729A.

[199] Y. Matsuki et al., "Dynamic nuclear polarization with a rigid biradical", *Ang. Chem. Int. Ed.* 48.27 (2009) 4996–5000.

[200] K.-N. Hu et al., "Dynamic nuclear polarization with biradicals", *J. Am. Chem. Soc.* 126.35 (2004) 10844–10845.

[201] K.-N. Hu et al., "High-frequency dynamic nuclear polarization using biradicals: A multifrequency EPR lineshape analysis", *J. Chem. Phys.* 128.5 ().

[202] K. Nunome et al., "ESR studies of local concentrations of radicals in polyethylene irradiated at 1.5, 4.2 and 77 K", *Chem. Phys. Lett.* 39 (1976) 542–546.

[203] T. Ichikawa, S. Kawahara and H. Yoshida, "Local distribution of alkyl radicals in γ-irradiated polyethylene studied by electron spin echo method", *Rad. Phys. & Chem.* 26 (1985) 731–737.

[204] B. van den Brandt et al., "Solid polarized targets at PSI: Recent developments", *PSTP2005 - Proceedings of the 11th international workshop on polarized sources, targets and polarimetry*, (Osaka, Japan), World Scientific, 2007 173–177.

[205] E. J. Lawton, J. S. Balwit and R. S. Powell, "Paramagnetic-resonance studies of irradiated high-density polyethylene. II. Effect of irradiation dose on the radical species trapped at room temperature", *J. Chem. Phys.* 33.2 (1960) 405–412.

[206] S.-I. Ohnishi et al., "On the ESR singlet spectra frequently observed in irradiated polymers at a large dose", *J. Poly. Sci.* 47.149 (1960) 503–507.

[207] A. Grishina and N. Bakh, "ESR study of the structural changes in polyethylene caused by high dose irradiation", *Vysokomol. Soedin.* 7.10 (1965), (Translated by E.O. Phillips) 1698–1700.

[208] M. Igarashi, "Free-radical identification by ESR in polyethylene and nylon", *J. Poly. Sci.* 21.8 (1983) 2405–2425.

[209] T. Kawashima et al., "ESR studies on the molecular mechanisms of fracture of polymers at low temperatures", *Poly. J.* 5 (1973) 135–143.

[210] M. Sakaguchi and J. Sohma, "ESR evidence for main-chain scission produced by mechanical fracture of polymers at low temperature", *J. Poly. Sci.* 13 (1975) 1233–1245.

List of Figures

List of Tables

Acknowledgements

Foremost, I would like to thank PD Dr. S. Goertz for his guidance and many fruitful discussions on the topics of the polarised target and generally helping to steer the ship in the right direction. Scientific endeavours are rarely possible without the assistance and support of a strong work group. I owe a great debt of gratitude to Dr. H. Dutz, in addition to my dear colleagues and comrades-in-arms S. Runkel and M. Bornstein, as well as all other past polarised target members I had the pleasure of working with.
Without the people involved in the irradiation facilities in Bonn, this work would not be possible. My sincerest thanks go to the operators, physicists and technicians working at ELSA. Here especially I would like thank Prof. Dr. W. Hillert and D. Proft, as well as Dr. M. Schedler for the many, many hours and days and weeks invested. The same applies to PD Dr. P.D. Eversheim and S. Birkenbach at the Cyclotron at the HISKP.
On the chemical analysis side, I would like to thank Prof. Dr. S. Höger for access to his laboratory in the Organic Chemistry department of the University of Bonn, as well as Dr. J. Vollmeyer for advice and guidance on the melt characteristics and the DSC measurements of polymer materials. Also, Prof. Dr. O. Schiemann of the Physikalische Chemie department of the University of Bonn, for laboratory time allowing some low temperature pulsed ESR measurements of our samples. In addition I would also like to mention Dr. H. Matsuoka who helped with the measurements and highlighted, in many hours of discussion, the advantages of pulsed ESR methods.
As well as my colleagues from the PT group in Bonn I would like to thank my colleagues from the polarised target group of the Ruhr University Bochum, particularly Prof. Dr. W. Meyer, Dr. G. Reicherz, Dr. J. Herick and Dr. A. Berlin, for all your efforts concerning the polarisation and analysis of the polymer materials, especially concerning the long hours and night shifts that were put in.
I would like to thank my family and friends for putting up with me in the taxing process of compilation, and my universal stressing about everything and sometimes anything. And finally I would like to express my appreciation and deepest respect for my very supportive and patient wife, Nadine, and my two daughters Hayleigh and Caelyn.